HIGHWAY RESEARCH RECORD

Number 128

Frost, Physical Properties and Stabilization

7 Reports

Subject Classifications

62 Foundations (Soils)
64 Soil Science

HIGHWAY RESEARCH BOARD
DIVISION OF ENGINEERING NATIONAL RESEARCH COUNCIL
NATIONAL ACADEMY OF SCIENCES—NATIONAL ACADEMY OF ENGINEERING

Washington, D. C., 1966 Publication 1372

Department of Soils, Geology and Foundations

Eldon J. Yoder, Chairman
Joint Highway Research Project
Purdue University, Lafayette, Indiana

Chester McDowell, Vice Chairman
Supervising Soils Engineer
Texas Highway Department, Austin

HIGHWAY RESEARCH BOARD STAFF

A. W. Johnson, Engineer of Soils and Foundations

J. W. Guinnee, Assistant Engineer of Soils and Foundations

DIVISION A

Chester McDowell, Chairman
Supervising Soils Engineer
Texas Highway Department, Austin

James E. Kelly, Vice Chairman
District Construction Engineer
Texas Highway Department, Waco

COMMITTEE ON SOIL-PORTLAND CEMENT STABILIZATION
(As of December 31, 1965)

James M. Hoover, Chairman
Civil Engineering Department
Iowa State University, Ames

William A. Cordon, Department of Civil and Irrigation Engineering, Utah State University, Logan
Earl B. Kinter, U. S. Bureau of Public Roads, Washington, D. C.
George R. Kozan, Chief, Soils Stabilization Section, U. S. Corps of Engineers, Waterways Experiment Station, Vicksburg, Mississippi
W. A. Lewis, Road Research Laboratory, Ministry of Transport, Harmondsworth, West Drayton, Middlesex, England
William H. Mills, Consulting Engineer, Atlanta, Georgia
C. E. Minor, Materials and Research Engineer, Washington Department of Highways, Olympia
James K. Mitchell, Associate Professor of Civil Engineering, Department of Civil Engineering, University of California, Berkeley
Peter J. Nussbaum, Research Engineer, Paving Development Section, Portland Cement Association, Skokie, Illinois
Radnor J. Paquette, Georgia Institute of Technology, Atlanta
J. F. Redus, Clark, Dietz, Painter and Associates, Memphis, Tennessee
E. G. Robbins, Portland Cement Association, Chicago, Illinois

COMMITTEE ON SOIL-BITUMINOUS STABILIZATION

(As of December 31, 1965)

Walter H. Zimpfer, Chairman
Civil Engineering Department
University of Florida, Gainesville

K. O. Anderson, Department of Civil and Municipal Engineering, University of Alberta, Edmonton, Canada
Moreland Herrin, Professor of Civil Engineering, Department of Civil Engineering, University of Illinois, Urbana
Charles C. Ladd, Assistant Professor of Civil Engineering, Massachusetts Institute of Technology, Cambridge
Vytautas P. Puzinauskas, Associate Research Engineer, The Asphalt Institute, University of Maryland, College Park
Hugh A. Wallace, Special Products Engineer, Golden Bear Oil Company, Dallas, Texas
H. Fred Waller, Jr., Miller-Warden Associates, Raleigh, North Carolina
Hans F. Winterkorn, Professor of Civil Engineering, Princeton University, Princeton, New Jersey

DIVISION C

O. L. Lund, Chairman
Assistant Engineer of Materials and Tests
Nebraska Department of Roads, Lincoln

L. F. Erickson, Vice Chairman
Research Engineer
Idaho Department of Highways, Boise

COMMITTEE ON PHYSICO-CHEMICAL PHENOMENA IN SOILS

(As of December 31, 1965)

Hans F. Winterkorn, Chairman
Professor of Civil Engineering
Princeton University, Princeton, New Jersey

Gail C. Blomquist, School of Civil Engineering, Michigan State University, East Lansing
James H. Havens, Director of Research, Kentucky Department of Highways, Lexington
J. F. Hemwall, The Dow Chemical Company, Midland, Michigan
Earl B. Kinter, U. S. Bureau of Public Roads, Washington, D. C.
Joakim G. Laguros, Department of Civil Engineering, University of Oklahoma, Norman
R. C. Mainfort, Michigan State Highway Department, Lansing
Edward Penner, Division of Building Research, National Research Council of Canada, Ottawa
Elmer A. Rosauer, Engineering Experiment Station, Iowa State University, Ames
J. B. Sheeler, Associate Professor of Civil Engineering, Civil Engineering Department, Iowa State University, Ames
Mehmet A. Sherif, Department of Civil Engineering, University of Washington, Seattle
F. L. D. Wooltorton, Truffles, Pigbush Lane, Loxwood, Billingshurst, Sussex, England

COMMITTEE ON FROST ACTION

(As of December 31, 1965)

L. F. Erickson, Chairman
Research Engineer
Idaho Department of Highways, Boise

Hamilton Gray, Chairman, Department of Civil Engineering, Ohio State University, Columbus
L. E. Gregg, L. E. Gregg and Associates, Consulting Engineers, Lexington, Kentucky
Wilbur M. Haas, Department of Civil Engineering, Michigan Technological University, Houghton
Frank B. Hennion, Assistant Chief, Civil Engineering Branch, Engineering Division, Military Construction, Office, Chief of Engineers, Department of the Army, Washington, D. C.
Alfreds R. Jumikis, Professor of Civil Engineering, College of Engineering, Rutgers, The State University, New Brunswick, New Jersey
Miles S. Kersten, Professor of Civil Engineering, University of Minnesota, Minneapolis
R. I. Kingham, Staff Engineer, The Asphalt Institute, University of Maryland, College Park
Clyde N. Laughter, Chief Soils Engineer, State Highway Commission of Wisconsin, Madison
O. L. Lund, Assistant Materials and Testing Engineer, Nebraska Department of Roads, Lincoln
A. E. Matthews, Engineer of Soils, Office of Testing and Research, Michigan State Highway Department, Lansing
George W. McAlpin, Deputy Chief Engineer (Research), Technical Services Subdivision, New York State Department of Public Works, Albany
Eugene B. McDonald, Materials Engineer, South Dakota Department of Highways, Pierre
Paul S. Otis, Materials and Research Engineer, New Hampshire Department of Public Works and Highways, Concord
R. G. Packard, Chief, Soil-Cement Laboratory, Portland Cement Association, Chicago
Edward Penner, Division of Building Research, National Research Council of Canada, Ottawa
Harold R. Peyton, Principal Investigator, Arctic Environmental Engineering Laboratory, University of Alaska, College
C. K. Preus, Materials and Research Engineer, Minnesota Department of Highways, St. Paul
James R. Schuyler, State Highway Engineer, New Jersey State Highway Department, Trenton
Willis H. Taylor, Jr., Assistant Chief Construction Engineer, Louisiana Department of Highways, Baton Rouge
K. B. Woods, Goss Professor of Engineering, Purdue University, Lafayette, Indiana

Foreword

This Record includes seven papers that range in content from the results of applied research to those that report fundamental data of a scientific nature.

Although some of the papers will be of interest to those whose engineering specialty includes soils, geology and foundations, they should also interest individuals in charge of different branches of engineering operations. Materials engineers concerned with testing proprietary and natural materials for damaged areas, and engineers responsible for design and construction of roads over highly frost-susceptible areas may find the paper by Penner, Oosterbaan and Rodman helpful. Shen and Mitchell's paper will interest engineers who design multilayer pavements of components exhibiting different properties of strength and volume change. The papers by Jones, and Justo and Hariharan, should interest engineers charged with the proportioning of the components employed in stabilized mixtures and with determining limits of compaction and layer thickness to satisfy structural requirements. The paper by Farouki provides information for those concerned with embedment of electric power cables—an item of construction becoming more common in urban areas. In addition, it provides information of an applied nature and data that adds to our knowledge of thermal conductivity and resistance to transmission of heat by different soil types and different soil states. All of these papers should be of interest to those engaged in teaching.

All of the foregoing papers concern researches based on the mechanistic approach toward increasing knowledge of the behavior of soil and pavement structures. However, because of the complexity of the soil, water, load, and temperature interrelationships, the mechanistic approach to the study of soil behavior is now being increasingly supplemented by comprehensive investigations of the fundamental physico-chemical aspects of interaction between these factors.

The papers by Rao and by Roderick and Demirel add to our fundamental scientific knowledge. They should be of interest to soil engineers, soil scientists, and to researchers looking ever deeper into the physico-chemical properties of soils, and to those engaged in teaching this branch of soil science. The paper by Rao presents results on determinations of subpressures that develop in soil under thermal gradients embracing freezing temperatures and the resulting hydrodynamic moisture transfer to the zone of freezing. The Roderick-Demirel paper reports researches employing physico-chemical studies to determine interactions between soil colloids amd water vapor.

Contents

Performance of City Pavement Structures Containing Foamed Plastic Insulation

E. PENNER, Research Officer, Division of Building Research, National Research Council, Ottawa;
M. D. OOSTERBAAN, Construction Engineer, Plastics Development and Service, Dow Chemical Co., Midland, Michigan; and
R. W. RODMAN, Roads and Drainage Engineer, City of Sudbury, Ontario

This paper presents one winter's results of two 100-ft city pavement sections insulated with a 2-in. thickness of extruded polystyrene plastic foam in Sudbury, Ontario, Canada. The experimental results consisted of temperature measurements, frost-depth measurements with methylene blue gages, elevation measurements for frost heave and Benkelman beam deflections following the thawing period.

The insulation reduced frost penetration by 35 in. during a 2600 degree-day winter. Thermoconductivity measurements showed that no deterioration occurred in the insulating properties of the insulation. Frost penetration in the control area was approximately 65 in., which compares favorably with the depth predicted by the U. S. Army Corps of Engineers from measurements in granular base course beneath snow-cleared airport runways.

•THE CONCEPT of thermally insulating frost-susceptible subgrades has been used widely on Norwegian railroads since the turn of the century (1). The practice has been to replace frost-susceptible soil in the freezing zone with a layer of peat blocks or other highly fibrous materials. Such materials usually contain more water than soil. When wet peat freezes a proportionately larger quantity of latent heat is released and hence the freezing plane moves downward more slowly. The frostline may also be attenuated with a dry insulating layer of high thermal resistance placed in the pavement structure. This is the basis of a technique that has received attention recently.

The first full-scale field trials with a dry insulation using extruded polystyrene plastic foam with surface skins were described by Oosterbaan and Leonards (2) and Young (3). An earlier study, which compared predicted and measured frost penetration depths beneath small concrete slabs, also included a small amount of data on an insulating layer of cellular glass (4).

The desirability of decreasing frostline penetration in highways and streets in areas of seasonal frost arises because the design pavement thickness, based strictly on load-carrying capacity, is usually less than the thickness required to prevent frost penetration into the subgrade. Consequently, detrimental frost action ensues if the subgrade is frost-susceptible.

If an insulating material is embodied in the pavement structure it should retain its thermal resistance over the lifetime of the road in spite of a varying moisture regime in the surrounding material. Further, the insulating layer should not interfere significantly with the stability of the pavement structure, either because of the flexible nature of the insulation or by creating an unfavorable water condition in the other components of the road.

The amount of insulation required will depend on the type of pavement structure, the thermal constants of the various layers, and the climate. As there are some difficulties

Paper sponsored by Committee on Frost Action and presented at the 45th Annual Meeting.

associated with the prediction of reliable thermal patterns in pavement structures, field trials have been initiated.

In the present paper the results of one winter's observations are given for two street sections in the City of Sudbury insulated with extruded polystyrene plastic foam with surface skins. The project was a joint undertaking by Dow Chemical of Canada Ltd., the City of Sudbury, and the Division of Building Research of the National Research Council of Canada.

CONSTRUCTION AND INSTRUMENTATION

Insulated sections were constructed at two locations in Sudbury, on Antwerp and Byng Streets, which were unpaved streets slated for reconstruction and surfacing. Figure 1 shows a plan view of both the insulated and control sections on Antwerp Street. The 100-ft insulated section was 35 ft wide and extended beneath the east sidewalk over most of its length and to the edge of the sidewalk on the west side. Letters A to G give the seven thermocouple locations; the circled numbers are the locations of the frost-depth gages.

A similar plan view shows the Byng Street location (Fig. 2). This site was instrumented with frost-depth gages only. The insulated area was 108 ft long and 35 ft wide. Again, the insulation extended underneath the proposed sidewalk area on the east side but the sidewalk was not constructed before the first winter's observations.

Figures 3 and 4 show cross-sections of the pavement structure and thermocouple depths for both the insulated and control areas on Antwerp Street. The pavement design on the east half of Antwerp Street consisted of $3\frac{1}{2}$ in. of asphaltic concrete, 3 in. of "A" base material, 9 in. of "B" subbase and 2 in. of insulation. On the west half, an additional 7 in. of "B" subbase was placed below the insulation. The control area

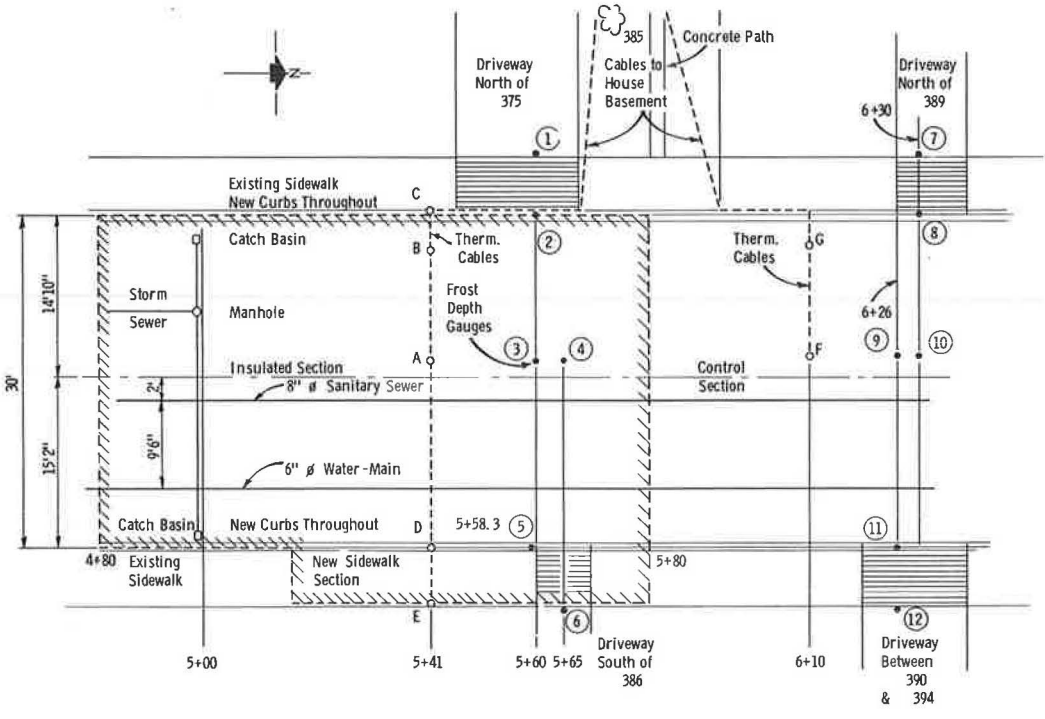

Figure 1. Plan of insulated and control section on Antwerp Street with locations of thermocouples and frost-depth gages.

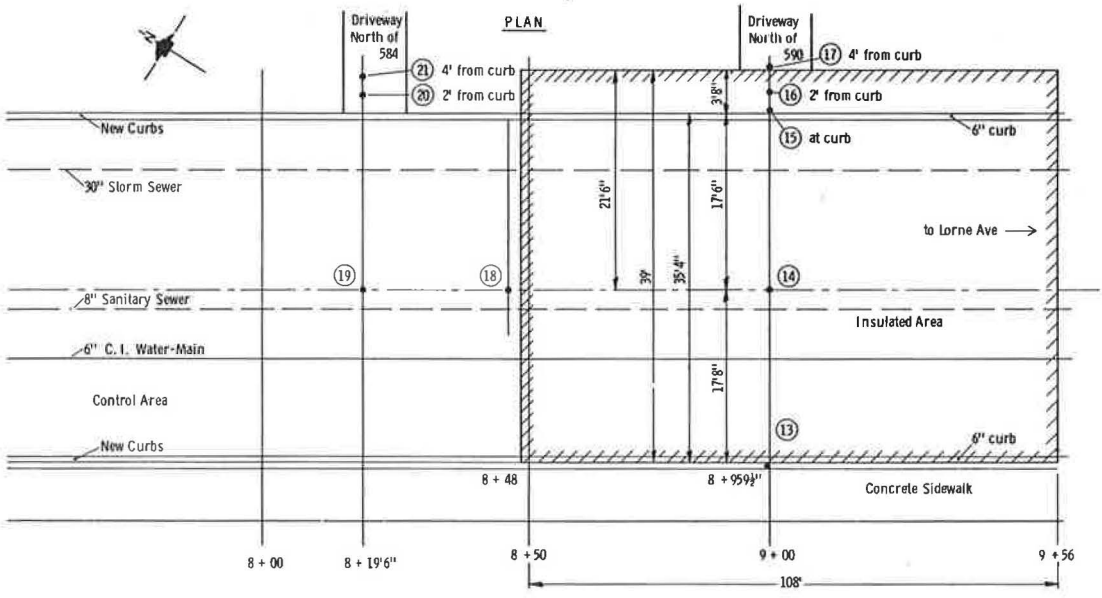

Figure 2. Plan view of insulated and control areas on Byng Street showing location of frost depth.

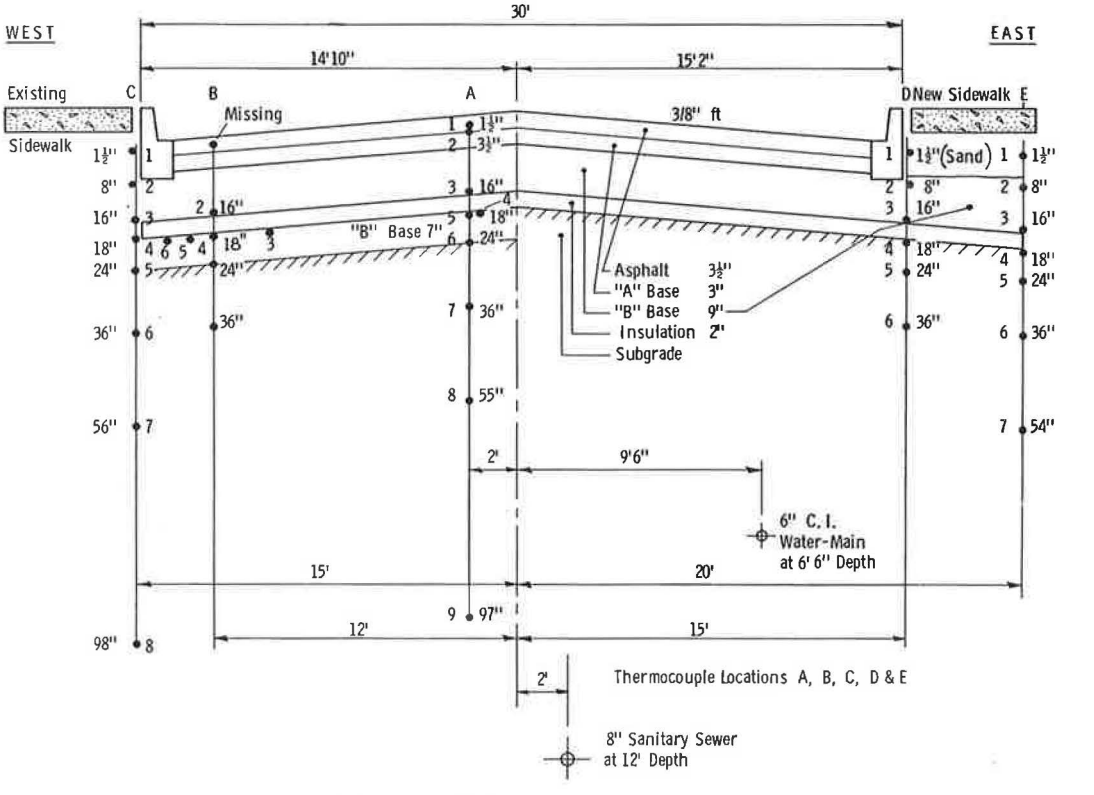

Figure 3. Pavement design and thermocouple locations of insulated section at Station 5+41, Antwerp Street.

was uniform on both sides consisting of 3½ in. of asphaltic concrete, 3 in. of "A" base course, and 18 in. of "B" subbase.

Cross-sections of the pavement structure on Byng Street are shown in Figures 5a and 5b. The pavement design of 3½ in. of asphaltic concrete, 3 in. of "A" base course

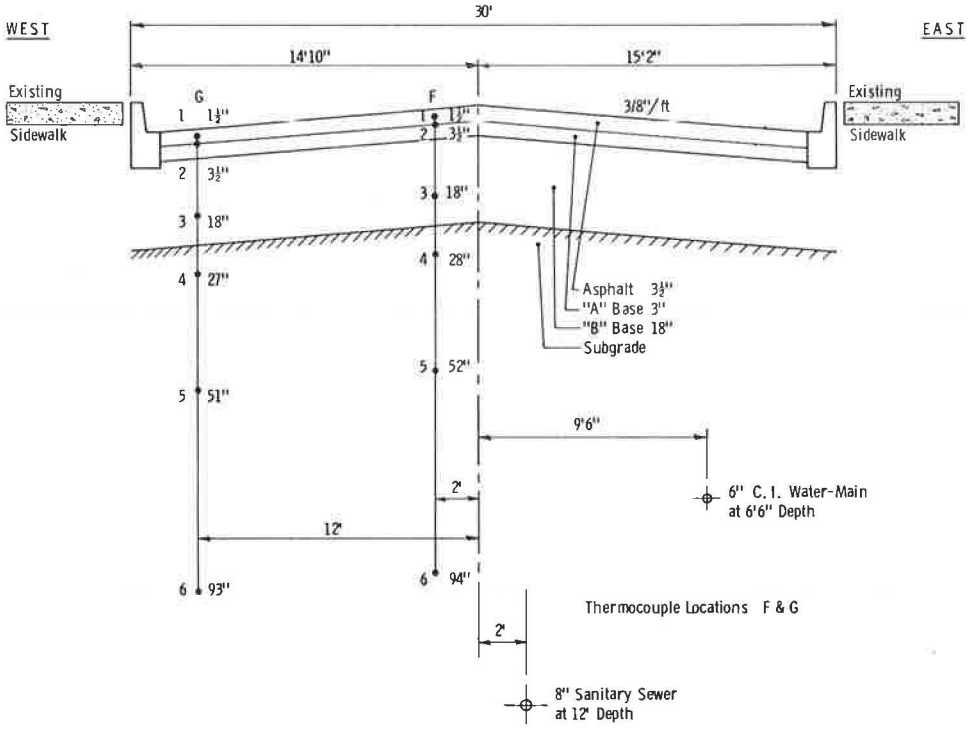

Figure 4. Pavement design and thermocouple locations of control section at Station 6+10, Antwerp Street.

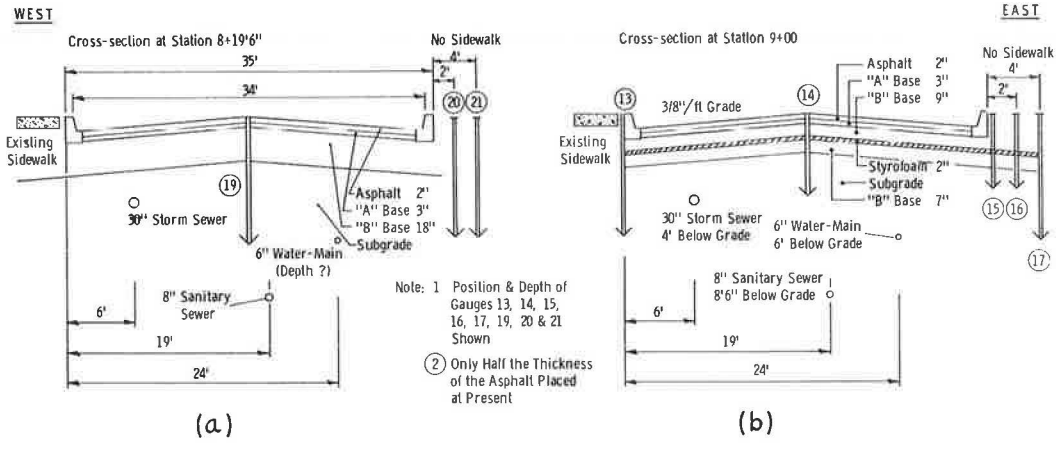

Figure 5. Cross-section of insulated and control areas on Byng Street showing pavement structure and locations of frost-depth gages.

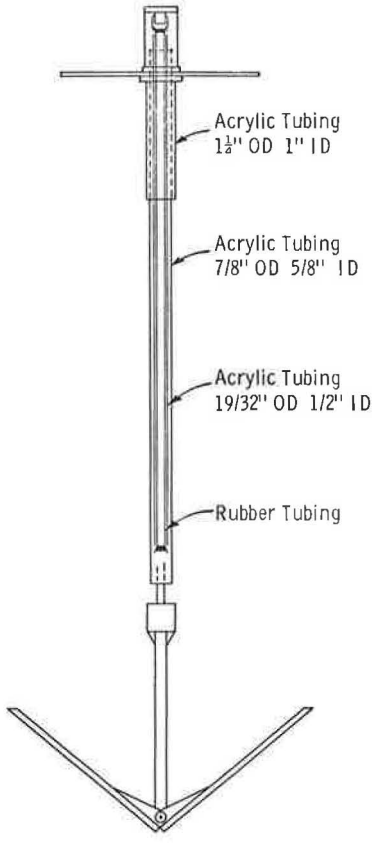

Figure 6. Frost-depth gage.

and 18 in. of "B" subbase was based on the standard practice of the City of Sudbury for the subgrade soils at both locations. Only 2 in. of asphaltic concrete was placed at Byng Street prior to freeze-up. The remaining 1½ in. was scheduled for placement in the summer of 1965.

Frost-Depth Gages

The frost-depth gages (Fig. 6) were of Swedish design, the details of which have been published (5). Briefly, the gage consists of two telescoping lucite tubes. The inner plastic tube contains a soft rubber tube and the annulus between the rubber tube and plastic outer tube is filled with an aqueous solution of methylene blue. The thin annulus of solution can expand easily on freezing by compressing the inner rubber tube. The outer tube, anchored at the surface, can move vertically in case of heave or settlement without damaging the gage. The gages were read weekly to follow the progress of the freezing plane by this method.

Thermocouple Installation

Fifty 20-gage copper-constantan thermocouples were installed on Antwerp Street (Figs. 3 and 4) and connected to a panel located in the basement of a house adjacent to the experimental area. Twenty thermocouples were connected to a suitably preamplified millivolt recorder for continuous measurements and the remaining thirty were read either daily or weekly depending on the depth of installation. In most cases the thermocouples located in the upper strata of the pavement and above the insulation were connected to the recorder; the lower ones were read with a standard manually operated potentiometer. An automatic thermoelectric ice bath was used as a reference temperature.

A Stevenson screen containing a thermograph was installed on the Antwerp Street site for air temperature measurements.

Frost Heave Measurements

Elevations at the tops of the frost-depth gages were determined weekly to measure frost heave. Every three weeks, elevations were determined on the surface of the road on a 20-ft grid system.

Site Preparation

Site preparation for the placing of the extruded polystyrene insulation boards (2 ft by 4 ft by 2 in.) was to fine grade and hand rake the surface. The panels, placed in a staggered fashion, were held in place with 6-in. wooden dowels. No attempt was made to seal the cracks between adjacent boards. The subbase was end-dumped from trucks and then bladed over the insulation by track vehicles riding on an 8-in. cushion of the subbase material.

The Byng Street experimental site had a gentle upward slope of 1.5 percent from south to north. On Antwerp Street, the slope was about 4 percent in the same direction.

TABLE 1

GRADING REQUIREMENTS

Tyler Screen Size Square Openings	Percent Passing	
	"A" Base Course	Modified Granular "B" Subbase
4 in.		100
2½ in.		85-100
1 in.		60-100
⅞ in.	100	57-100
⅝ in.	75-100	48-100
No. 4	35-60	25-92
No. 8		15-85
No. 14	15-35	10-75
No. 28		
No. 48	5-20	5-38
No. 100	4-15	4-22
No. 200	3-8	3-8

The east side of the pavement was about 6 in. lower than the west side at both locations. This had some bearing on the drainage and deflection pattern of both test sections.

BASE-COURSE MATERIALS AND SOILS

The particle-size grading requirements for both the "A" base course and "B" subbase materials are given in Table 1. These were compacted in accordance with the usual practice followed by the City of Sudbury.

As both installations were built on previously unpaved streets, the first few feet of material below the surface varied considerably. Although it was hoped that the insulation on the east half of Antwerp Street could be placed directly on natural

TABLE 2

SOIL TEST DATA ON ANTWERP STREET PRIOR TO PRESENT CONSTRUCTION
September 14, 1964
Hole 1, Station 5+45, 6 ft west of centerline
Hole 2, Station 4+96, 2 ft west of centerline

Hole	Depth (ft)	W_n	W_L	W_p	γ	Description
1	0-2	—	—	—	—	Sandy gravel fill with slag and ashes; dry.
	2-4	22.3	—	—	—	As above to 2.5 ft, then brown silty fill to 3.9 ft, then 1 in. peat, then dense brown silt.
	4-5.7	22.0	22.7	22.1	125	Brown cohesive sand silt with numerous oxidized stains. Hit obstruction at 5.7 ft. Move rig 2 ft.
	6-8	22.6	—	—	—	Brown moist silt.
	8-10	18.6	25.3	19.3	—	Brownish grey, stratified, fissured cohesive silt. Could not jack sample. Silt partings at frequent intervals.
2	0-2	—	—	—	—	Dry sandy gravel fill with slag and ashes to 20 in., then brown clayey silt.
	2-4	23.2	35.1	22.1	121	
	4-6	20.1	—	—	—	Grey and brown coarse silt, very moist 4.5 to 4.7 ft.
	6-8	15.4	17.9	17.5	132	
	8-10	21.8	—	—	—	Dense brown silt, thin clay seams, moist only.

Note: W_n = natural moisture, W_L = liquid limit, W_p = plastic limit, γ = natural unit weight.

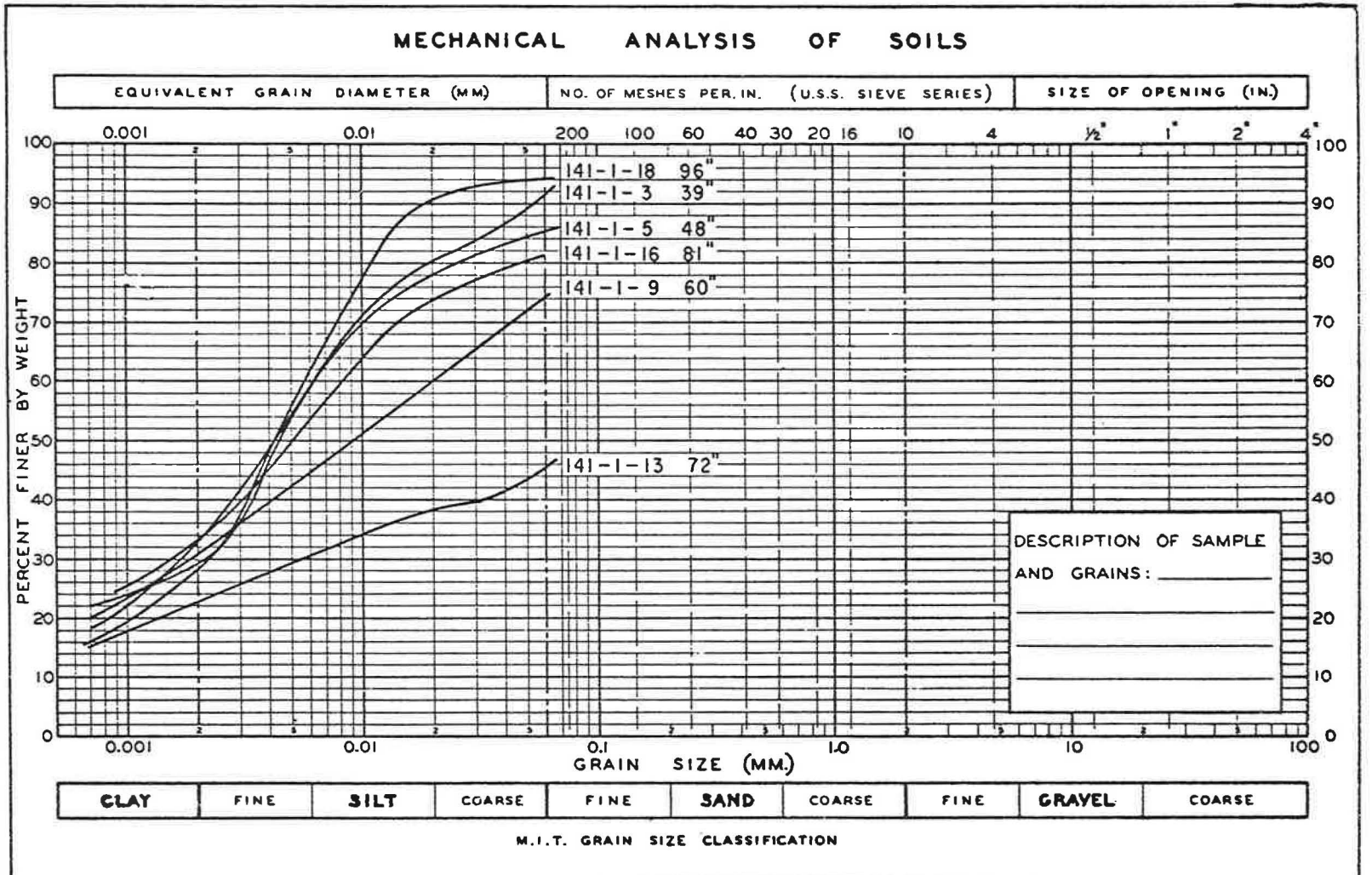

Figure 7. Hydrometer analyses of soil samples at Station 5+41, 2 ft west of centerline.

subgrade soils, this was in fact not the case. At the Antwerp site, the upper few feet consisted of fill material of slag and ashes mixed with silt. Grain-size curves for samples of the subgrade below 39 in. are given in Figure 7. These show 18 to 26 percent in the clay sizes, most of the remaining percentage in the silt size, and a small amount of fine sand. The moisture contents ranged from 17 to 22 percent by weight just before construction. Test results and a description of the soils on Antwerp Street are given in Table 2.

The Byng Street installation was constructed on a previously filled low-lying swampy area. Again, the upper materials consisted of a slag-ash fill intermixed with silts. Below 3 ft the organic residues and silts were too soft to sample with a hand auger.

RESULTS

Air Temperature and Freezing Index

The air freezing index based on degree-days F, calculated from thermograph measurements on the site, was 2600 (Fig. 8). The average for 1954-1960 at the Sudbury airport 12.5 miles NE of the city was 2387.

The design freezing index for the area is 3200 degree-days (6). The freezing index was 1770 degree-days at a depth of 1½ in. in the asphaltic concrete over the insulated area and 1500 at the same depth in the control area. This gives an "n-factor" of 0.68 for the insulated area and 0.58 for the control area.

Subsurface Temperatures

The average daily air temperatures are shown in Figure 9a for the winter of 1964-65. Figures 9b and 9c show the temperatures at various depths (2 ft off centerline) of the control area and insulated area respectively. The shaded area gives the temperature difference across the 2 in. of insulation.

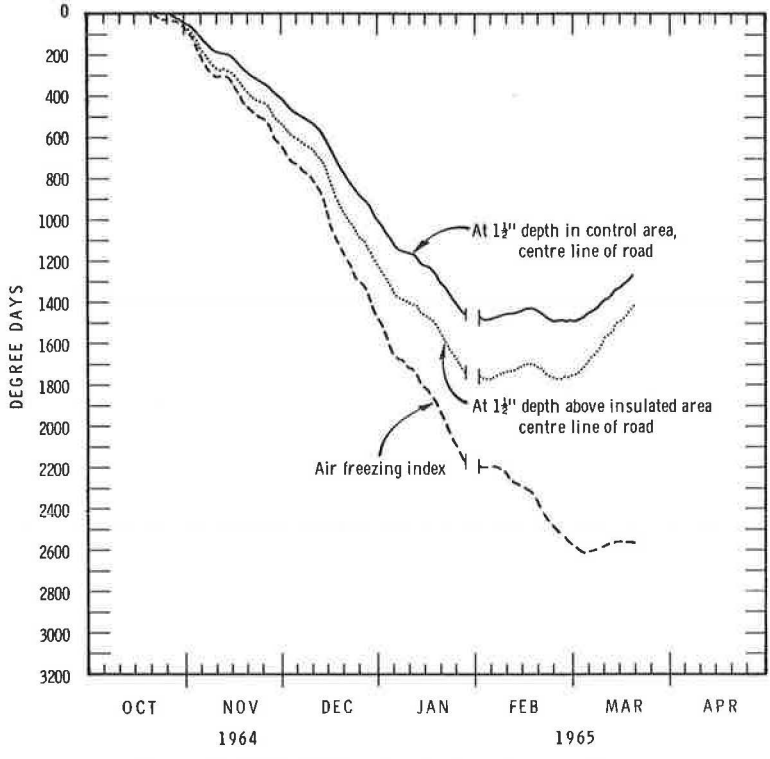

Figure 8. 1964-65 freezing index, Antwerp Street.

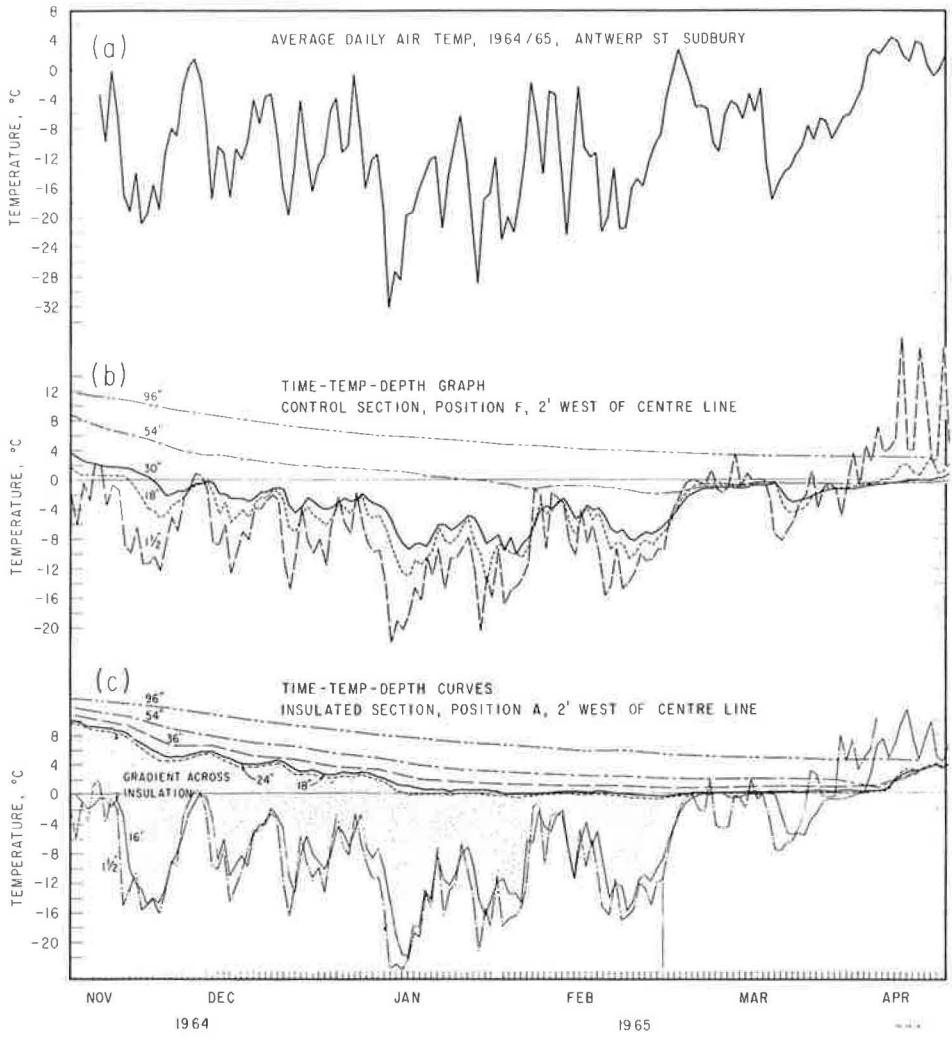

Figure 9. Air and ground temperatures on Antwerp Street.

When the soil and air temperature records were started, on November 16, 1964, all the material above the insulation was frozen. The 0-deg C isotherm did not reach the 18-in. level in the control area until the end of November.

Thermal response of the base-course materials to air temperature was much more rapid above the insulation than at similar depths in the control section. This particular feature is shown by the small differences between the temperature at 1½ in. and 16 in. The differences were usually much greater in the control area (Fig. 9b).

The frostline, based on the depth of the 0-deg C isotherm, was below the insulation for 80 days at position A, 2 ft west of centerline. The maximum penetration—12 in. below the insulation—was on March 2, 1965 (Fig. 10a). The minimum temperature just beneath the insulation at this position was -0.9 C on February 28, 1965. The average temperatures were +0.8 C during January, -0.45 C during February, and -0.15 C during March. At the top of the natural subgrade soil the minimum temperature was -0.4 C.

At position B, 12 ft west of centerline (3 ft from the west edge of the insulation), the period of frost penetration was 65 days (Fig. 10b). The maximum penetration was 9 in. at this position on March 2, 1965. The minimum temperature just beneath the insulation at this point was -0.3 C on March 2, 1965. The average temperature at this point during February and March was about 0 C.

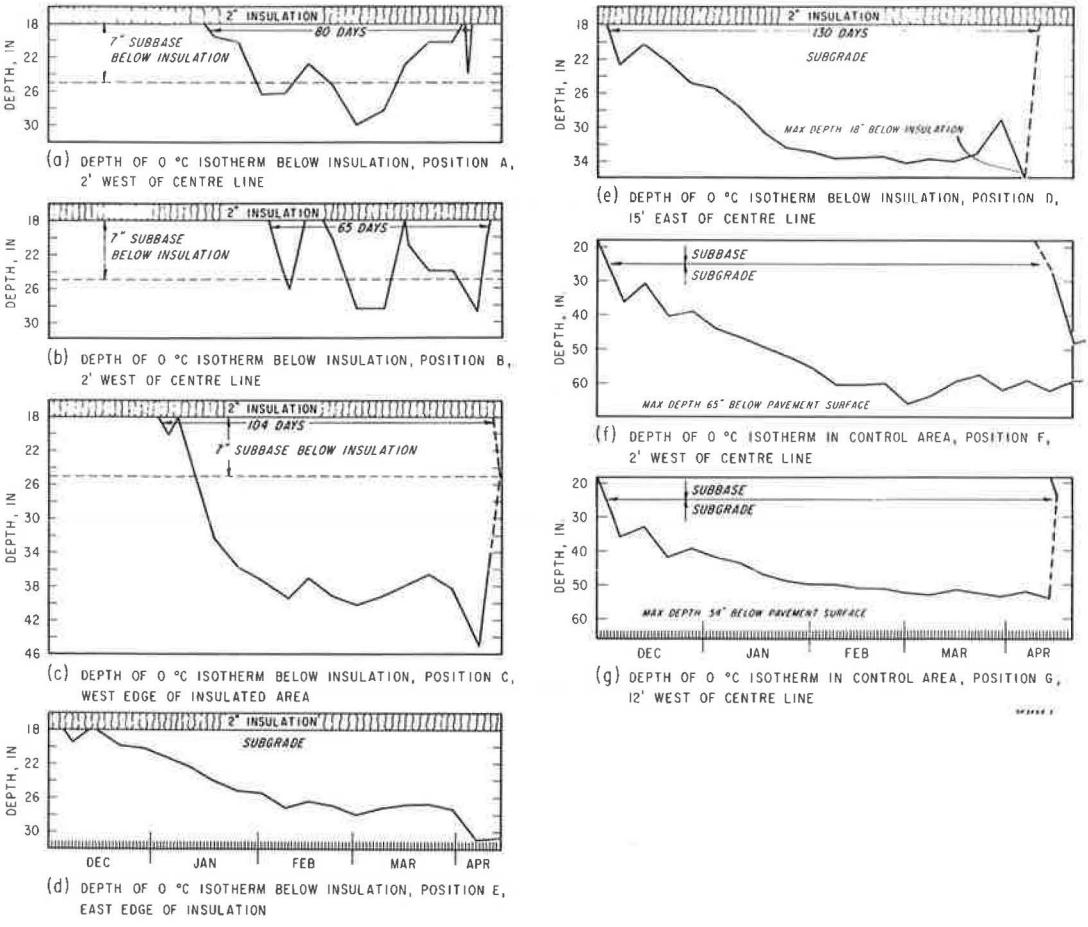

Figure 10. Frost penetration on Antwerp Street.

Directly below the west edge of the insulation (position C), the period of freezing below the insulation was 104 days and the maximum frost penetration was 27 in. (Fig. 10c).

For the east half of the street the insulation was placed directly on the subgrade; the thermocouple positions in this area were D and E. At position D (which is at the curbline on the east side, 5 ft in from the east edge of the insulation) the period of frost penetration below the insulation was over a longer period and to a greater depth than at a comparable position on the west side (Figs. 10b and 10e). This aspect is discussed in detail later in this paper.

The depths of the 0-deg C isotherm for the two positions in the control section are given in Figures 10f and 10g. The minimum temperature at the 18-in. depth was -14 C on January 30, 1965. The minimum temperature at the 30-in. depth was -10 C on February 4, 1965. The maximum frost penetration at this point was 65 in.

Comparison of Frost-Depth Gages with Zero Isotherms

Figure 11a gives the comparison of frostline depth as a function of time between gage measurements and those estimated from temperature gradients. The comparison is favorable in the control area as long as the frostline was actively penetrating downwards. In the insulated areas the gages indicated a greater penetration (average of 5.5 in.) than did temperature measurements when the frostline was in the vicinity of the insulation. This is perhaps not unexpected since the thermal conductivity of the plastic gage is much greater than that of the insulation.

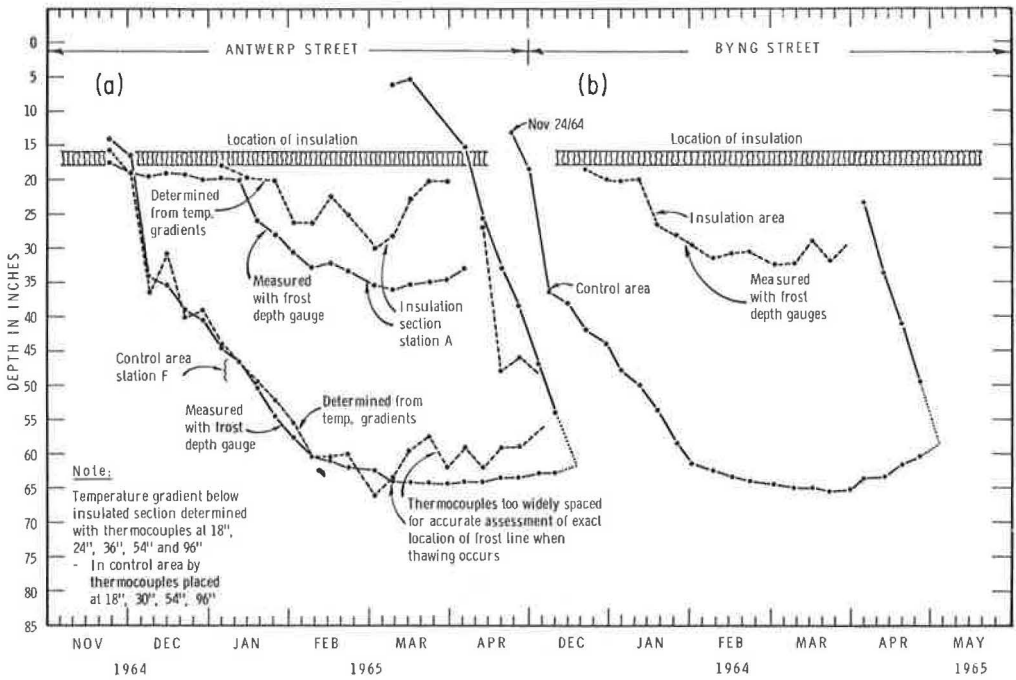

Figure 11. Frost depth determinations with frost-depth gages and temperature measurements.

There was also poor agreement toward the end of the freezing period when the frost-line was receding in the control area. A part of the disagreement results from estimating the freezing plane from widely spaced thermocouples, particularly when thawing was occurring both from the top and the bottom of the frozen layer. During the active thawing period the frozen layer was too close to zero degrees to estimate accurately the location of the freezing plane from temperature gradients.

Frost penetration as measured by frost-depth gages on Byng Street is shown in Fig. 11b. The depth of freezing was about the same (65 in.) as on Antwerp Street in the control area. The frost penetration curve beneath the insulation shows a trend similar to that at the Antwerp Street location. No temperature measurements were carried out at this site, but consideration of the difference between the gage and thermocouple frost depths indicates that the actual frost penetration was about 27 in. (9 in. below the insulation).

Frost Heave Measurements

Figure 12 gives the results of surface elevation measurements on Antwerp Street. The first measurements (January 21) showed some settlement in the insulated area. By this date the control area had heaved a maximum of 0.3 ft in one spot, but in general the heave was less than 0.2 ft. By February 20, 7 in. of frost penetration had occurred beneath the insulation at the centerline. The west side (with the additional 7 in. of subbase beneath the insulation) showed no heaving; the east side (without the additional subbase) had heaved 0.1 ft, and at a position 2 ft off centerline it was slightly less. As shown, additional heaving occurred in March but by April 12 the pavement in the insulated area was back to its original position.

At the Antwerp Street location, heaving was greatest on the east side, where drainage conditions were known to be poor, and least on the west side. The average heave in the insulated area was one-third to one-half of the heave in the areas to the north and south.

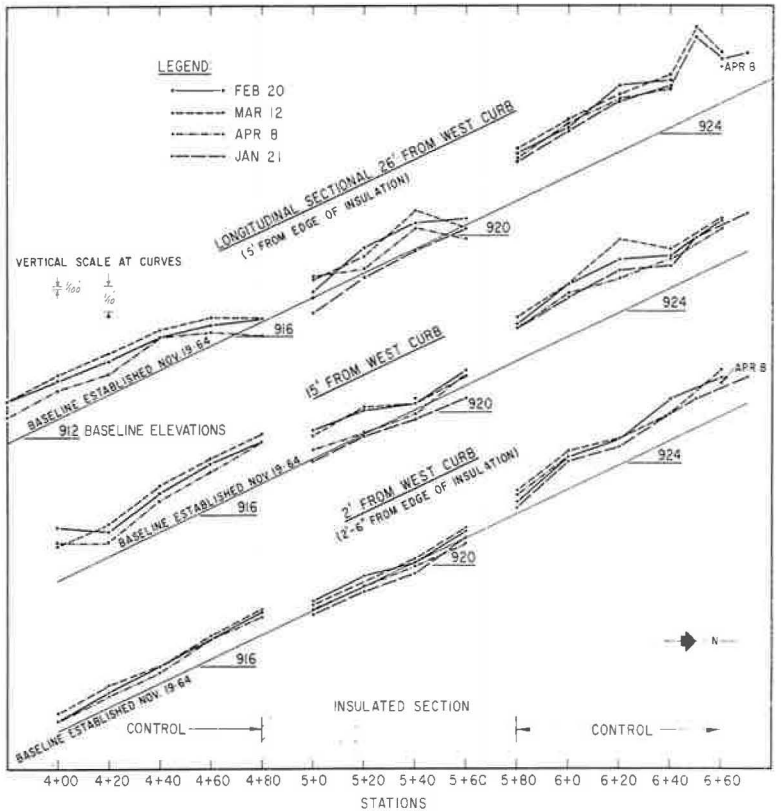

Figure 12. Frost heave measurements on Antwerp Street.

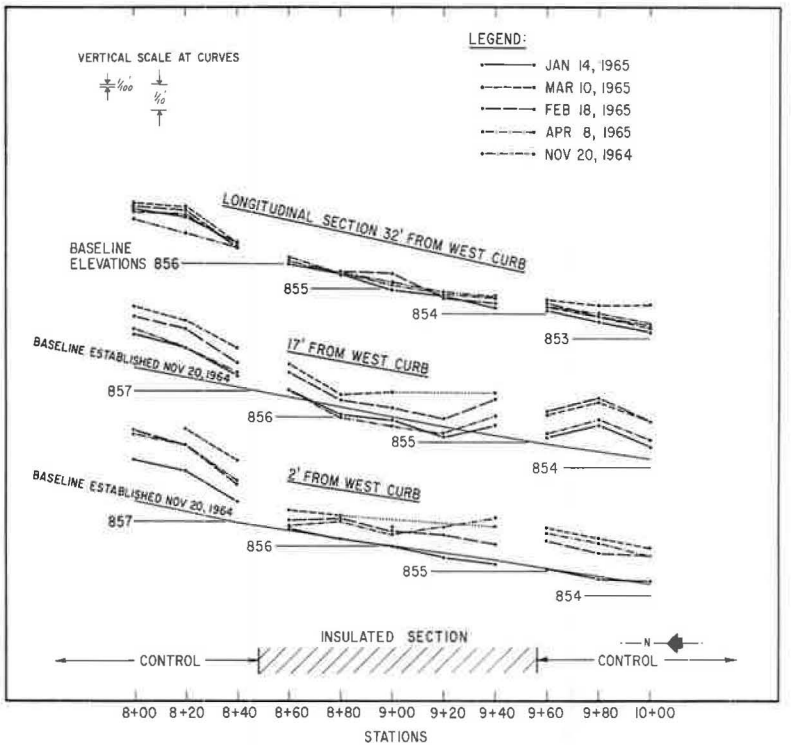

Figure 13. Frost heave measurements on Byng Street.

The heaving pattern was the same on Byng Street (Fig. 13). Heaving was greatest in the central areas beyond the ends of the insulated section and the onset of heaving in the insulated area was consistent with the time of frost penetration of the insulation and the underlying subbase. More heaving occurred on the east side, where drainage conditions were poor, than on the west side. Again, the average heave in the insulated section was about one-half of the heave in the control areas.

Prediction of Frost Penetration Depth

The variable material in the subgrade at both locations reduced the possibility of obtaining meaningful theoretical frost-depth predictions—even for the center of the road where one-dimensional heat flow might be anticipated. It is of interest, however, to compare the frost depth measured in the control section with the design curve for frost penetration obtained by the U. S. Army Corps of Engineers (7) from measurements

TABLE 3

ASSUMED PROPERTIES FOR FROST PENETRATION PREDICTION, ANTWERP STREET
Freezing Index, 1500 and 2600 degree-days F; Freeze Time, 126 days; Mean Annual Temperature, 37 F

Layer	Thickness, d (ft)	Water Content, w (%)	Density, γ_d (lb/cu ft)	Thermal Conductivity, k (BTU/ft-hr-deg F)	Volumetric Heat Capacity, c (BTU/cu ft-deg F)	Latent Heat of Fusion, L (BTU/cu ft)
Asphalt	0.29	0	143	0.84	30.4	0
"A" base	0.25	6.0	135	1.76	29.3	1160
"B" base	1.50	8.0	130	1.90	29.9	1490
Subgrade	—	22.7	102	1.05	34.7	3330

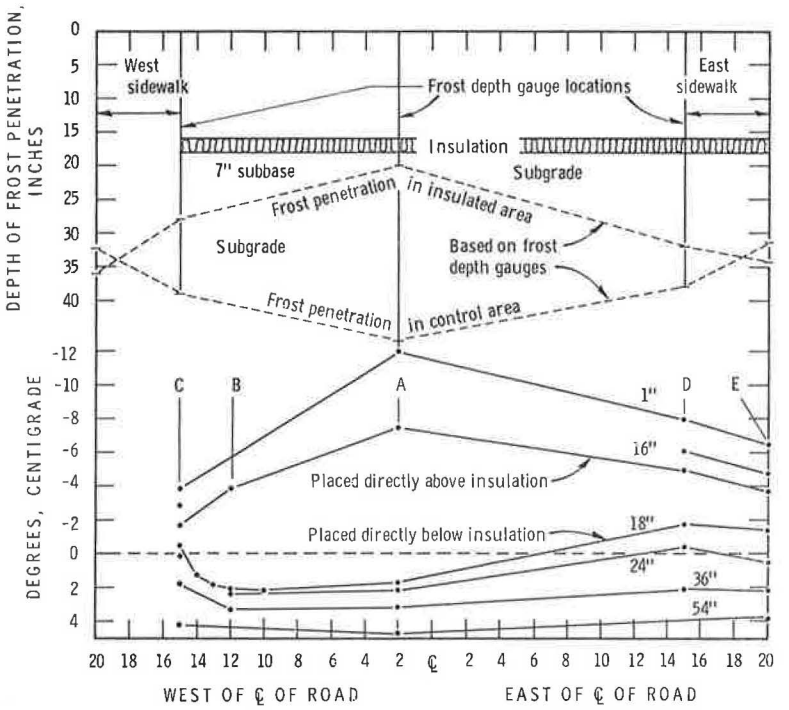

Figure 14. Cross-section of temperature pattern in insulated road section (5+41) and depth of frost penetration in insulated and control section, Antwerp Street, January 12, 1965.

in granular base courses beneath cleared airport runways and by the prediction based on the Modified Berggren Method.

For a 2600 degree-day freezing index (based on air temperature measurements on the Antwerp site) the design curve predicts 65 to 70 in. of frost penetration; the Modified Berggren Method predicts 81 in. (8). This compares favorably with the experimental value of 65 in. in the control area (2 ft west of centerline). For a 1500 degree-day freezing index the Modified Berggren Method predicts a frost penetration of some 63 in. The soil properties used in this calculation are given in Table 3.

Maximum frost penetration 2 ft west of centerline in the insulated area was 30 in. For this type of pavement, depth to insulation, and climatic conditions, 2 in. of this insulation attenuated frost penetration by some 35 in.

Soil Temperature Pattern and Edge Effects

A weekly temperature pattern was plotted for the control section (at Station 6+10) and the insulated section (Station 5+41) on Antwerp Street to follow the thermal changes in the ground. Figure 14 shows such a graph for January 12, 1965. The thermal pattern is not only influenced by the insulation but obviously also by snow-clearing practices. The east side of the roadway was also more shaded than the west side. These factors, in addition to the variability of the subgrade, ruled out the possibility of making meaningful comparisons between the thermal edge effects observed with theoretically computed values.

One anomaly was the earlier and deeper frost penetration of the insulation 15 ft east of center (location D) than at location B, 12 ft west of centerline. Figure 14 shows the temperature at 18 in. (directly below the insulation) to be above freezing at A (2 ft west of centerline) and at B (3 ft from the west edge of the insulation), but -1.8 C at D, which was 5 ft from the east edge of the insulation. Temperature distributions of this type persisted during the entire winter but were most marked during the period when the frostline was actively progressing downward. At the time of maximum frost penetration the frostline was 4 in. deeper at D than at A. This was not a temperature measurement error because the methylene blue frost-depth gages also showed a similar trend as can be observed from Figure 14. Based on temperature measurements, the period when freezing occurred beneath the insulation was about 130 days at D and only about 65 days at B.

During construction it was noted that the drainage was poor on the east side and, following a heavy rain during construction, the desired compaction was difficult to obtain. The poor compaction resulted in greater pavement deflections as will be shown later. The subbase and subgrade materials were sampled for moisture content immediately after thawing at locations A and D. The subbase at the center of the road had an average moisture content of 6 percent. At D the subbase was completely saturated, as water was seen to rise in boreholes above the depth of the insulation.

Because the thermal conductivity of soils increases with moisture content, the differences noted in the cooling rate between the center of the road and the east side might be attributed in part to the influence that moisture content has on heat conduction. It was deemed desirable, however, to inspect the insulation and to measure its moisture content and thermal conductivity. A 2-ft-wide trench was excavated from the centerline to the east edge of the insulation in early June and samples of the insulation were removed from the center and east side of the installation near the position of the thermocouples at Station 5+41. In the area where poor compaction was obtained beneath the insulation some of the panels had hairline cracks which were attributed to poor subgrade support.

Evaluation of Antwerp Street Insulation After Nine Months' Service

Two samples, approximately 14 in. square, were taken from two insulation panels near the center of the road (location A), and two more were taken between locations D and E which were in the "wet" zone. The samples were sealed in polyethylene bags for transportation and for the thermal tests.

Thermal conductivities were determined on a guarded hot plate apparatus 12 in. square at a mean temperature of 75 F and at a temperature difference of 40 deg.

The measured average K value of panels 1 and 2 near the center of the road was 0.23 (BTU-in.)/(sq ft/hr/deg F). The samples were then reversed with respect to hot and cold sides and the conductivity values were redetermined. The measured K was 0.23. Since stone indentations made a somewhat unsatisfactory thermal contact with the plate, the outside portions of the insulation were shaved off to leave a 1-in. thickness of insulation. This was oven-dried to constant weight and its K value in the dry state was determined to be 0.24. The moisture content of panel 1 was 22.8 percent by weight or 0.77 percent by volume. Its measured dry density was 2.1 lb/cu ft. The moisture content of panel 2 was 11.6 percent by weight, 0.43 percent by volume and its density was 2.28 lb/cu ft.

Panels 3 and 4 from the wet area (east side) had an average thermal conductivity of 0.25 before drying. The average moisture content of panel 3 was 4.7 percent by weight and 0.16 percent by volume when tested in the wet state. The center 1½-in. layer had a moisture content of 2.63 percent by weight (0.092 percent by volume). It is concluded that the unusual heat flow pattern observed on the east side of Antwerp Street was not due to any change in the thermal conductivity of the insulation.

Benkelman Beam Rebound Measurements

Deflection measurements by the Ontario Department of Highways were made 6 to 8 ft in from the curb at intervals on both the control and insulated sections under 9000-lb dual loads. The deflection for the particular section given in Table 4 is an average of five. This information is also shown in Figure 15.

The deflections were greater for the insulated sections at both locations. At Antwerp Street the greater deflections on the east side for both control and insulated areas are considered to be the result of poor subgrade support and inadequate drainage. On the west side the deflections of the insulated section were 0.005 to 0.010 in. greater than the deflections of the control section. The mean fall deflection of 0.035 in. is considered quite tolerable for this street. There was also an additional 6 in. of subbase on the west side.

At the Byng Street location the increased deflection of the insulated section is considered to be the result of two factors.

One, the pavement surface is 2 in. of asphaltic concrete. This relatively thin surface may not be adequate to distribute the loads to an acceptable amount at the depth of the insulation.

TABLE 4

AVERAGE BENKELMAN BEAM DEFLECTIONS, INCHES

Date	Antwerp Street				Byng Street			
	Insulated		Control		Insulated		Control	
	East	West	East	West	East	West	East	West
April 22, 1965	0.079	0.043	0.052	0.042	0.095	0.072	0.039	0.040
May 19, 1965	0.055	0.041	0.051	0.036	0.078	0.052	0.025	0.034
June 3, 1965	0.046	0.032	0.051	0.036	—	—	—	—
June 17, 1965	0.050	0.036	0.042	0.028	0.064	0.047	0.022	0.024
June 30, 1965	0.048	0.040	0.041	0.028	0.062	0.047	0.021	0.023
July 14, 1965	0.047	0.035	0.043	0.028	0.064	0.066	0.020	0.044
July 27, 1965	0.049	0.038	0.037	0.029	0.066	0.042	0.021	0.024
August 12, 1965	0.043	0.031	0.028	0.022	0.055	0.050	0.019	0.020
August 24, 1965	0.043	0.033	0.034	0.022	0.058	0.050	0.019	0.020

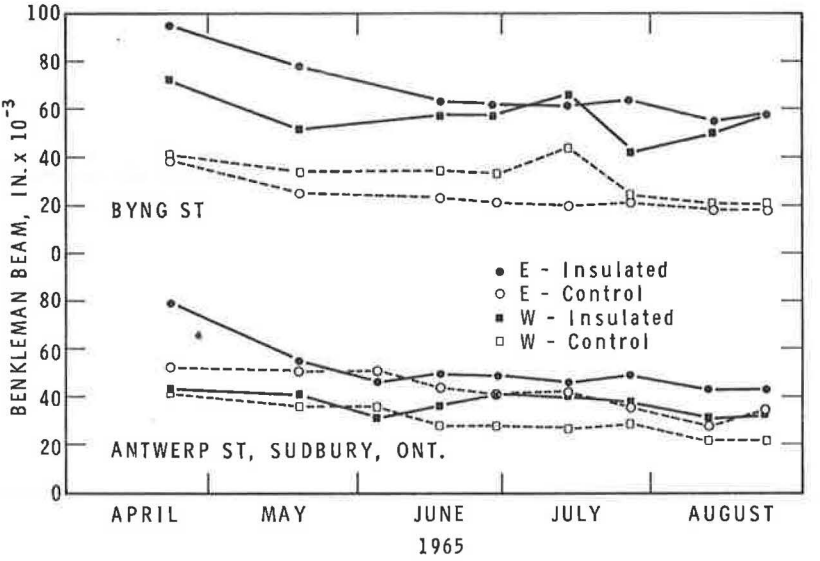

Figure 15. Benkelman beam deflections on Antwerp and Byng Streets.

Two, the frost penetration into the upper 9 in. of the subgrade soil has been slow enough to create a large amount of ice lensing (0.10-ft surface heave for 9 in. frost penetration, compared with 0.24-ft surface heave for 40 in. frost penetration into the subgrade in the control section, based on frost-depth gage measurements).

These ice layers subsequently released a large amount of moisture into the subgrade soil at the end of freezing which would lower the bearing capacity of the normally weak subgrade. Furthermore, the smaller slope on this street attenuated drainage of this excess moisture. This factor is considered to be the most significant and is most probably the cause of the large deflections of the insulated section on Byng Street.

Minimum rebound values in the fall of the year were estimated at 20 to 30 for the control sections at both streets. For the insulated sections, 40 and 50 are estimated for Antwerp and Byng Streets, respectively.

CONCLUSIONS

For the conditions at Sudbury, Ontario, 2 in. of the particular insulation used attenuated 35 in. of frost penetration during a winter when the air freezing index approached the design value. This insulating layer also reduced the amount of heave by one-half to two-thirds of that measured in an uninsulated pavement.

Poor drainage conditions at the east side of the installations caused greater frost penetration, large pavement deflections in the Benkelman beam test, and eliminated the possibility of obtaining meaningful results on thermal effects at the edge of the insulation.

The methylene-blue frost-depth gages are accurate in uninsulated sections. In insulated sections the gage predicts frost penetrations that are too large.

The thermal properties of the insulation were unaffected by 9 months' exposure to severe moisture conditions.

Benkelman beam deflection tests showed that the insulated sections had somewhat larger deflections. Where the asphaltic concrete surface was $3\frac{1}{2}$ in. the deflections in the insulated section were 0.005 to 0.010 in. more than deflections of the control section. The estimated mean fall rebound values in the insulated area (0.040 to 0.050 in.) are considered tolerable. On Byng Street the large rebound values in the insulated section are considered a result of the relatively large amount of ice lens formation in the top of the subgrade and the thin (2 in.) asphaltic concrete surface.

ACKNOWLEDGMENTS

The authors wish to express their appreciation to the Ontario Department of Highways for carrying out the Benkelman beam measurements. This paper is a joint contribution from The Dow Chemical Company, Midland, Michigan; the City of Sudbury; and the Division of Building Research, National Research Council, Canada.

REFERENCES

1. Skaven-Haug, Sv. Protection Against Frost Heaving on the Norwegian Railroads. Géotechnique, Vol. 9, No. 3, pp. 87-106, 1959.
2. Oosterbaan, M. D., and Leonards, G. A. Use of an Insulating Layer to Attenuate Frost Action in Highway Pavements. Highway Research Record 101, pp. 11-27, 1965.
3. Young, F. D. Experimental Foamed Plastic Base Course. Highway Research Record 101, pp. 1-10, 1965.
4. Quinn, W. F., and Lobacz, E. F. Frost Penetration Beneath Concrete Slabs Maintained Free of Snow and Ice, With and Without Insulation. Highway Research Board Bull. 331, pp. 98-115, 1962.
5. Gandahl, R. Bestämning av Tjälgräns—I Mark Med Enkel Typ av Tjälgransmätare. Statens Vaginstitut, Report 30, Stockholm, 1957.
6. Linell, K. A., Hennion, F. B., and Lobacz, E. F. Corps of Engineers' Pavement Design—Areas of Seasonal Frost. Highway Research Record 33, pp. 76-128, 1963.
7. Corps of Engineers, U. S. Army. Addendum No. 1, 1945-47, to Report on Frost Penetration, 1944-45. Corps of Engineers, U. S. Army, New England Division, Boston, 1949.
8. Sanger, F. J. Degree-Days and Heat Conduction in Soils. Presented at International Conference on Permafrost, Purdue University, Nov. 1963.

An Experimental Study of Subpressure in a Freezing Soil System

R. N. S. RAO, Professor of Civil Engineering, Prairie View A&M College of Texas

ABRIDGMENT

•IN MOST regions of the modern world, the frost problem is a factor of major concern to all. The attempts to solve this problem have resulted in many studies to understand the exact nature of frost development in soils. The present paper discusses one aspect of this problem, namely the subpressure developed and its relationship to the causes of frost problems.

The fundamental laws of hydrodynamics indicate that the moisture-migration in the upward direction against gravity in a porous medium is feasible only if there is some form of pressure drop in the direction of flow. In nature, the groundwater table is at atmospheric pressure. In freezing soil, therefore, the absolute pressure in the frozen zone above the groundwater table should be less than atmospheric pressure for upward moisture migration to be feasible. The author is of the opinion that this pressure drop is due to temperature drop. The deviation from this simple cause is due to other side effects such as surface atmospheric pressure.

Factors Affecting Subpressure

The factors influencing pressure conditions in a freezing soil are many, such as porosity of the soil, particle size, shape of particle, intensity of cold spell, deviation of cold spell, and depth of the groundwater table. Any analytical method of evaluation would be quite tedious, if not impossible. The strain and effort involved in such an evaluation would not be commensurate with the problem. The more direct experimental approach is quicker and more dependable in such situations of random variables; therefore, the study undertaken used the experimental method.

In this study the soil freezing system has been considered mainly as a porous medium subject to a freezing thermal gradient. The moisture movement is a secondary effect, although it is the immediate cause of frost heave and breaking up of pavements. The study involved experimental freezing of soil samples in the laboratory under controlled conditions where variation of several influencing factors was possible.

A series of soil freezing experiments was conducted at the Frost Action Research Laboratory of Rutgers University. The material presented in this paper is based on these experiments. The experiments simulated the conditions of natural soil freezing in New Jersey. The particular case selected, since it focused the main points of the study, was one where water exists at a fixed depth from the ground surface at a constant nonfreezing temperature. The study is limited to one type of highly frost-susceptible silty soil, Penn Soil. Figure 1 is a diagram of the instrumented soil sample used in these experiments. Details on the experimental procedure and data are given elsewhere (1).

Relationship Between Influencing Factors and Subpressure

The study correlated the observed phenomenon of induced subpressure in freezing soil to one of the main physical properties of the soil, porosity (which in a way represents other physical properties such as pore size and specific surface) and the freezing

Paper sponsored by Committee on Frost Action and presented at the 45th Annual Meeting.

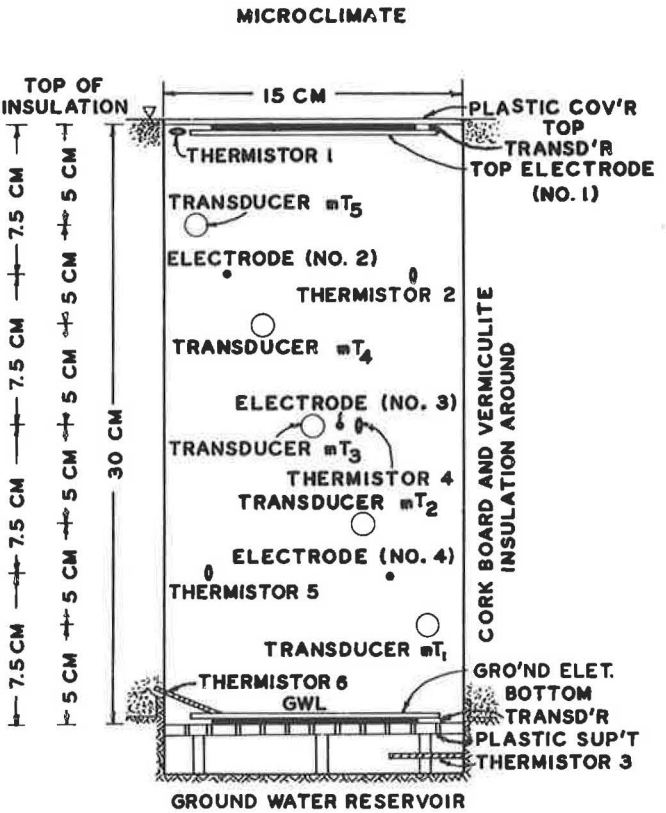

Figure 1. Instrumented soil sample.

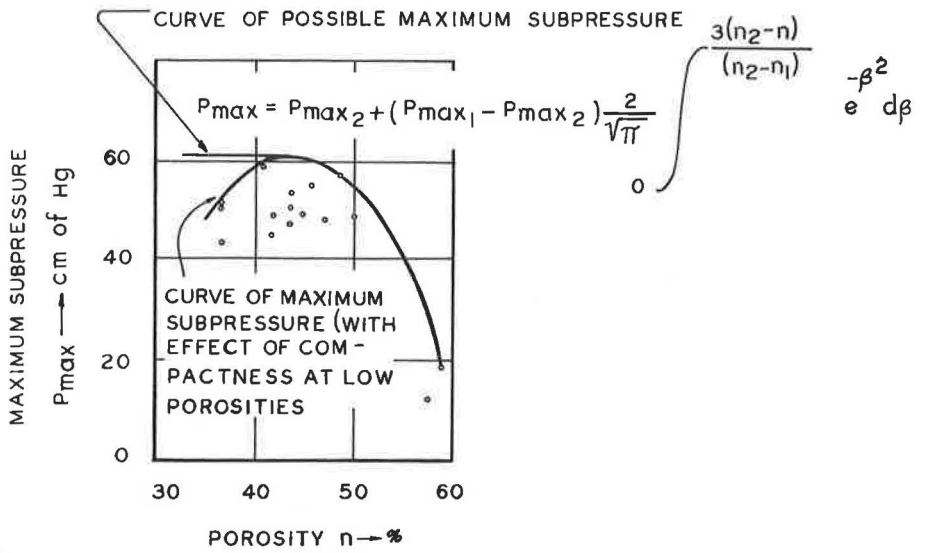

Figure 2. Maximum subpressure as a function of porosity.

thermal gradient, the chief cause which triggers the whole freezing moisture-migration process. The effect of the time element involving the development of the subpressure in an unsteady state of thermal condition was recognized. The findings show the relationships between the following factors: (a) the maximum induced subpressure and porosity of the soil; (b) the maximum subpressure and frost depth; (c) the maximum subpressure and the surface subfreezing temperature; (d) the maximum subpressure and the freezing thermal gradient; and (e) the subpressure at a point and depth (subpressure profile). A combined empirical equation for the maximum induced subpressure as a function of all the above influencing factors is also evolved which is a combination of the individual relationships developed.

Notation

p_{max_1}, p_{max_2}, p_{max} = maximum induced subpressure in freezing soil of porosities n_1, n_2, and n;
β = arbitrary variable of integration;
p_m = subpressure induced at the frost boundary;
h = depth of groundwater table from the ground surface;
ξ, ξ_0 = frost depth and optimum frost depth;
m_1, m_2, a_2, b_2, c_2, k_1, k_2 = constants;
T_S = ground surface subfreezing temperature; and
p = induced subpressure in the freezing soil layer at a depth z from the ground surface and above groundwater table.

Subpressure and Porosity of the Soil

In a given type of soil, the maximum induced subpressure under any subfreezing thermal gradient depends on the porosity of the soil. In a practical experimental range of porosity, the experimental results indicate that the maximum induced subpressure decreases with increasing porosity. The pattern of the decaying curve conforms to the curve represented by Gauss' error function, which is given by

$$p_{max} = p_{max_2} + \left(p_{max_1} - p_{max_2}\right) \frac{z}{\sqrt{\pi}} \int_0^{\frac{3(n_2 - n)}{(n_2 - n_1)}} e^{-\beta^2} d\beta \qquad (1)$$

This relationship is illustrated in Figure 2. The curve gets modified according to the range of limits of error function chosen in any particular case.

Subpressure and Frost Depth

The next area studied relates to the relationship between the maximum induced subpressure and the frost depth. The maximum induced subpressure in a freezing soil depends on the frost depth. The experimental results indicate that the maximum subpressure increases rapidly with the increase in frost depth, starting from zero at the ground surface. It reaches a maximum value at the optimum frost depth, which is usually a little closer to the ground surface than to the groundwater table. The optimum frost depth is defined as the frost depth at which the induced subpressure profile is maximum for a given soil of a given porosity. Thereafter it will begin to decrease with further increase in the frost depth, reaching zero value when the frost depth reaches the groundwater table. Both the increasing subpressure from the ground surface to the optimum frost depth and the decreasing subpressure from optimum frost depth to the groundwater table vary parabolically with depth but at different rates. The maximum subpressure at any porosity as indicated by Eq. 1 corresponds to the peak value of the subpressure profile at optimum frost depth. The peak value of the subpressure at any frost depth is given by

$$p_m = p_{max}\left[1 - \left(1 - \frac{\xi}{\xi_0}\right)^{m_1}\right] \tag{2}$$

for frost depth ξ less than optimum frost depth ξ_0, and for frost depth ξ greater than the optimum frost depth ξ_0,

$$p_m = p_{max}\left[1 - \left(\frac{\xi - \xi_0}{h - \xi_0}\right)^{m_2}\right] \tag{3}$$

These relationships are illustrated in Figure 3. The dotted line in the figure indicates the theoretical case of frost depth approaching the groundwater table of constant nonfreezing temperature.

Subpressure, Freezing Thermal Gradient, and Frost Depth

The study also included the correlation of the maximum induced subpressure to the freezing ground surface temperature and freezing thermal gradient. The experimental evidence indicated the following relationship between the surface subfreezing temperature T_S and the maximum frost depth ξ that it can induce in the given soil

$$\xi = a_2 T_S^2 + b_2 T_S + c_2 \tag{4}$$

The maximum induced subpressure p_m can now be expressed as a function of porosity of the soil (n) and the surface subfreezing temperature T_S by combining Eqs. 1, 2 and 4 or 1, 3 and 4 as the case may be, depending on whether the frost depth ξ is less than or greater than the optimum frost depth ξ_0. The expression will be

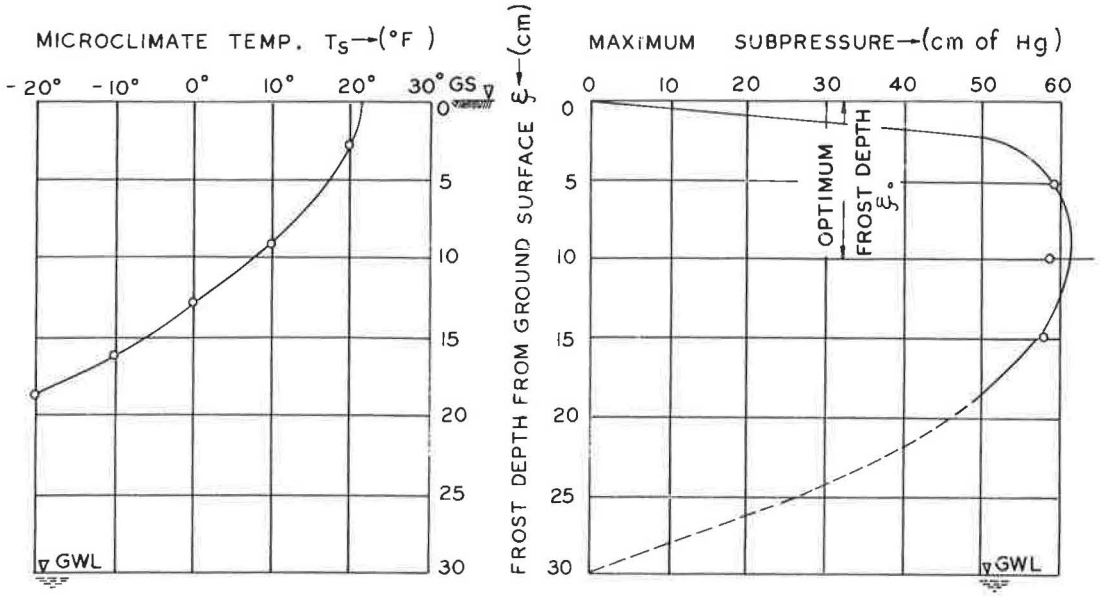

Figure 3. Relationship between maximum subpressure, frost depth, and microclimate temperature for Penn Soil (prosity 4%).

$$p_m = \left[p_{max_2} + \left(p_{max_1} - p_{max_2} \right) \frac{2}{\sqrt{\pi}} \int_0^{\frac{3(n_2 - n)}{(n_2 - n_1)}} e^{-\beta^2} d\beta \right] \left[1 - \left(1 - \frac{a_2 T_S^2 + b_2 T_S + c_2}{\xi_0} \right)^{m_1} \right] \quad (5)$$

$$p_m = \left[p_{max_2} + \left(p_{max_1} - p_{max_2} \right) \frac{2}{\sqrt{\pi}} \int_0^{\frac{3(n_2 - n)}{(n_2 - n_1)}} e^{-\beta^2} d\beta \right] \left[1 - \left(\frac{a_2 T_S^2 + b_2 T_S + c_2 - \xi_0}{h - \xi_0} \right)^{m_2} \right] \quad (6)$$

Subpressure Profile

The foregoing discussion relates to the maximum induced subpressure (p_m) in a given soil of known porosity (n) under a given freezing surface temperature T_S. However, at any instant the subpressure in the soil layer varies between ground surface and the groundwater table (both are at atmospheric pressure). It is observed that the maximum subpressure (p_m) always occurs at the frost boundary. This is consistent with the theoretical reasoning based on the concept of the varying internal energy of

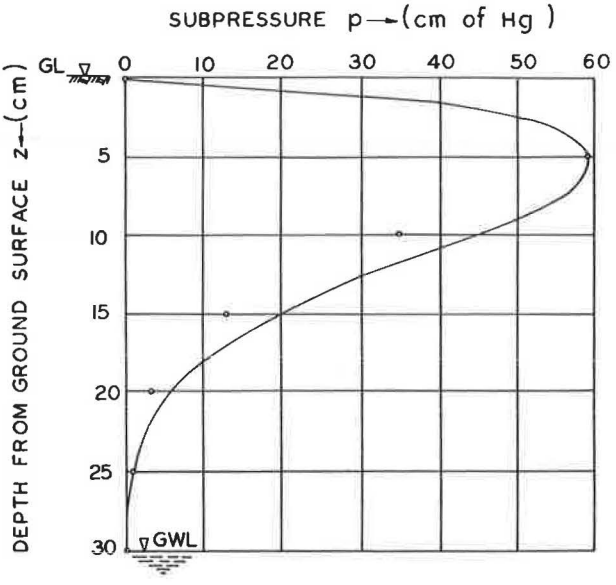

Figure 4. Subpressure profile in freezing Penn Soil (porosity 42%, frost depth 5 cm).

soil moisture at varying temperature from the ground surface to the groundwater table. The subpressure profile resembles a skew frequency distribution curve. The subpressure at any depth as a function of depth of soil layer z can be expressed as

$$p = p_m \left(\frac{z}{\xi}\right)^{k_1} \left(1 - \frac{z - \xi}{h - \xi}\right)^{k_2} \tag{7}$$

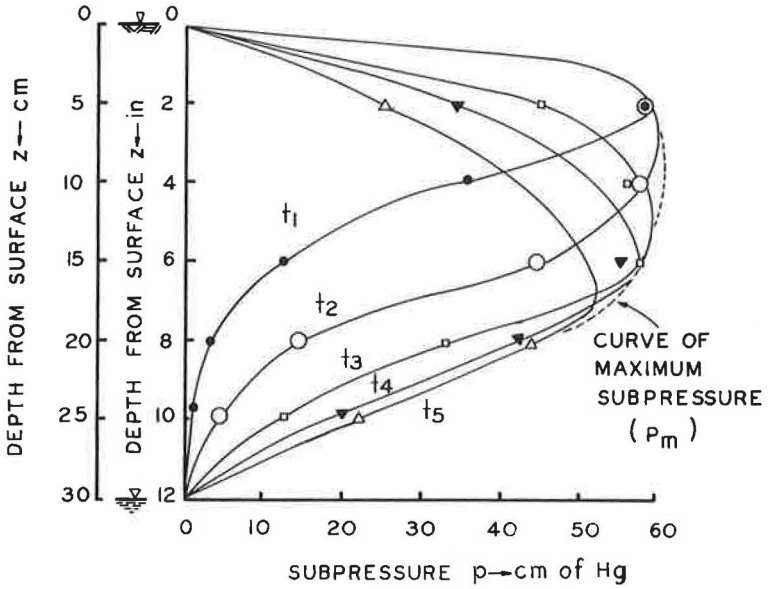

Figure 5. Subpressure profiles in the freezing soil system at different intervals of time after start of cold spell (Penn Soil, porosity 42%).

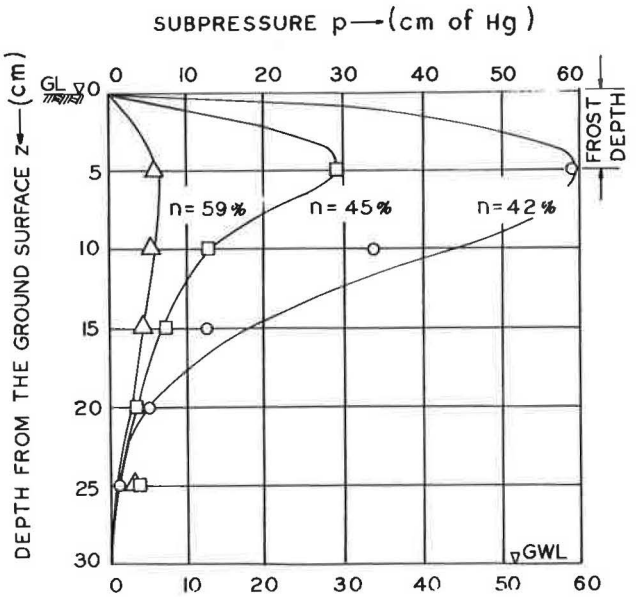

Figure 6. Subpressure profile in Penn Soil (frost depth 5 cm; different porosities).

This is illustrated in Figure 4. Figure 5 shows the relationship of subpressure profile and p_m curve. The variation of subpressure profile for the same frost depth and for the same soil but under different porosities is illustrated in Figure 6. The subpressure p can be expressed as a function of T_s and n only by substituting the values of p_m and ξ in Eq. 7 from Eqs. 4, 5, and 6.

Application and Limitations of the Study

The study presented in this paper has its limitations. It has only indicated the pattern of relationship. Extensive experimental data are necessary to get a practical set of quantitative charts and equations, since many of the constants in the equations presented in this paper have to be obtained from such experimentation.

There is also room for broadening the scope of the study by extending the problem into the quality of water and the pattern of the cold spell. The charts and graphs thus developed could readily be used by practicing engineers.

ACKNOWLEDGMENT

This paper is based on the Ph. D. thesis that the author submitted to Rutgers University in 1964. The author wishes to acknowledge the help he received from his major advisor, Dr. A. R. Jumikis, and the other faculty members at Rutgers in conducting this study.

REFERENCES

1. Rao, R. N. S. An Experimental Study of Subpressure in a Freezing Soil System. Thesis, Rutgers Univ., 1964.
2. Highway Research Board. Frost Action in Soils. HRB Bibliography 3, Washington, 1948.
3. Briggs, L. G. The Mechanics of Soil Moisture. Bulletin No. 10, U. S. Dept. of Agriculture, Soils Division, Washington, 1897.
4. Jumikis, A. R. Suction Force in Soils upon Freezing. ASCE Proc., June 1954.
5. Jumikis, A. R. Experimental Studies on Moisture Transfer in a Silty Soil Upon Freezing as a Function of Its Porosity. Rutgers University (Mimeographed), New Brunswick, 1963.

Physical Properties of Granular Materials with Reference to Thermal Resistivity

OMAR T. FAROUKI, Assistant Professor, San Jose State College

Various approaches to the engineering aspects of the problem of thermal resistivity of backfill materials for underground power cable systems are described. A study is made of the effect on the thermal resistivity of the percentage and the nature of binder added to a Rothfuchs graded granular skeleton of quartzitic sand and gravel. Addition of kaolinite in percentages up to 16 percent shows that the optimum amount is in the vicinity of 8 percent. The use of calcium carbonate, fly ash, lime and lime-fly ash as binders in an amount of 8 percent shows that the nature of the binder has little effect on the thermal resistivity of the cemented backfill material in the nearly dry state, as the value of this resistivity is controlled chiefly by the oriented water films. However, the nature of the binder becomes important as its amount increases to 16 percent and more.

The compressive strength of a nearly dry cemented backfill material containing 8 percent binder is found by experiment to increase linearly with its thermal conductivity, provided the binder does not react chemically with the quartz grains (as lime does). This experimental relation agrees with hypothetical relations derived on the basis of Debye's equation for the thermal conductivity in terms of the speed of sound. The derivation assumes a linear relation between the speed of sound in a generalized cemented granular material and its compressive strength, as has been previously established experimentally in the particular case of concrete.

A study was made of the effect on thermal resistivity of the method by which a given moisture content of a backfill material is attained, whether from the dry side or the wet side. It is shown that a material dried out from the saturated to the air-dry state has a considerably lower thermal resistivity than if it were simply mixed and densified in the air-dry state. When the material dries out, the thermal resistivity increases linearly as the logarithm of the moisture content decreases. However, when moisture is added to the dry material, the thermal conductivity increases linearly as the logarithm of the moisture content increases.

A comprehensive equation for the thermal conductivity of a generalized soil is developed to include the effect of moisture migration in both the film and the vapor phase.

•THE SCIENTIFIC and engineering study presented in this paper was occasioned by the problem faced by the electric power industry of developing economical backfill materials possessing dependable low thermal resistivities even at low moisture contents. The design of a suitable material composition or system of high dependable thermal conductivity or low resistivity involves the determination and selection of the best available constituents and their most effective combination with respect to mineral composition and granulometry. The effective and economical densification of the material with available equipment necessitates a consideration of such mechanical properties as workability and the related property of shear strength. The total engineering and scientific

Paper sponsored by Committee on Physico-Chemical Phenomena in Soils and presented at the 45th Annual Meeting.

problem thus involves practically all the physical properties of such backfill materials and the mutual interrelation of these properties.

The mechanical properties of granular materials were considered in a previous paper by Farouki and Winterkorn (6). The present paper contains a study of the thermal properties and of the relations between thermal and mechanical properties. It also includes the development of a comprehensive equation for the thermal conductivity of a soil, which takes into account the phenomenon of moisture migration.

THERMAL PROPERTIES OF GRANULAR MATERIALS

If a backfill material is to have a good thermal conductivity, it should possess a continuous granular skeleton composed of quartz grains, because quartz is the common rock mineral having the best thermal conductivity. A high density of the material must be easily obtainable, which means that the material should be well-graded. To prevent segregation of the different grain sizes during handling and densification, a small amount of binder, such as clay, should be added. Since this binder usually has a lower intrinsic thermal conductivity than the quartz grains, there is an optimum percentage of binder. Additional amounts would only result in interference with the packing of the granular skeleton, and would therefore cause a decrease in the thermal conductivity. A series of experiments was performed to determine the optimum percentage of binder. Another series of experiments was performed using different binders to determine the effect of the nature of the binder. In both series the binder was added to the same type of granular skeleton which consisted of a quartz granular material made up according to the Rothfuchs (22) gradation to obtain a high density at a good workability.

The thermal conductivity of a granular material with a binder may have different values at the same density and moisture content, depending on whether this moisture content is approached from the saturated or completely dry state (32). Experiments were performed to investigate this phenomenon.

Method of Measuring Thermal Conductivity

The method used to measure the thermal conductivity is the transient method of Stalhane and Pyk (24) which was used by Van Rooyen (26). The essential feature of this method is the thermal probe which contains a heating wire and a thermocouple, and is located in the center of the soil. Readings of the temperature rise of the probe with time are taken, the time being measured from the instant the heating current is on.

The probe used was 6 in. long and 0.035 in. in diameter and contained a copper-constantan thermocouple as well as a constantan heating wire. The material under test was contained in a 6-in. brass cylinder of 4-in. diameter.

TABLE 1

GRAIN-SIZE DISTRIBUTION[a]

Sieve	Percent of Fraction
3/8 in.-No. 4	32.2
No. 4-No. 8	22.7
No. 8-No. 16	16.0
No. 16-No. 30	11.4
No. 30-No. 50	8.0
No. 50-No. 100	5.6
No. 100-No. 200	4.1

[a]Rothfuchs graded granular skeleton of sand and gravel.

Effect of Percentage of Binder on Thermal Conductivity

According to the existing empirical and theoretical formulas which show the effect of the clay content on the thermal conductivity, K, of a granular material, K decreases continuously as the percentage of clay added to the sandy material increases from zero. (See the nomogram of Makowski and Mochlinski (16) which is based on the work of Gemant (7) and Kersten (15).) The empirical formulas derived by Van Rooyen (26) also show a decrease in K as the clay content increases.

To determine the effect of increasing percentages of binder on thermal conductivity, a series of experiments was performed. Kaolinite was used as the binder

$$p_m = p_{max}\left[1 - \left(1 - \frac{\xi}{\xi_0}\right)^{m_1}\right] \tag{2}$$

for frost depth ξ less than optimum frost depth ξ_0, and for frost depth ξ greater than the optimum frost depth ξ_0,

$$p_m = p_{max}\left[1 - \left(\frac{\xi - \xi_0}{h - \xi_0}\right)^{m_2}\right] \tag{3}$$

These relationships are illustrated in Figure 3. The dotted line in the figure indicates the theoretical case of frost depth approaching the groundwater table of constant nonfreezing temperature.

Subpressure, Freezing Thermal Gradient, and Frost Depth

The study also included the correlation of the maximum induced subpressure to the freezing ground surface temperature and freezing thermal gradient. The experimental evidence indicated the following relationship between the surface subfreezing temperature T_S and the maximum frost depth ξ that it can induce in the given soil

$$\xi = a_2 T_S^2 + b_2 T_S + c_2 \tag{4}$$

The maximum induced subpressure p_m can now be expressed as a function of porosity of the soil (n) and the surface subfreezing temperature T_S by combining Eqs. 1, 2 and 4 or 1, 3 and 4 as the case may be, depending on whether the frost depth ξ is less than or greater than the optimum frost depth ξ_0. The expression will be

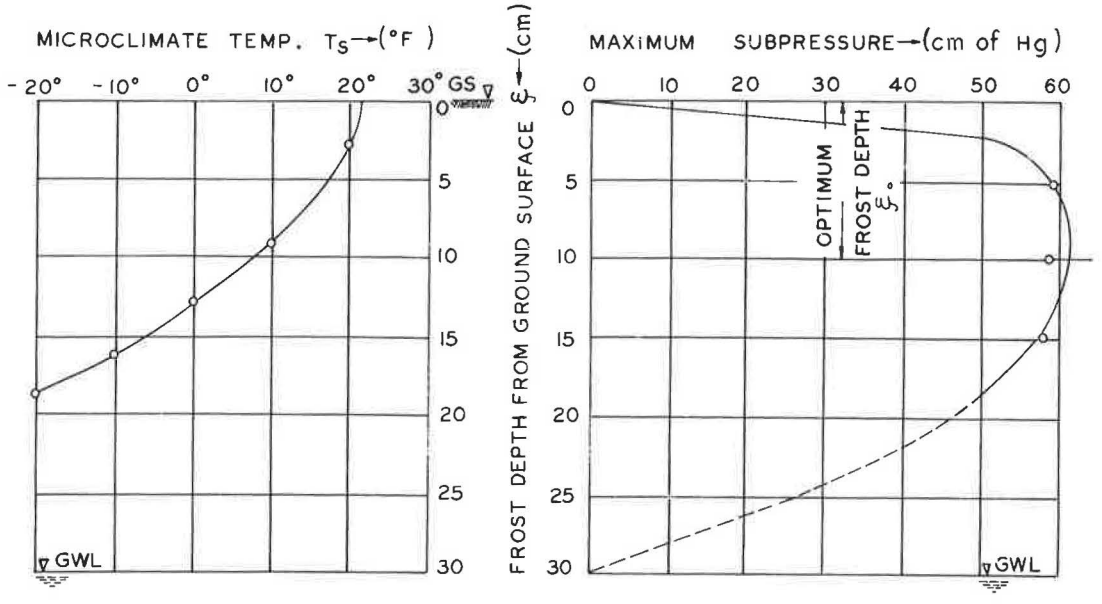

Figure 3. Relationship between maximum subpressure, frost depth, and microclimate temperature for Penn Soil (prosity 4%).

$$p_m = \left[p_{max_2} + \left(p_{max_1} - p_{max_2} \right) \frac{2}{\sqrt{\pi}} \int_0^{\frac{3(n_2 - n)}{(n_2 - n_1)}} e^{-\beta^2} d\beta \right] \left[1 - \left(1 - \frac{a_2 T_S^2 + b_2 T_S + c_2}{\xi_0} \right)^{m_1} \right] \quad (5)$$

$$p_m = \left[p_{max_2} + \left(p_{max_1} - p_{max_2} \right) \frac{2}{\sqrt{\pi}} \int_0^{\frac{3(n_2 - n)}{(n_2 - n_1)}} e^{-\beta^2} d\beta \right] \left[1 - \left(\frac{a_2 T_S^2 + b_2 T_S + c_2 - \xi_0}{h - \xi_0} \right)^{m_2} \right] \quad (6)$$

Subpressure Profile

The foregoing discussion relates to the maximum induced subpressure (p_m) in a given soil of known porosity (n) under a given freezing surface temperature T_S. However, at any instant the subpressure in the soil layer varies between ground surface and the groundwater table (both are at atmospheric pressure). It is observed that the maximum subpressure (p_m) always occurs at the frost boundary. This is consistent with the theoretical reasoning based on the concept of the varying internal energy of

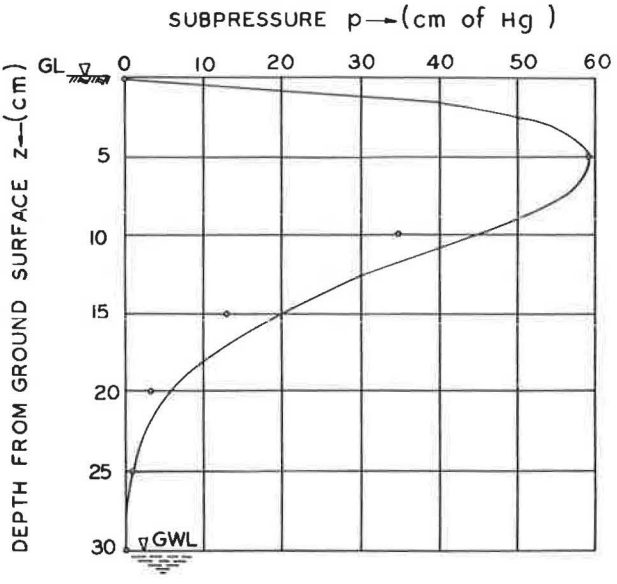

Figure 4. Subpressure profile in freezing Penn Soil (porosity 42%, frost depth 5 cm).

soil moisture at varying temperature from the ground surface to the groundwater table. The subpressure profile resembles a skew frequency distribution curve. The subpressure at any depth as a function of depth of soil layer z can be expressed as

$$p = p_m \left(\frac{z}{\xi}\right)^{k_1} \left(1 - \frac{z - \xi}{h - \xi}\right)^{k_2} \tag{7}$$

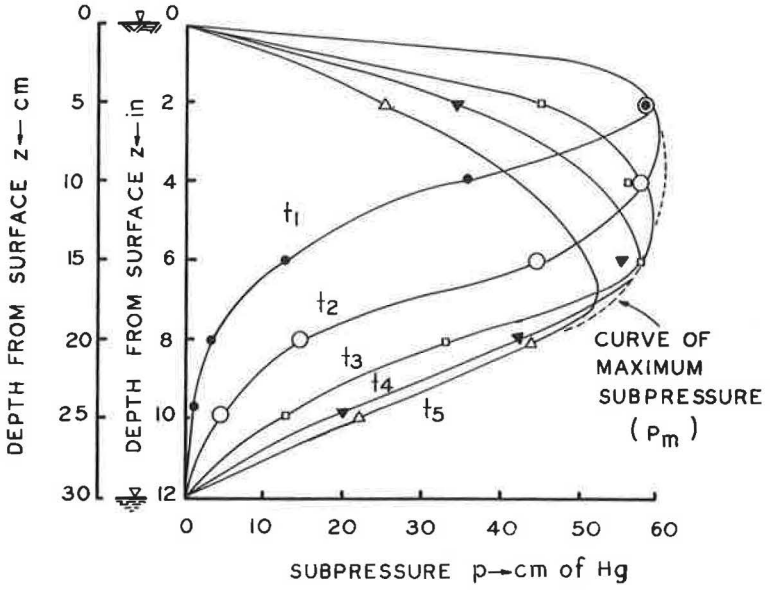

Figure 5. Subpressure profiles in the freezing soil system at different intervals of time after start of cold spell (Penn Soil, porosity 42%).

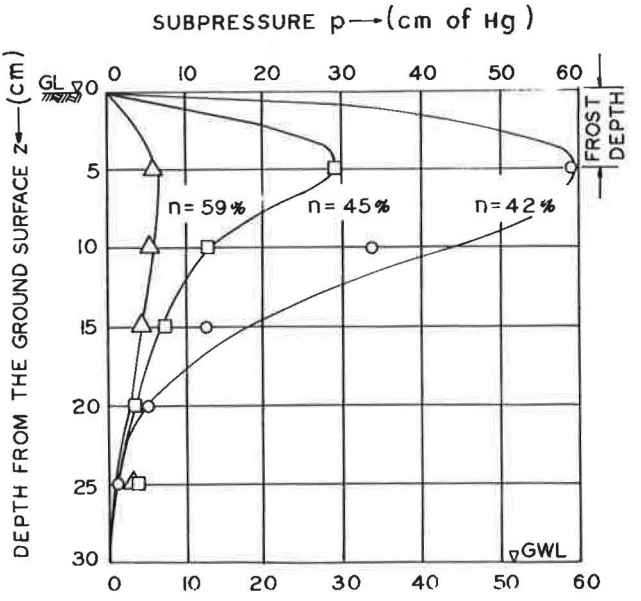

Figure 6. Subpressure profile in Penn Soil (frost depth 5 cm; different porosities).

This is illustrated in Figure 4. Figure 5 shows the relationship of subpressure profile and p_m curve. The variation of subpressure profile for the same frost depth and for the same soil but under different porosities is illustrated in Figure 6. The subpressure p can be expressed as a function of T_s and n only by substituting the values of p_m and ξ in Eq. 7 from Eqs. 4, 5, and 6.

Application and Limitations of the Study

The study presented in this paper has its limitations. It has only indicated the pattern of relationship. Extensive experimental data are necessary to get a practical set of quantitative charts and equations, since many of the constants in the equations presented in this paper have to be obtained from such experimentation.

There is also room for broadening the scope of the study by extending the problem into the quality of water and the pattern of the cold spell. The charts and graphs thus developed could readily be used by practicing engineers.

ACKNOWLEDGMENT

This paper is based on the Ph. D. thesis that the author submitted to Rutgers University in 1964. The author wishes to acknowledge the help he received from his major advisor, Dr. A. R. Jumikis, and the other faculty members at Rutgers in conducting this study.

REFERENCES

1. Rao, R. N. S. An Experimental Study of Subpressure in a Freezing Soil System. Thesis, Rutgers Univ., 1964.
2. Highway Research Board. Frost Action in Soils. HRB Bibliography 3, Washington, 1948.
3. Briggs, L. G. The Mechanics of Soil Moisture. Bulletin No. 10, U. S. Dept. of Agriculture, Soils Division, Washington, 1897.
4. Jumikis, A. R. Suction Force in Soils upon Freezing. ASCE Proc., June 1954.
5. Jumikis, A. R. Experimental Studies on Moisture Transfer in a Silty Soil Upon Freezing as a Function of Its Porosity. Rutgers University (Mimeographed), New Brunswick, 1963.

Physical Properties of Granular Materials with Reference to Thermal Resistivity

OMAR T. FAROUKI, Assistant Professor, San Jose State College

Various approaches to the engineering aspects of the problem of thermal resistivity of backfill materials for underground power cable systems are described. A study is made of the effect on the thermal resistivity of the percentage and the nature of binder added to a Rothfuchs graded granular skeleton of quartzitic sand and gravel. Addition of kaolinite in percentages up to 16 percent shows that the optimum amount is in the vicinity of 8 percent. The use of calcium carbonate, fly ash, lime and lime-fly ash as binders in an amount of 8 percent shows that the nature of the binder has little effect on the thermal resistivity of the cemented backfill material in the nearly dry state, as the value of this resistivity is controlled chiefly by the oriented water films. However, the nature of the binder becomes important as its amount increases to 16 percent and more.

The compressive strength of a nearly dry cemented backfill material containing 8 percent binder is found by experiment to increase linearly with its thermal conductivity, provided the binder does not react chemically with the quartz grains (as lime does). This experimental relation agrees with hypothetical relations derived on the basis of Debye's equation for the thermal conductivity in terms of the speed of sound. The derivation assumes a linear relation between the speed of sound in a generalized cemented granular material and its compressive strength, as has been previously established experimentally in the particular case of concrete.

A study was made of the effect on thermal resistivity of the method by which a given moisture content of a backfill material is attained, whether from the dry side or the wet side. It is shown that a material dried out from the saturated to the air-dry state has a considerably lower thermal resistivity than if it were simply mixed and densified in the air-dry state. When the material dries out, the thermal resistivity increases linearly as the logarithm of the moisture content decreases. However, when moisture is added to the dry material, the thermal conductivity increases linearly as the logarithm of the moisture content increases.

A comprehensive equation for the thermal conductivity of a generalized soil is developed to include the effect of moisture migration in both the film and the vapor phase.

•THE SCIENTIFIC and engineering study presented in this paper was occasioned by the problem faced by the electric power industry of developing economical backfill materials possessing dependable low thermal resistivities even at low moisture contents. The design of a suitable material composition or system of high dependable thermal conductivity or low resistivity involves the determination and selection of the best available constituents and their most effective combination with respect to mineral composition and granulometry. The effective and economical densification of the material with available equipment necessitates a consideration of such mechanical properties as workability and the related property of shear strength. The total engineering and scientific

Paper sponsored by Committee on Physico-Chemical Phenomena in Soils and presented at the 45th Annual Meeting.

problem thus involves practically all the physical properties of such backfill materials and the mutual interrelation of these properties.

The mechanical properties of granular materials were considered in a previous paper by Farouki and Winterkorn (6). The present paper contains a study of the thermal properties and of the relations between thermal and mechanical properties. It also includes the development of a comprehensive equation for the thermal conductivity of a soil, which takes into account the phenomenon of moisture migration.

THERMAL PROPERTIES OF GRANULAR MATERIALS

If a backfill material is to have a good thermal conductivity, it should possess a continuous granular skeleton composed of quartz grains, because quartz is the common rock mineral having the best thermal conductivity. A high density of the material must be easily obtainable, which means that the material should be well-graded. To prevent segregation of the different grain sizes during handling and densification, a small amount of binder, such as clay, should be added. Since this binder usually has a lower intrinsic thermal conductivity than the quartz grains, there is an optimum percentage of binder. Additional amounts would only result in interference with the packing of the granular skeleton, and would therefore cause a decrease in the thermal conductivity. A series of experiments was performed to determine the optimum percentage of binder. Another series of experiments was performed using different binders to determine the effect of the nature of the binder. In both series the binder was added to the same type of granular skeleton which consisted of a quartz granular material made up according to the Rothfuchs (22) gradation to obtain a high density at a good workability.

The thermal conductivity of a granular material with a binder may have different values at the same density and moisture content, depending on whether this moisture content is approached from the saturated or completely dry state (32). Experiments were performed to investigate this phenomenon.

Method of Measuring Thermal Conductivity

The method used to measure the thermal conductivity is the transient method of Stalhane and Pyk (24) which was used by Van Rooyen (26). The essential feature of this method is the thermal probe which contains a heating wire and a thermocouple, and is located in the center of the soil. Readings of the temperature rise of the probe with time are taken, the time being measured from the instant the heating current is on.

The probe used was 6 in. long and 0.035 in. in diameter and contained a copper-constantan thermocouple as well as a constantan heating wire. The material under test was contained in a 6-in. brass cylinder of 4-in. diameter.

TABLE 1

GRAIN-SIZE DISTRIBUTION[a]

Sieve	Percent of Fraction
3/8 in.-No. 4	32.2
No. 4-No. 8	22.7
No. 8-No. 16	16.0
No. 16-No. 30	11.4
No. 30-No. 50	8.0
No. 50-No. 100	5.6
No. 100-No. 200	4.1

[a]Rothfuchs graded granular skeleton of sand and gravel.

Effect of Percentage of Binder on Thermal Conductivity

According to the existing empirical and theoretical formulas which show the effect of the clay content on the thermal conductivity, K, of a granular material, K decreases continuously as the percentage of clay added to the sandy material increases from zero. (See the nomogram of Makowski and Mochlinski (16) which is based on the work of Gemant (7) and Kersten (15).) The empirical formulas derived by Van Rooyen (26) also show a decrease in K as the clay content increases.

To determine the effect of increasing percentages of binder on thermal conductivity, a series of experiments was performed. Kaolinite was used as the binder

in percentages up to 16 by weight of the granular skeleton. The kaolinite was added to a quartz sand and gravel graded according to the Rothfuchs equation. The grain-size distribution of the granular skeleton is given in Table 1. The fractions were separated from well-washed filter sands and gravels having rounded grains and uniform characteristics.

The granular material with the added kaolinite was first tested in the air-dry state without any previous wetting. The material was then removed from the test cylinder, mixed well with enough water to saturate it and then redensified in the cylinder. The thermal resistivity was measured in the saturated state and moisture was then gradually removed from the material by suction. The thermal resistivity was measured at lesser moisture contents and finally in the driest state that could be obtained. Each material, of course, remained at the same dry density as its moisture content decreased.

For each moisture content, the measured thermal resistivity was plotted against the logarithm of the moisture content. The results obtained are shown in Figure 1 which

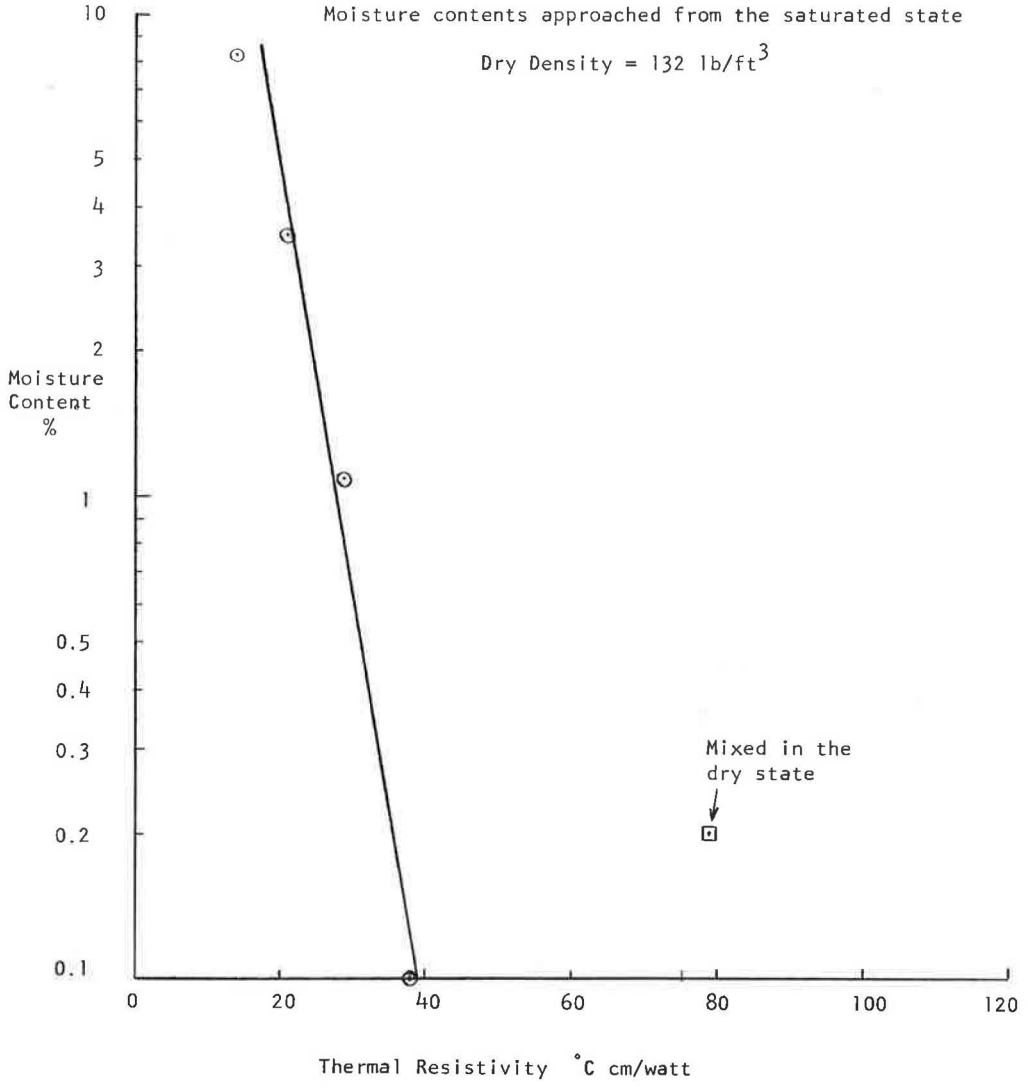

Figure 1. Thermal resistivity of Rothfuchs graded sand and gravel + 8 percent kaolinite.

gives the data for the material containing 8 percent kaolinite. The value of the thermal resistivity for the material mixed and tested in the dry state is also plotted for comparison. The data show that when the material is dried out from the saturated state, it has a considerably less resistivity in the dry state than it would have if it were simply mixed and tested in the dry state.

For a given percentage of kaolinite, the data fell on a straight line (Fig. 2) suggesting the following relation between the thermal resistivity, ρ, and the moisture content, w, percent:

$$\log w = a - \frac{\rho}{b} \qquad (1)$$

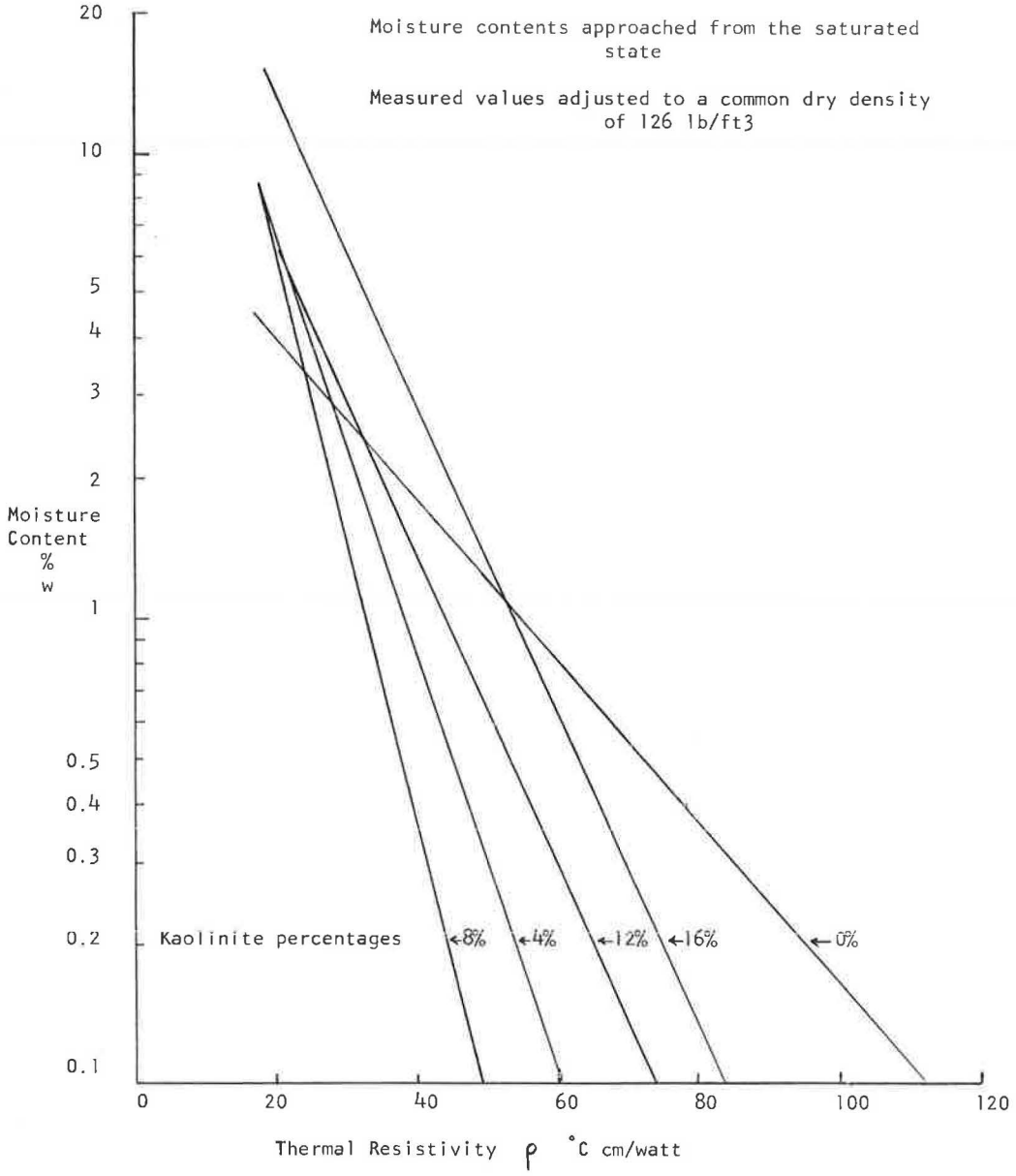

Figure 2. Thermal resistivity of Rothfuchs graded sand and gravel at various percentages of kaolinite binder.

where a and b are positive constants for a material having a given kaolinite percentage at a constant dry density. Figure 2 shows that the addition of a kaolinite binder causes a large decrease in ρ at low moisture contents. However, at moisture contents near saturation, the kaolinite causes little change in ρ, or even a small increase.

Figure 3 shows the variation of the measured values of the thermal resistivity of the materials, in the driest state that could be obtained, with the percentage of kaolinite. There is an optimum percentage of kaolinite around 8 percent. The important binding effect of the kaolinite is clearly shown by the large reduction in resistivity which is obtained by adding 4 percent kaolinite. This effect continues to decrease the resistivity as more kaolinite is added, up to about 8 percent.

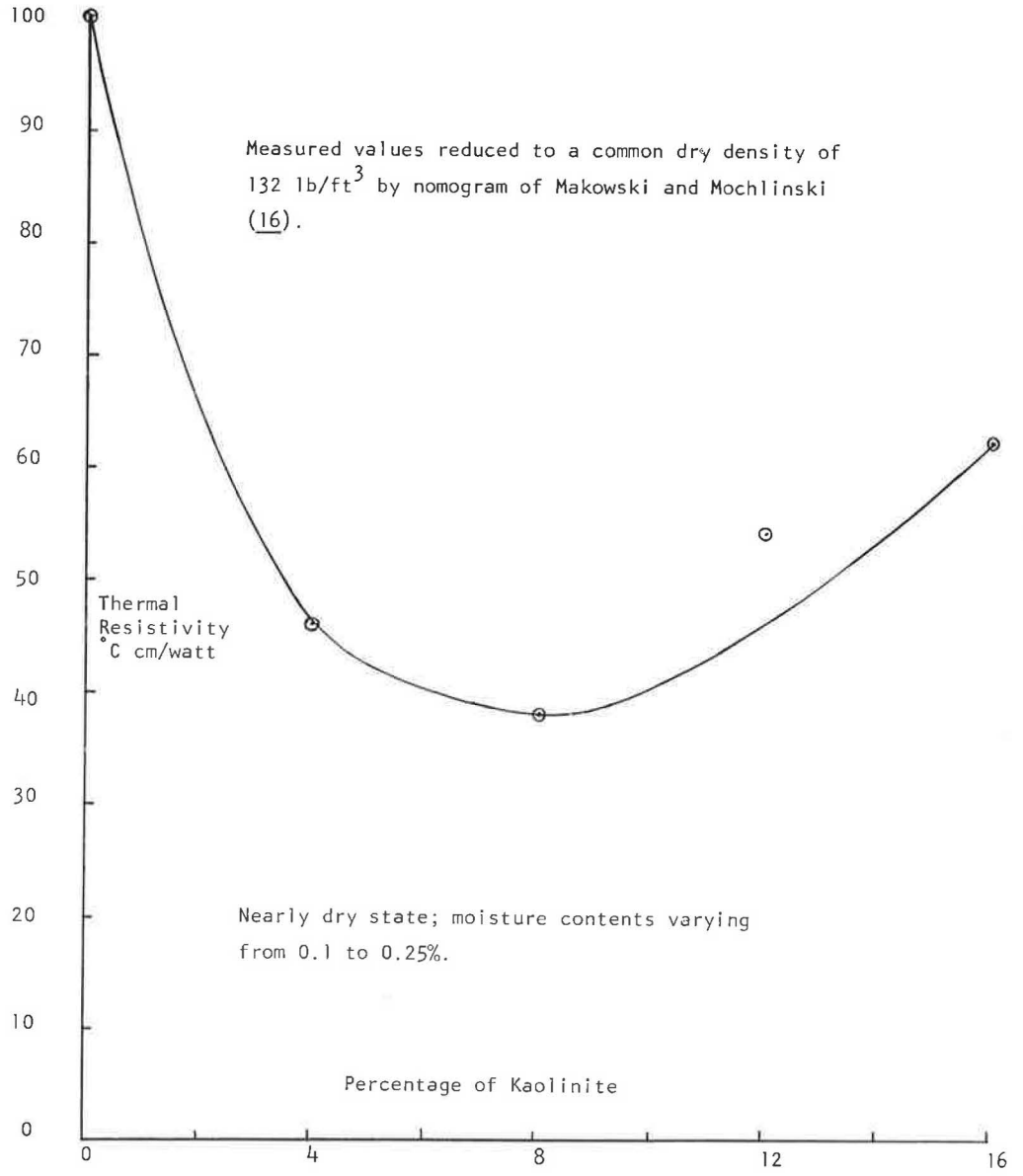

Figure 3. Thermal resistivity of Rothfuchs graded sand and gravel with various percentages of kaolinite.

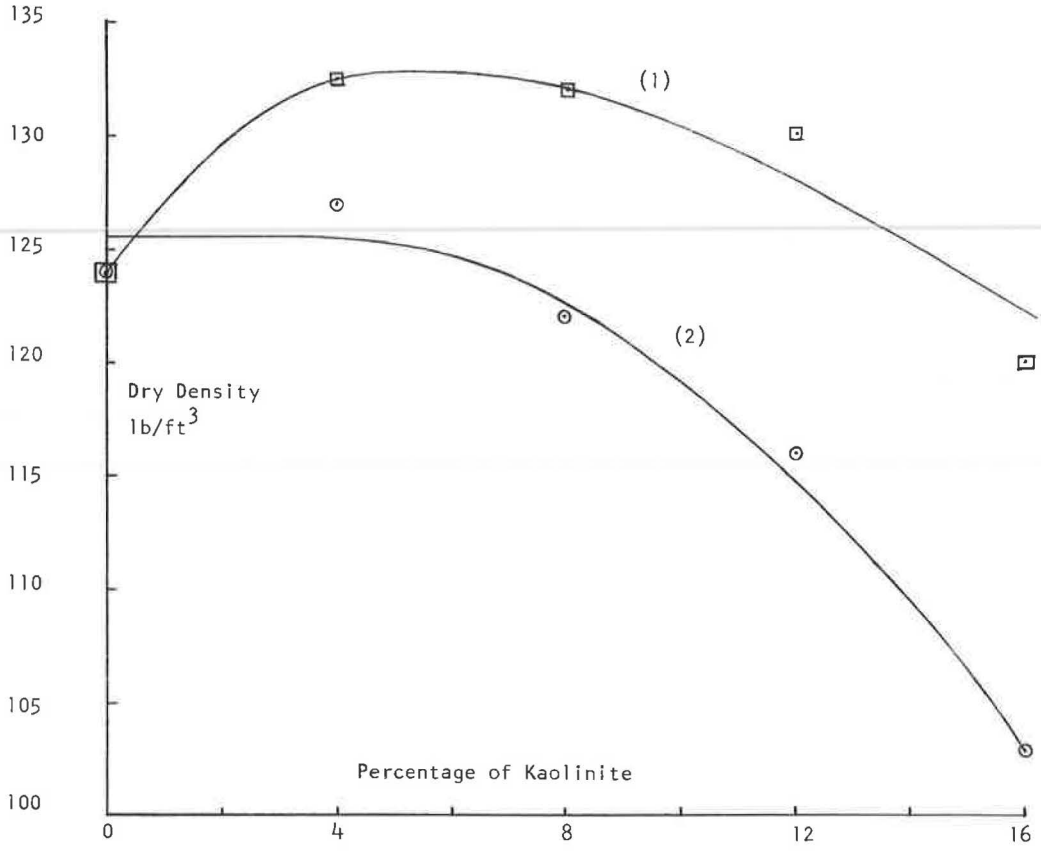

Figure 4. Dry densities of Rothfuchs graded sand and gravel, with various percentages of kaolinite: (1) dry densities of total mixture; (2) dry densities of the skeleton of sand and gravel.

The greatest dry densities obtained during the densification of the different mixtures were at 4 and 8 percent kaolinite. With 12 percent kaolinite the mixture was much less workable. Figure 4 shows the dry densities of the total mixture obtained by the same method of densification with nearly the same effort. The resulting dry densities of the skeleton of sand and gravel are also shown. The skeleton dry density remains practically constant up to about 8 percent kaolinite, and then begins to drop sharply. It appears, therefore, that as more kaolinite than 8 percent is added, there arises an appreciable interference of the kaolinite with the packing of the sand and gravel particles to the extent that the skeleton may become largely disconnected. The resulting decrease in the skeleton dry density and the interposition of excess kaolinite between the skeletal grains is responsible for the increase in resistivity when more kaolinite than 8 percent is added, since the intrinsic resistivity of kaolinite is greater than that of the quartz grains.

Effect of Nature of Binder on Thermal Conductivity

Besides kaolinite, other binders were added to the Rothfuchs graded sand and gravel. Calcium carbonate, fly ash, lime or lime-fly ash (1:2 by weight) were used as binders in the optimum amount of 8 percent. The material with the added binder was densified in the saturated state and the thermal resistivity measured. The moisture was then removed by suction and ρ measured at decreasing moisture contents and in the driest state that could be obtained. Again, ρ was found to increase linearly as log w decreased. The data obtained on the materials in the driest state are given in Table 2, after being

TABLE 2

THERMAL RESISTIVITIES[a]

Binder Added	Thermal Resist. (°C cm/watt)
8 percent kaolinite	35
8 percent calcium carbonate	41
8 percent fly ash	43
8 percent lime	52
2.7 percent lime + 5.3 percent fly ash	50

[a]Rothfuchs graded sand and gravel + 8 percent binder at 0.2 percent moisture and 135 pcf dry density.

slightly adjusted to the same moisture content and dry density, using the nomogram of Makowski and Mochlinski (16).

The range of variation of the resistivities of the dry materials is not too great. The common constituents of these materials are quartz grains, which have a low resistivity (11° C cm/watt), and also the oriented water films. For these materials, it therefore appears that the presence of the oriented water films, rather than the nature of the binder, may control the value of the thermal resistivity.

The resistivity values of these materials are close to the resistivity of ice which is 45° C cm/watt. In the light of the foregoing conclusion, this may be quite significant. The oriented water films, controlling the value of the resistivity, are in an ice-like condition.

Considering the foregoing evaluation of the effect of binder percentage, it may be expected that the oriented water films also control the resistivity of the system when the amount of binder is less than 8 percent. However, when the percentage exceeds 8, the intrinsic resistivity of the binder begins to play an appreciable part in determining the resistivity of the system. The influence of the oriented water films therefore decreases. The nature of the binder may then become important, especially at percentages of 12 to 16.

Thermal Resistivities at Increasing or at Decreasing Moisture Contents

At a given moisture content, a granular material may be expected to have different values of thermal resistivity according to whether the moisture content was attained starting from the saturated state or from the completely dry state. To obtain data on this effect, experiments were performed on a Rothfuchs graded backfill sand to which 8 percent of calcium carbonate was added as a binder. Some of the results are shown in Figure 5. At increasing moisture contents the binding effect does not exist. However, as the material decreases its moisture content this effect increases, reaching a maximum in the dry state. This is the chief reason for the increasing divergence of the curves in the two cases as the moisture content decreases. At intermediate moisture contents, these curves are relatively close together, since moisture migration and its accompanying heat transfer may play a large part in both cases at this point.

In the case of decreasing moisture contents, the linearity of the relation between the resistivity and the logarithm of the moisture content has been established. With increasing moisture contents, however, there may not be such a linear relation because the mechanism of heat transmission differs, especially at lower moisture contents, due to the binding effect. The limited data obtained on this and similar systems showed some deviation from such a linear relation, but tended to agree more closely with Kersten's (15) relation. The latter, applying to the case of increasing moisture contents, indicates a linearity between the thermal conductivity (not the resistivity) and the logarithm of the moisture content at a given dry density.

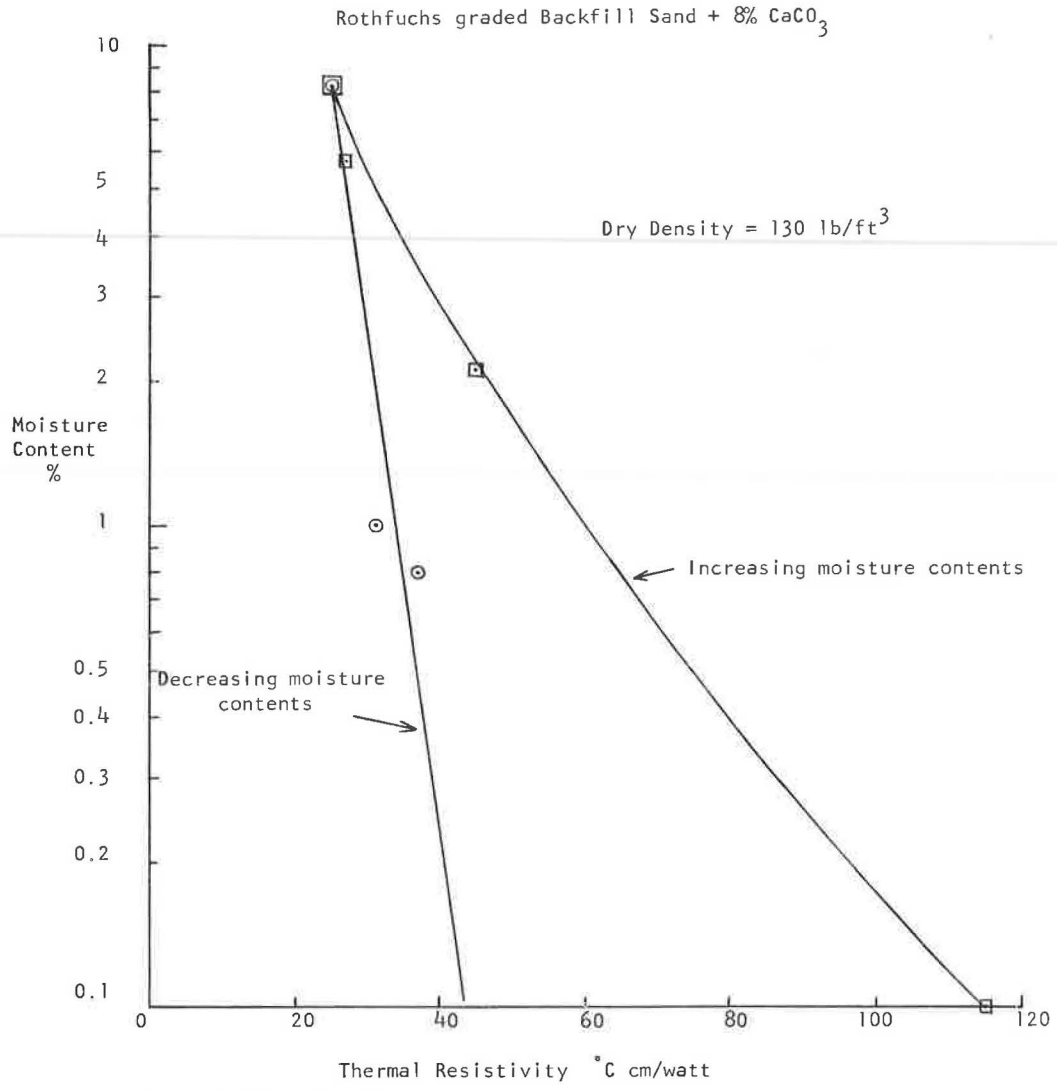

Figure 5. Thermal resistivities at increasing or decreasing moisture contents.

RELATIONS BETWEEN THERMAL AND MECHANICAL PROPERTIES

The equation for thermal conductivity in terms of the speed of sound, as derived by Debye (4), is used in developing a relation between the thermal conductivity of a cemented granular material and its compressive strength. The material considered is one which is practically in the dry state, having oriented water films but no free water. The presence of free water would give rise to moisture migration during heat transmission, which would complicate the problem.

Debye's Equation

Debye (4) conceived that the transmission of heat through crystalline nonmetallic solids takes place by means of thermoelastic waves. Bragg (3) and Meissner (17) visualized the atoms in the crystal lattice as linked together by springs. If the temperature at one end is increased, the atoms vibrate more intensely at that end, and these increased vibrations are propagated along from atom to atom at a characteristic speed. The speed with which the thermal energy is transmitted, and therefore the thermal

conductivity, depend on the strength of the bonds between the atoms. This strength is also the chief factor influencing the mechanical properties such as the modulus of elasticity and the hardness. As a result, a relation exists between the thermal conductivity and the mechanical properties of crystalline nonmetallic solids (5).

On the basis of his conception of heat transmission, Debye derived the following equation (4) for heat conductivity, K (cal/°C cm sec)

$$K = \frac{1}{4} v \lambda \delta c_v \tag{2}$$

where

v = average speed of propagation of elastic waves, in cm/sec;
λ = mean free path of phonons, in cm;
δ = density of solid, in gm/cm^3; and
c_v = specific heat of solid at constant volume, in cal/gm° C.

A cemented granular soil material consists of various nonmetallic solids (grains and binder) usually held together by oriented water films to form a solid system. The oriented water films are in an ice-like state (28). The thermal resistivity of a cemented granular material depends on the intrinsic resistivities of its components, but it may be chiefly controlled by the weakest links in the system. These may be the oriented water films or the binder itself, as long as the skeleton grains consist of a material such as quartz which has a low resistivity. Debye's equation may be applicable to these weakest links, and since they may control the resistivity of the system, Debye's equation may be also applicable to the cemented system as a whole. This would indicate a relationship between the thermal conductivity of this system and the speed of sound in it.

Relation Between Speed of Sound in Concrete and the Concrete's Compressive Strength

Jones (13), Parker (18), and Kaplan (14) all found a definite linear relation between the speed, v, of sound waves in concrete and its compressive strength R_c, the concrete being tested at a certain age. The variation in R_c was obtained by varying the water-cement ratio, keeping other factors constant. This linear relation held for many different proportions of aggregate to cement as well as for different admixtures and for different types of coarse aggregate (such as rounded gravel, crushed limestone, crushed granite). Figure 6 shows this linear relationship as obtained by Jones (13) using an irregular river aggregate at different aggregate-to-cement proportions. All the tests were done at 28 days. With the exception of line (1), the lines are practically parallel, indicating a relation of the form

$$v = A + BR_c \tag{3}$$

where A and B are constant for a concrete having a given proportion of aggregate to cement, and where variation of this proportion causes a change in A but not in B (in this equation R_c is the cube strength). Evaluation of Jones' data shows that the average slope, B, equals 0.443 ft in.^{2}/lb sec. Also, the intercept of the lines at zero compressive strength (value A) is related to the ratio, f, of the volume of cement to the volume of total aggregate by the equation A = 13,555 - 3,407f. Eq. 3 thus becomes

$$v = 13{,}555 - 3{,}407f + 0.443\ R_c \tag{4}$$

which gives v in ft/sec when R_c is in psi.

Concrete is merely a special case of the general cemented granular material in which the binding agent may be different from portland cement. Eq. 3 may therefore be applicable, at least in qualitative terms, to the general cemented granular material. This

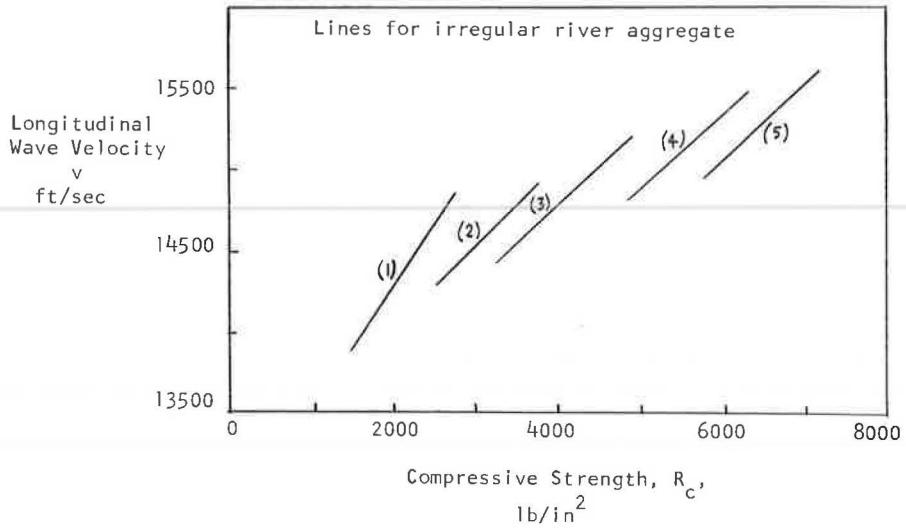

Cement: Fine Aggregate: Coarse Aggregate (by volume)

Curve (1) 1 : 3 : 6

(2) 1 : 2 1/2 : 5

(3) 1 : 2 : 4

(4) 1 : 1 1/2 : 3

(5) 1 : 1 : 2

Figure 6. Relation between velocity of sound in a concrete and its compressive strength at 28 days (13).

would indicate a relation between the speed of sound in such a material and its compressive strength, the one increasing as the other increases.

Relation Between Thermal Conductivity and Compressive Strength of a Cemented Granular Material

Combining Debye's equation with Eq. 3 or 4 gives tentative equations for the thermal conductivity, K, of the cemented granular material in terms of its compressive strength R_c:

$$K = \frac{1}{4} \lambda \delta c_v (A + B R_c) \quad (5)$$

or

$$K = \frac{30.5}{4} \lambda \delta c_v (13,555 - 3,407f + 0.443 R_c) \quad (6a)$$

Eq. 6a is obtained using Eq. 4 which applies to a special concrete; the factor 30.5 converts v from ft/sec to cm/sec.

These derived equations for K are tested against experimental data in the following paragraphs.

Evaluation of Data onThermal Conductivity and Compressive Strength of Cemented Granular Materials

Measurements were made of the compressive strengths of the dry cemented granular materials which were tested for thermal resistivity. The compressive strength was

TABLE 3

DATA FOR MATERIALS WITH VARIOUS BINDERS ADDED TO A ROTHFUCHS GRADED GRANULAR SKELETON

Binder	Dry Density (pcf)	Moisture Content (%)	Failure Load (lb)	Compressive Strength (psi)	Thermal Resist. (°C cm/watt)	Thermal Conduct. (watt/°C cm)
4 percent kaolinite	132.5	0.1	32.5	10.3	52	0.0192
8 percent kaolinite	132	0.1	35	11.1	38	0.0263
12 percent kaolinite	130	0.1	35	11.1	65	0.0154
16 percent kaolinite	120	0.3	49	15.6	80	0.0125
8 percent $Ca\ CO_3$	138	0.1	6	1.9	45	0.0222
8 percent fly ash	140	0.1	12	3.8	43	0.0232
8 percent lime	134	0.15	144	45.8	56	0.0179
8 percent lime-fly ash	141	0.15	80	25.4	46	0.0218

measured by determining the load required to crush 2- by 2-in. cylinders of dry cemented material, these cylinders being small-scale replicas of the 6- by 4-in. material cylinders used in the thermal resistivity tests. The data obtained are given in Table 3 and may be evaluated by dividing the tested materials into two groups. Group No. 1 comprises those materials having 8 percent of binder. These materials thus have the same grain-size distribution and may be expected to have a similar spatial arrangement of their grains. Group No. 2 comprises materials in which the same binder (kaolinite) is present but in different percentages.

Evaluation of Group No. 1 Data. —For these materials, the compressive strength is plotted against the thermal conductivity in Figure 7. The experimental points for three of the materials (those with kaolinite, calcium carbonate or fly ash binder) lie close to a straight line, indicating the existence of a linear relation between the thermal conductivity, K, and the compressive strength, R_c, of these materials:

$$K = A' + B' R_c \qquad (7)$$

where A' and B' are positive constants. The kaolinite, fly ash or calcium carbonate binder is joined to the granular skeleton of the material by means of oriented water films only. Although such films also exist when a lime binder is present, the lime behaves differently in that it reacts chemically with the quartz grains to form additional bonds of a chemical nature which may give the cemented material a greater strength. This would explain why the compressive strengths of the two materials containing lime are much higher than those of the other three materials and do not agree with Eq. 7. This view is further supported by the observation that the compressive strength of the material containing a lime-fly ash binder (2.7% lime to 5.3% fly ash) is between the strength of the material having a pure lime binder and that of the material having a pure fly ash binder.

Eq. 7 thus applies to cases in which the binder does not react chemically with the granular skeleton. It is applicable to systems having a grain-size distribution and binder percentage (8%) similar to those tested. Under such conditions Eq. 7 is valid. Since this equation is of the same form as Eq. 5, the general reasoning on which the derivation of the latter equation was based may be valid. This involved the following suppositions, which may therefore be valid:

1. Debye's equation may be applied to a cemented material as a whole, at least in qualitative terms, to show a relation between the thermal conductivity and the speed of sound, the one increasing with the other; and
2. The speed of sound in a cemented material is related to its compressive strength, the one increasing with the other.

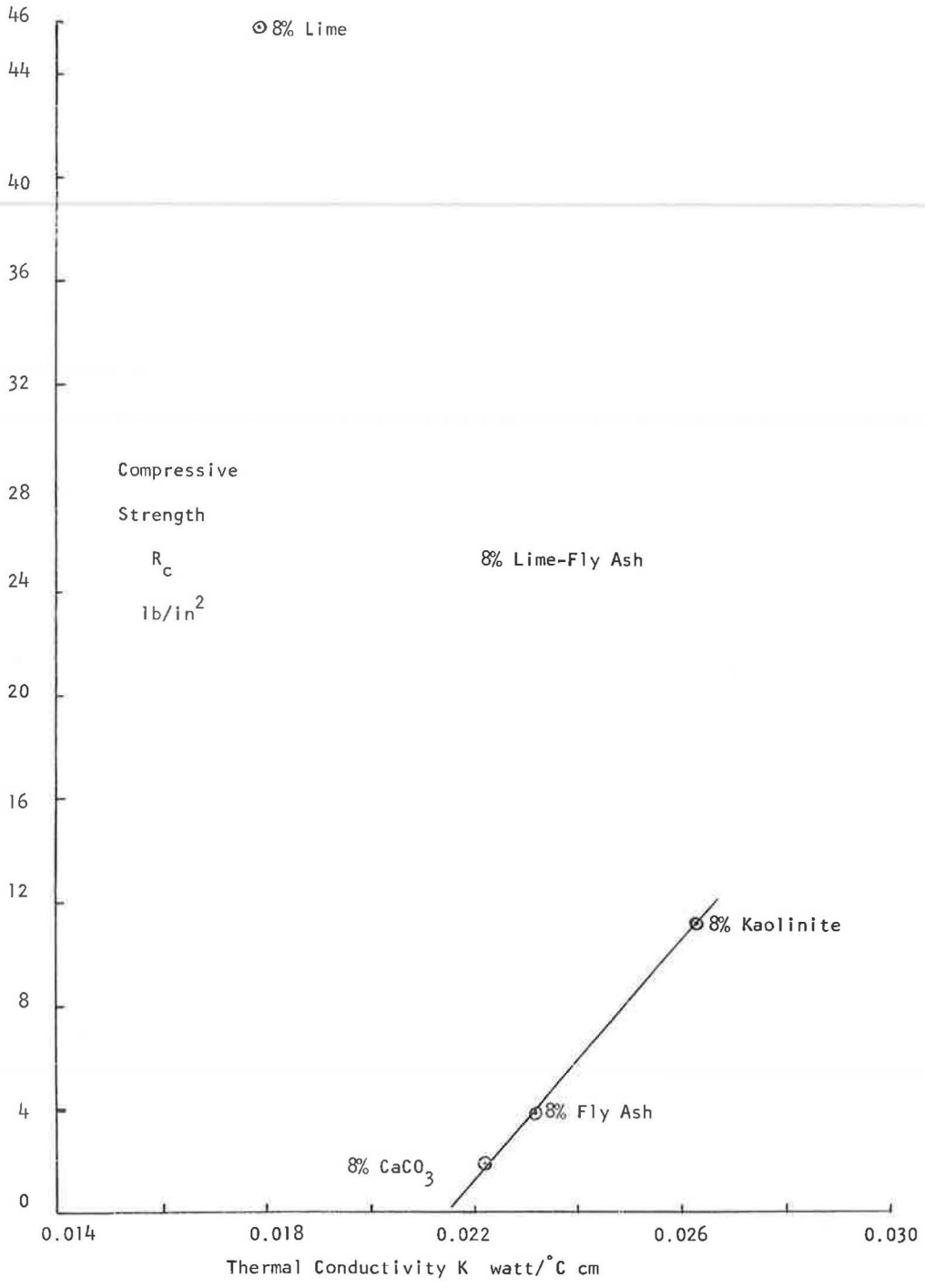

Figure 7. Compressive strength vs thermal conductivity for cemented granular materials with 8 percent binder.

The experimental data do not permit determination of the factors on which the constants A' and B' depend. If it is assumed, however, that these constants are as suggested by Eq. 5, a tentative conclusion may be drawn. This assumption gives

$$A' = \frac{1}{4} A \lambda \delta c_v \text{ and } B' = \frac{1}{4} B \lambda \delta c_v$$

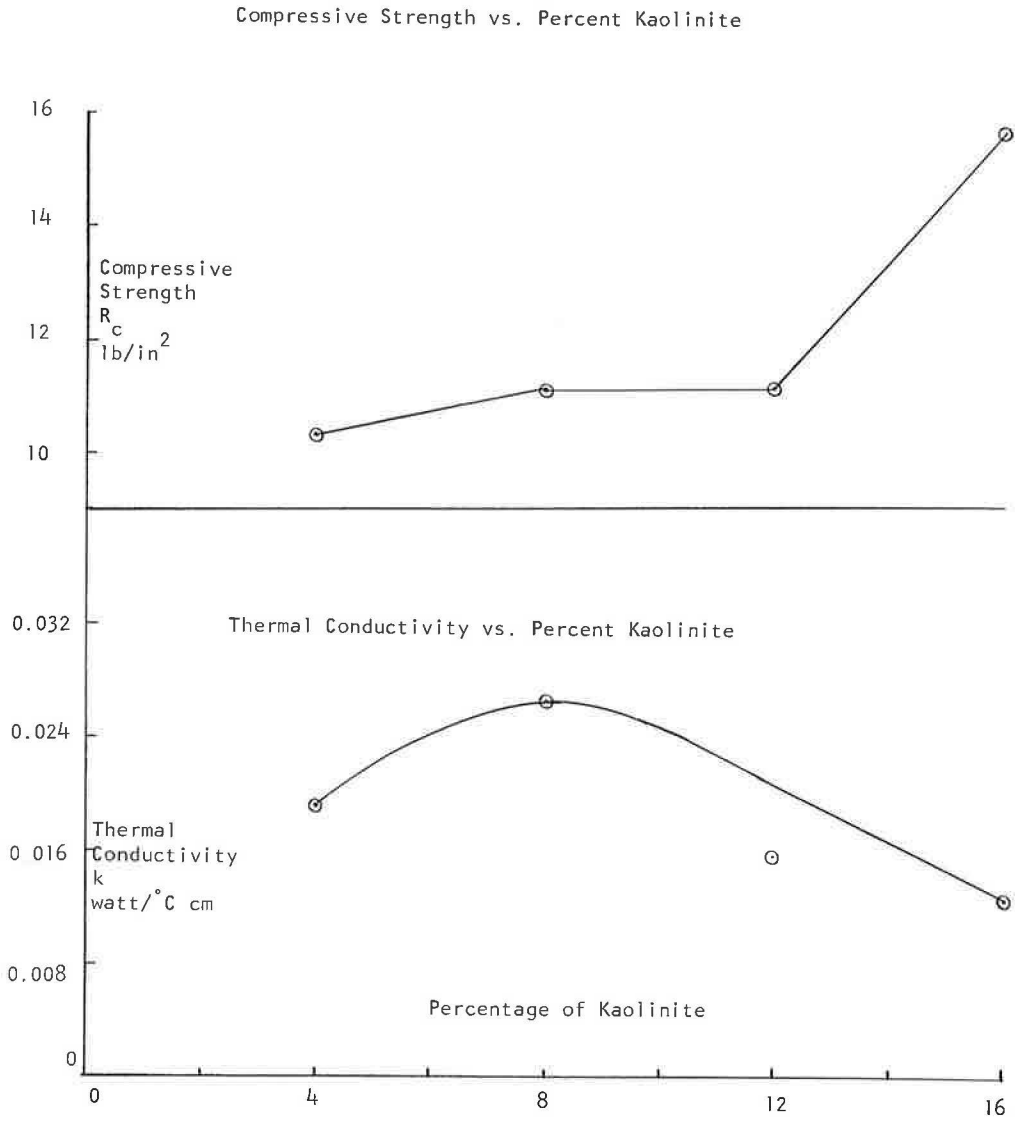

Figure 8. Compressive strengths and thermal conductivities of Rothfuchs graded sand and gravel having various percentages of kaolinite.

Since A′ and B′ are constant for materials with kaolinite, calcium carbonate or fly ash binder, the product $\lambda\ \delta\ c_v$ may also be constant. Since the density δ and the specific heat c_v vary only to a slight extent, the mean free path λ appears to be somewhat constant for these materials. The nature of the binder does not appear to affect the average value of λ for the system. As long as the binder establishes oriented water films between the quartz grains, the travel of the phonons between these grains is dominated by the oriented water films rather than by the nature of the binder. This view is suggested because the presence of the oriented water films is the common element in these materials.

Evaluation of Group No. 2 Data. —The compressive strength and thermal conductivity data of the materials in group No. 2 have been plotted in Figure 8 against the percentage of kaolinite. Both the compressive strength and the thermal conductivity increase as the percentage of kaolinite increases from 4 to 8 percent. Sufficient data were not obtained to determine whether the increase of one with the other occurs linearly in this range. From 8 to 12 percent kaolinite there is no change in the compressive strength, but the thermal conductivity starts to decrease. The compressive strength increases as the kaolinite percentage increases from 12 to 16, whereas the thermal conductivity continues to decrease.

The different patterns of behavior may be explained by considering how the system changes as kaolinite is added to it. Part of the kaolinite added will go to fill the voids between the granular skeleton and part will interfere with the packing of the grains, pushing them somewhat farther apart. For percentages of kaolinite up to about 8 percent, most of the kaolinite may be expected to go in the voids of the skeleton with only a small amount causing interference in the arrangement of the skeleton. Figure 4 shows the effect of increasing percentages of kaolinite on the dry density of the skeleton. This dry density remains practically constant up to about 8 percent kaolinite content. Hence the system remains essentially of the same type, i. e., a continuous granular skeleton with a binder in its voids.

As the kaolinite content increases from 8 to 12 percent, a transition may occur from one mode of behavior to another. An increasing portion of the binder now starts to interfere with the arrangement of the granular skeleton, but most of the binder nevertheless goes to fill the voids. Beyond 12 percent kaolinite, however, most of the binder causes interference in the skeleton arrangement, interposing itself between the quartz grains. The bonds between the grains of kaolinite, rather than those between the kaolinite grains and the quartz grains, now become the determining factor with respect to the strength of the whole system. Since the former bonds are stronger, the compressive strength starts to increase rapidly, resulting in a different system which does not possess a continuous granular skeleton.

The decrease in the thermal conductivity in the range 8 to 16 percent kaolinite is due to the important role played by the intrinsic resistivity of the kaolinite in this range. This feature has been discussed previously.

Eq. 6 which applies to a special type of concrete was tested to determine if it could also apply to a granular material with a kaolinite binder. This equation may be rewritten

$$k = \alpha\ (13,555 - 3,407f + 0.443\ R_c) \qquad (6b)$$

where $\alpha = 7.62\ \lambda\ \delta\ c_v$. It gives k in cal/°C cm sec when R_c is in psi and α is in cgs units. Table 4 gives the values of α calculated at different values of f where $f = \frac{\text{volume of kaolinite}}{\text{volume of granular skeleton}}$. At each value of f, the measured values of K and R_c were used (from Table 3). The value of R_c was multiplied by a factor of 1.1 to obtain the equivalent cube strength from the measured cylinder strength. Assuming a value of 2.5 gm/cm^3 for δ, and 0.2 cal/gm °C for c_v, the values of λ were calculated (Table 4). Winterkorn (31) calculated a λ of 4×10^{-7} cm for quartz $\|$, and a λ of 0.4×10^{-7} cm for quartz glass. Thus Eq. 6 gives quite reasonable values of λ for the granular material with kaolinite binder.

TABLE 4

VALUES OF α AND λ AT DIFFERENT f VALUES FROM EQ. 6

Percent Kaolinite by Wt	f	α	λ (cm)
4	0.041	3.4×10^{-7}	0.9×10^{-7}
8	0.081	4.7×10^{-7}	1.2×10^{-7}
12	0.121	2.9×10^{-7}	0.8×10^{-7}
16	0.161	2.3×10^{-7}	0.6×10^{-7}

The value of λ is maximum at 8 percent kaolinite. With the values of λ and α in Table 4, Eq. 6 represents accurately the relation between k and R_c as obtained by experiment at different percentages of kaolinite.

Further Conclusions From Data of Both Groups. —Eq. 7 is not expected to apply at a given percentage of binder when this percentage is between 8 and 16 due to the important roles played in this range by (a) the strength of the bonds between the binder grains, and (b) the intrinsic resistivity of the binder. However, since the influence of these two properties is not important when the percentage of binder is between 4 and 8, Eq. 7 may apply at a constant percentage in this range. Again, the conditions are that no chemical bonds are formed by the binder, and the granular skeleton keeps the same grain size composition.

The factor λ may be conceived as the effective average mean free path for the whole material. The experimental results indicate that, at a binder percentage of 8 percent, the value of λ depends chiefly on the oriented water films. As the amount of binder decreases below 8 percent, the quantity of oriented water films decreases, causing a decrease in λ. At percentages above 8 percent, λ depends on both the oriented water films and the nature of the binder. The effect of the latter results in a decrease of the effective λ. The nature of the binder may become the controlling factor when the amount of binder reaches 16 percent.

A COMPREHENSIVE EQUATION FOR THERMAL CONDUCTIVITY

The existing theoretical and empirical formulas for the thermal conductivity of a soil (27) do not take into account the contribution of moisture migration to heat transfer. As this factor may be quite important, an attempt is made here to introduce it, together with some other factors, into a comprehensive equation for the thermal conductivity of a general soil.

Bouyoucos (2) was the first to carry out systematic laboratory experiments on moisture migration in soils due to a thermal gradient. He found that there existed for each soil a moisture content which gave rise to the maximum amount of migration. At greater or smaller moisture contents, the migration was less. For the materials employed, moisture migration occurred chiefly in the liquid phase due to a greater water affinity at the lower temperatures. This view is supported by Winterkorn (29) and by the experiments of Gowda and Winterkorn (8). On the other hand, some workers have maintained on the basis of their experiments that migration in the vapor phase due to vapor pressure gradients is the predominating mechanism (9, 10, 12, 21, 25). To account for the fact that the observed moisture migration is greater than that predicted by the simple vapor diffusion theory, W. O. Smith (23), Philip and De Vries (19), and Woodside and Kuzmak (34) postulated a transfer mechanism consisting of a series of evaporation and condensation steps together with a discontinuous film flow. This postulate gives better agreement with experimental data (20).

Considering the types of soils used in the various experiments on moisture migration, two essential conclusions pertaining to unsaturated soils may be drawn (20):

1. Transfer in the film phase predominates in clayey soils, especially at moisture contents near the plastic limit and at optimum compaction, and
2. Transfer in the vapor phase predominates in sandy soils.

Migration in the vapor phase is maximum at a certain moisture content of a sandy soil (12) just as migration in the film phase is maximum at a certain moisture content of a clayey soil (2).

Let w_m denote the moisture content at which moisture transfer in the film phase is maximum. The data of Bouyoucos (2) show that $w_m \approx 20$ percent for a clay soil, $w_m \approx 14$ percent for a silt loam, and $w_m \approx 7.5$ percent for a sandy loam. The value $w_m \approx 20$ percent for a clay soil coincides in general with the plastic limit. The exact value of w_m depends on the water affinity of the soil and hence on the type and percentage of clay. For a soil containing a fraction c of clay, it may therefore be assumed that $w_m \approx 20c$ percent; an amount of 2 should be added to this value, however, if the soil is predominantly sandy, so as to allow for the moisture adsorbed by the sand grains which is unavailable for hydration of the clay portion.

When w = 0, there can be no moisture transfer in the film phase. The data of Bouyoucos show that the transfer is also zero when $w = 2w_m$. We may assume that the amount of moisture transferred in the liquid phase, T_L, varies parabolically as w increases from 0 to $2w_m$, having a maximum value of β gm/cm^2 sec per °C/cm when $w = w_m$. This assumption gives rise to the following equation for T_L at any moisture content, w,

$$T_L = \frac{1}{2} \frac{w(2w_m - w)}{w_m} \beta \text{ gm/cm}^2 \text{ sec per } ^\circ\text{C/cm} \tag{8}$$

which satisfies the conditions just stated. The amount of heat transferred in calories, h_L, is numerically the same as T_L since the specific heat of water is 1 cal/gm °C.

Vapor transfer in soils may cause an appreciable heat transfer due to the large latent heat of evaporation of water. From the data of Rollins et al. (21) as evaluated by Philip and De Vries (19), we may take the moisture content at which vapor transfer is maximum to be that corresponding to m = 0.5, approximately; m denotes the fraction of voids filled with water. At this value of m, there is an appreciable amount of free water which can be easily transferred, and also a sufficient volume of pore space in which the vapor can move.

Let the value of the maximum vapor transfer (at m = 0.5) be γ gm/cm^2 sec per °C/cm. At m = 0 (dry condition) and at m = 1 (saturated condition) the transfer is zero. Assume that the amount of vapor transferred, T_V, varies parabolically between these two points with a maximum value of γ at m = 0.5. This gives the following equation for T_V at any value of m:

$$T_V = \frac{1}{(0.5)^2} m(1 - m) \gamma \text{ gm/cm}^2 \text{ sec per } ^\circ\text{C/cm} \tag{9}$$

which satisfies the stated conditions. As a result, the amount of heat transferred is

$$h_V = 580\ T_V \text{ cal/cm}^2 \text{ sec per } ^\circ\text{C/cm} \tag{10}$$

The value T_L depends on w, whereas T_V depends on m. At a constant value of w, a sandy soil may have different values of m, depending on its dry density. The dry density may be such that m = 1 when no vapor migration can occur, or it may be such that m < 1 when an appreciable migration may occur. Thus at a constant w, T_V can vary in the case of a sandy soil. However, for a clayey soil the value of w determines the thickness of the water film around the grains and hence its condition of restraint. It therefore determines the value of T_L because the liquid transfer is chiefly due to the variation of the restraint with temperature.

In clayey soils having appreciable air voids, migration in the vapor phase may occur simultaneously with migration in the liquid phase. It may be assumed that the heat transfer due to such a vapor transfer is given by Eqs. 10 and 9 in which γ has to be experimentally determined.

The first quantity of water that interacts with a soil tends to collect between the grains. The water wedges thus formed improve the intergranular contacts. The thermal conductivity is thereby increased by an amount h_w watt/°C cm.

If there is more water in the soil, this forms films around the grains. There will be two zones of oriented water in these films, one adjacent to the solid grains at the solid-water interface, and the other at the water-air interface. If the total water content is large, there is a zone of free water in between, the thickness of which increases as more water is added. To determine the additional contribution to heat transfer due to the higher thermal conductivity of the oriented water, as compared with free water, we have to know the thicknesses of the two oriented water films. In the case of kaolinite, the oriented water at the air-water interface is much thicker and may be several hundred molecules thick (11). This would give a thickness in the order of 10^{-5} cm. If S cm^2/cm^3 is the specific surface of the soil, and k_o is the thermal conductivity of the oriented water, then its contribution to heat transfer is, approximately,

$$h_o = 10^{-5} S k_o \tag{11}$$

k_o may be nearer to the thermal conductivity of ice than to that of free water.

Let V_s, V_w, and V_a be the partial volumes (cm^3/cm^3) of the solids, water and air in a given soil, and let k_s, k_w, and k_a be the respective thermal conductivities. Assuming that the heat flow paths through the three phases (solids, water, and air) are parallel and that contributions to the heat transfer are additive, we obtain the following equation for the thermal conductivity, k, of the given soil

$$k = k_s V_s + k_w (V_w - 10^{-5} S) + k_a V_a + h_L + h_V + h_w + h_o \tag{12}$$

That is

$$k = k_s V_s + k_w (V_w - 10^{-5} S) + k_a V_a + \frac{4.19}{w_m^2} w(2w_m - w) \beta +$$

$$4.19 \times 580 \times \frac{1}{(0.5)^2} m(1 - m) \gamma + h_w + 10^{-5} S k_o \tag{12}$$

where the k values are in watt/°C cm and the factor 4.19 converts calories/sec to watts.

Eq. 12 assumes perfect intergranular contact and does not take into account the interfacial resistance between the grains. It may therefore be expected to give values of k that are too high.

The values of β and γ in Eq. 12 have to be determined experimentally for the particular soil. For a sandy soil, the liquid transfer T_L is small so that the term containing β may be assumed zero; also, the value of S is relatively small, so that $10^{-5} S k_o$ is negligible. For a clayey soil both h_L and h_V may have appreciable values, and $S \approx 2 \times 10^4$ cm^2/cm^3 (30). The value k_o may be taken as 1/45 watt/°C cm which is the conductivity of ice.

Without the terms h_L, h_V, and h_w Eq. 12 reduces to

$$k = k_s V_s + k_w (V_w - 10^{-5} S) + 10^{-5} S k_o + k_a V_a \tag{13}$$

which would be identical with Birch and Clarke's (1) equation for a parallel mechanism of heat flow if $k_o = k_w$. Calculations show that Eq. 13 gives too high a value for k because it assumes perfect intergranular contact. However, if a series mechanism of heat flow is assumed, an equation is obtained which gives too low a value for k, that is,

$$\frac{1}{k} = \frac{1}{k_s} V_s + \frac{1}{k_w} (V_w - 10^{-5} S) + 10^{-5} S \frac{1}{k_o} + \frac{1}{k_a} V_a \tag{14}$$

Let k' be the mean of the values of k given by Eqs. 13 and 14. We may modify Eq. 12 by introducing k' as follows

$$k = k' + h_L + h_V + h_W \tag{15}$$

which should give more accurate values of k than Eq. 12.

Eq. 15 may be expected to provide more accurate predictions in the case of a granular material having a binder at moisture contents approached from the saturated state, than in the case where the moisture content of the material is approached from the dry state. In the former case, as has been shown previously, the binding effect improves the intergranular contacts considerably.

There are few data available from which the magnitudes of β and γ may be calculated. Further research is required to obtain such data and to determine how β and γ vary with the type of soil and its porosity. The variation of the amount of moisture transferred with the moisture content, and the point at which the maximum transfer occurs, have to be more precisely determined for both types of transfer.

From the experiments of Rollins et al. (21) on a fine sand, we obtain

$$\gamma = 5.4 \times 10^{-7} \text{ gm/cm}^2 \text{ sec per } ^\circ\text{C/cm}$$

Gowda and Winterkorn (8) obtained values for the thermo-osmotic transmission coefficients for various clays and for New Jersey Hagerstown soil and its homoionic modifications. From this data, β varies from 0.9×10^{-6} to 3.4×10^{-6} gm/cm^2 sec per °C/cm.

CONCLUSIONS

The presence of a binder in a granular material considerably reduces its thermal resistivity in the dry state (attained from a moist state) as compared with the resistivity without a binder. For the Rothfuchs granular skeleton used, the optimum binder percentage is 8 percent. As the binder percentage gets smaller, the resistivity of the system becomes controlled chiefly by the oriented water films set up by the binder. As the binder percentage increases above 8 percent, the intrinsic resistivity of the binder becomes more important and eventually controls. The system changes from one type (an essentially continuous granular skeleton) to another (a discontinuous skeleton) as the percentage of binder passes through 8 percent. There is a transition region centered around this value. With a different gradation of the granular skeleton, the center of the transition region would be different.

For dry cemented materials containing binders at the optimum percentage or below, the thermal conductivity increases linearly with the compressive strength, provided no chemical reaction occurs between binder and skeletal grains. The experimental data show good agreement with Eqs. 5 and 6, which justifies the general reasoning on which the derivation of these equations is based.

Further experimental observations on heat and moisture transfer in various soils are needed to permit refinement of the developed comprehensive equation for thermal conductivity.

ACKNOWLEDGMENTS

The author wishes to express his gratitude to Hans F. Winterkorn, Princeton University, for his advice and guidance during the preparation of the dissertation on which this paper is based. The Consolidated Edison Company of New York supplied the funds for the research undertaken.

REFERENCES

1. Birch, F., and Clark, H. The Thermal Conductivity of Rocks and Its Dependence upon Temperature and Composition. Amer. Jour. Sci., Vol. 238, pp. 529-558, 613-635, 1940.

2. Bouyoucos, G. J. Effect of Temperature on the Movement of Water Vapor and Capillary Moisture in Soils. Jour. of Agricultural Res., Vol. 5, pp. 141-172, 1915.
3. Bragg, W. H., and Bragg, W. L. X-rays and Crystal Structure. London, Bell & Sons Ltd., 4th ed., 1924.
4. Debye, P. Vorträge über die Kinetische Theorie der Materie und Elektrizität. Leipzig and Berlin, 1914.
5. Eucken, A., and Kuhn, G. Ergebnisse neuer Messungen der Wärmeleitfähigkeit fester Krystallisierter Stoffe bei 0° und -190° C. Zeitschrift für phys. Chem. Vol. 134, pp. 193-219, 1928.
6. Farouki, O. T., and Winterkorn, H. F. Mechanical Properties of Granular Systems. Highway Research Record No. 52, pp. 10-42, 1964.
7. Gemant, A. The Thermal Conductivity of Soil. Jour. of Applied Physics, Vol. 21, pp. 750-754, 1950.
8. Gowda, K. R. S., and Winterkorn, H. F. Theoretical and Experimental Exploration of the Practical Possibilities of Electro-Osmosis. Final Rept. on Beach Sand Stabilization Res., Pt. 5, 1949.
9. Gurr, C. G., Marshall, T. J., and Hutton, J. T. Movement of Water in Soil Due to a Temperature Gradient. Soil Sci., Vol. 74, pp. 335-345, 1952.
10. Hadley, W. A., and Eisenstadt, R. A Critical Soil Moisture Condition Affecting Buried Transmission Cables. Transactions AIEE, Pt. 3, Power Apparatus and Systems, Vol. 72, pp. 849-851, 1953.
11. Henniker, J. C., and McBain, J. W. The Depth of a Surface Zone of a Liquid. Stanford Res. Inst., Tech. Rept. N 6 ori 154 T. O. 11, 1948.
12. Hutcheon, W. L. Moisture Flow Induced by Thermal Gradients within Unsaturated Soils. In Water and Its Conduction in Soils, Highway Research Board Spec. Rept. 40, pp. 113-133, 1958.
13. Jones, R. Testing Concrete by Ultrasonic-Pulse Technique. Proc., Highway Research Board, Vol. 32, pp. 258-275, 1953.
14. Kaplan, M. F. The Effects of Age and Water/Cement Ratio upon the Relation Between Ultrasonic Pulse Velocity and Compressive Strength of Concrete. Magazine of Concrete Res., Vol. 11, No. 32, July 1959.
15. Kersten, M. S. Thermal Properties of Soils. Bull. No. 28, Eng. Expt. Sta., Univ. of Minnesota, 1949.
16. Makowski, M. W., and Mochlinski, K. An Evaluation of Two Rapid Methods of Assessing the Thermal Resistivity of Soil. London, Proc., Inst. of Electrical Eng., Vol. 103, Pt. A, pp. 453-470, 1956.
17. Meissner, A. Leistungssteigerung durch thermische Verbesserung der Isolierstoffe. Elektrotech. und Maschinenbau, Vol. 53, No. 25, pp. 289-293, 1935.
18. Parker, W. E. Pulse Velocity Testing of Concrete. Proc. ASTM, Vol. 53, pp. 1033-1043, 1953.
19. Philip, J. R., and De Vries, D. A. Moisture Movement in Porous Materials Under Temperature Gradients. Trans. Amer. Geophysical Union, Vol. 38, pp. 222-232, 1957.
20. Rollins, R. L. Discussion and Review of Symposium Papers on Water and Its Conduction in Soils. Highway Research Board Bull. 287, pp. 24-29, 1961.
21. Rollins, R. L., Spangler, M. R., and Kirkham, D. Movement of Soil Moisture Under a Thermal Gradient. Proc., Highway Research Board, Vol. 33, pp. 492-508, 1954.
22. Rothfuchs, G. Wie sind möglichst dichte Asphalt und Bitumenmischungen zu erzielen? Bitumen, März 1935, Heft 3, 1935.
23. Smith, W. O. Thermal Transfer of Moisture in Soils. Trans. Amer. Geophysical Union, Vol. 24, pp. 511-523, 1943.
24. Stalhane, B., and Pyk, S. A New Method for Determining the Coefficients of Thermal Conductivity. Teknisk Tidskrift, Vol. 61, pp. 383-393, 1931.
25. Taylor, S. A., and Cavazza, L. The Movement of Soil Moisture in Response to Temperature Gradients. Soil Sci. Soc. of America Proc., Vol. 18, pp. 351-358, 1954.

26. Van Rooyen, M. Soil Thermal Resistivity. Doctor's thesis, Dept. of Civil Eng., Princeton Univ., 1958.
27. Van Rooyen, M., and Winterkorn, H. F. Theoretical and Practical Aspects of the Thermal Conductivity of Soils and Similar Granular Systems. Highway Research Board Bull. 168, pp. 143-205, 1957.
28. Winterkorn, H. F. The Condition of Water in Porous Systems. Soil Science, pp. 109-115, August 1943.
29. Winterkorn, H. F. Fundamental Similarities Between Electro-Osmotic and Thermo-Osmotic Phenomena. Proc., Highway Research Board, Vol. 27, pp. 443-455, 1947.
30. Winterkorn, H. F. Introduction to Engineering Soil Science. Princeton Univ., 1960.
31. Winterkorn, H. F. Behavior of Moist Soils in a Thermal Energy Field. Clays and Clay Minerals, Vol. 9, pp. 85-103, 1962.
32. Winterkorn, H. F. Second Progress Report of Research Study on Soil Thermal Resistivity Characteristics. Dept. of Civil Eng., Princeton Univ., 1963.
33. Winterkorn, H. F. Disc. of Characteristics of Soil Affecting Cable Ratings. By A. G. Milne and K. Mochlinski. London, Inst. of Electrical Eng., 1964.
34. Woodside, W., and Kuzmak, J. M. Effect of Temperature Distribution on Moisture Flow in Porous Materials. Trans. Amer. Geophysical Union, Vol. 39, pp. 676-680, 1958.

Water Vapor-Sodium Montmorillonite Interaction

G. L. RODERICK, Assistant Professor of Civil Engineering, University of Rhode Island; and
TURGUT DEMIREL, Associate Professor of Civil Engineering, Iowa State University

The interaction of water vapor with sodium montmorillonite was investigated with X-ray diffraction and sorption isotherm (gravimetric method) experiments. Expansion of the montmorillonite occurs in three increments. The data suggest that interlayer water builds up in a laminar fashion. The hysteresis of sorption isotherms is apparently due to the formation of a thixotropic structure and to attractive interlayer forces. BET parameters from adsorption isotherm data reflect adsorption only on external surfaces. Free energy data, computed from adsorption isotherm data and X-ray data, allow separation of the free energy change on adsorption into two components: one for adsorption on external surfaces, and one for adsorption on, and separation of, internal surfaces. The data also permit the estimation of swelling pressures exerted by sodium montmorillonite due to the uptake of interlayer water from the vapor phase.

•CLAY-WATER systems are of prime importance in the engineering use of soils; for example, in the prediction of bearing capacity, skin friction on piles, or settlement. Past research on these matters has emphasized mechanical aspects of soil-water systems. It has been recognized, however, that some problems such as secondary consolidation, swelling pressures, and cohesion are not solvable by a mechanistic approach. Therefore, it appears that a more fundamental knowledge of the clay-water system is essential for understanding and predicting the soil-mechanics behavior of clays.

The objectives of this study were to obtain some fundamental knowledge of the sodium montmorillonite water system from successive adsorption-desorption isotherms of water vapor on the montmorillonite, and from X-ray diffraction data obtained during adsorption and desorption.

EXPERIMENTAL PROGRAM

Material

Sodium montmorillonite was chosen as the material for this investigation because the expansive clays are the most troublesome in soil engineering practice. Also, this choice provided the opportunity to study the phenomenon of interlay adsorption of water.

The homoionic sodium montmorillonite sample was prepared from a commercially available Wyoming bentonite, Volclay-SPV, produced by ion exchange (1, 2).

Methods of Investigation

Sorption Isotherm Study. —Sorption isotherms of water vapor on sodium montmorillonite were determined by gravimetric method (3). Figure 1 shows the adsorption apparatus. Bulb A was the permanent water reservoir vapor source. B was a simple

Paper sponsored by Committee on Physico-Chemical Phenomena in Soils and presented at the 45th Annual Meeting.

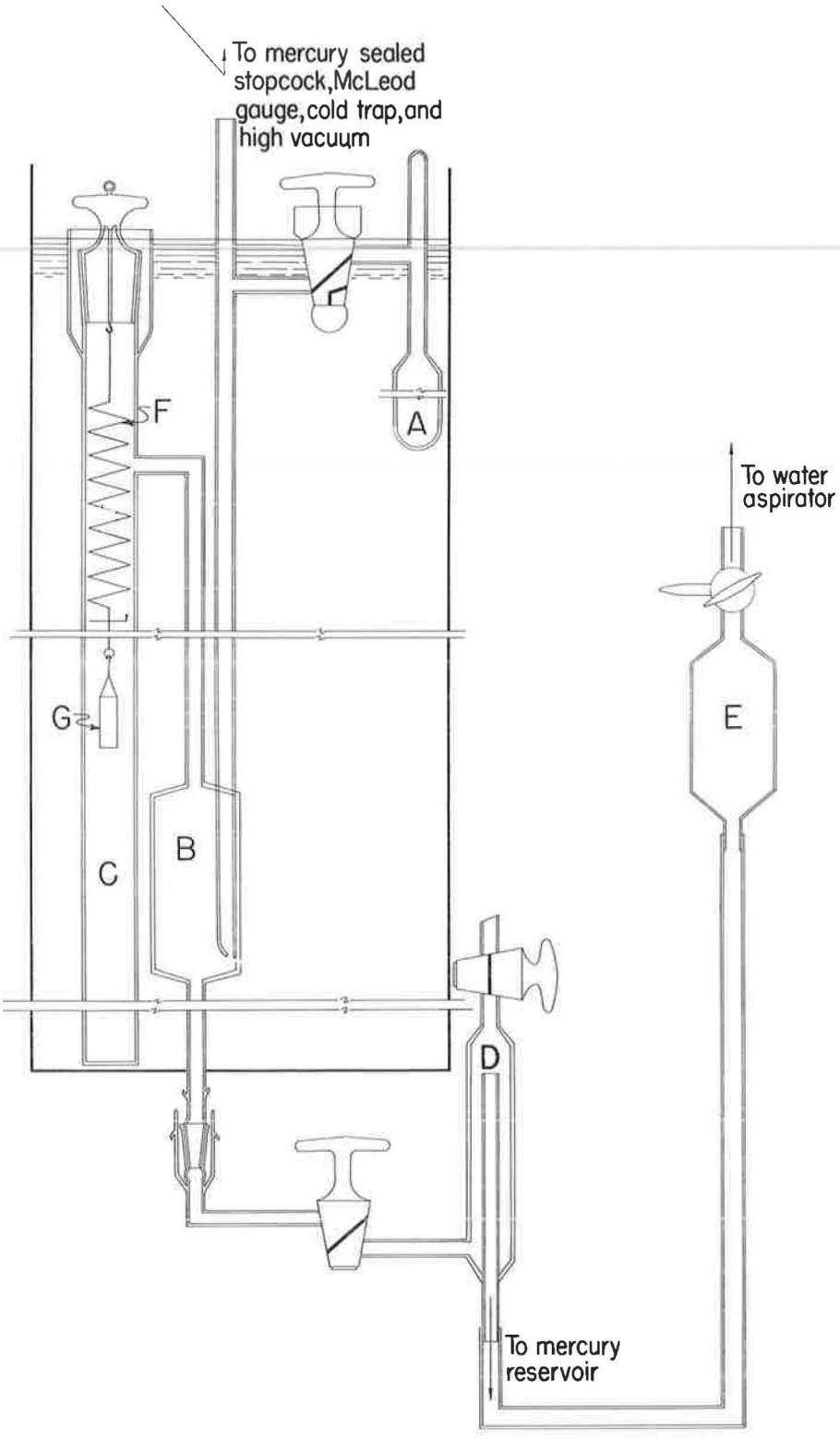

Figure 1. Adsorption apparatus.

mercury manostat-manometer combination for transferring vapor into the adsorption chamber, C, and for measuring vapor pressures. Mercury in B could be raised or lowered through air trap D into the mercury reservoir E. All glass parts were pyrex; all stopcocks were mercury-sealed, and high-vacuum silicone grease was used at all joints. A McBain-Bakr quartz spring balance, F, was suspended into the adsorption chamber from a mercury-sealed ground glass stopper, and a thin walled glass tubing sample holder, G, was suspended from the balance hangdown loop. The water reservoir, manostat-manometer, and adsorption chamber were immersed in a water thermostat maintained at 24.4 C. The apparatus was connected to a high-vacuum system by means of a mercury-sealed stopcock.

The sodium montmorillonite sample, in the sample holder, was dried for several weeks in an evacuated desiccator containing phosphorous pentoxide. The initial sample weight was 158.7 mg with a certified analytical balance. The sample was then placed in the adsorption chamber which, after a brief evacuation, was closed off by the manostat while the triple-distilled water in the reservoir was degassed by a repeated freezing-pumping-thawing process. With the reservoir closed off from the system, the adsorption chamber and sample were degassed by pumping at 10^{-5} mm Hg for several days. The manostat was then closed, the vacuum system closed off, and the water reservoir opened to allow water vapor into the right side of the system.

After thermal equilibrium at 24.4 C was attained, an initial pressure reading, p_o, was taken with a cathetometer reading to 0.02 mm, and corrected for temperature, gravity, and meniscus. An initial balance reading was made with an optical reader; one division on the reader corresponded to 0.0239 mg of mass increase of the sample. A small increment of vapor was then transferred to the chamber through the manostat arrangement. A period of 24 hr was sufficient for the system to attain equilibrium. After this period the pressure difference on the manometer and the spring balance extension were measured. The equilibrium pressure, p, in the chamber was found by making the required corrections on the pressure difference observed and subtracting it from the saturation pressure, p_o. The balance extension was converted to mass increase and divided by the initial sample weight to give the mass of vapor, q, adsorbed by one gram of montmorillonite. More and more vapor was transferred in the same manner until saturation pressure was attained.

In the vicinity of saturation an additional technique was used. After the vapor transfer, a small amount of condensation was formed in the chamber side of the manometer by cooling with a few cubic centimeters of cool water. Before saturation this condensation disappeared rapidly. At saturation the time for disappearance increased to several minutes. The mass of vapor adsorped just before and at saturation differed by less than 0.1 percent.

The desorption isotherm was obtained by condensing more and more vapor back into the water reservoir by cooling it with water. The sample was pumped at relative pressures, p/p_o, below 0.3.

The adsorption apparatus, optical reader and cathetometer were all securely mounted on a rigid steel frame tied to a heavy soapstone table top to prevent differential movements. The experimental error in determining p/p_o was calculated to be ± 0.003 for all pressure ranges. The experimental error in determining q was $\pm 3 \times 10^{-5}$ gm/gm at low pressures and $\pm 3 \times 10^{-4}$ gm/gm near saturation pressure.

X-ray Diffraction Study. —The apparatus used in the X-ray study consisted of a Rigaku-Denki controlled atmosphere high-temperature X-ray diffractometer attachment converted to serve as an adsorption chamber. The furnace and its support base were removed, and a stainless steel sample holder (Fig. 2) was constructed to take their place. This sample holder could be aligned by using the translation, rotation, and inclination controls provided for alignment of the furnace. The arrangement of the water reservoir source for vapor, the manometer for pressure readings, the mercury-sealed stopcock connection between the reservoir and adsorption chamber, and the X-ray windows are shown in Figure 3. The stopcock was fastened securely to a small brass cylinder which was in turn attached to a larger cylinder which fit snugly over the top of the adsorption chamber. A glass tube was attached to the exhaust port coupling by a kovar metal tube and supplied the connection between the adsorption chamber and the portable vacuum system.

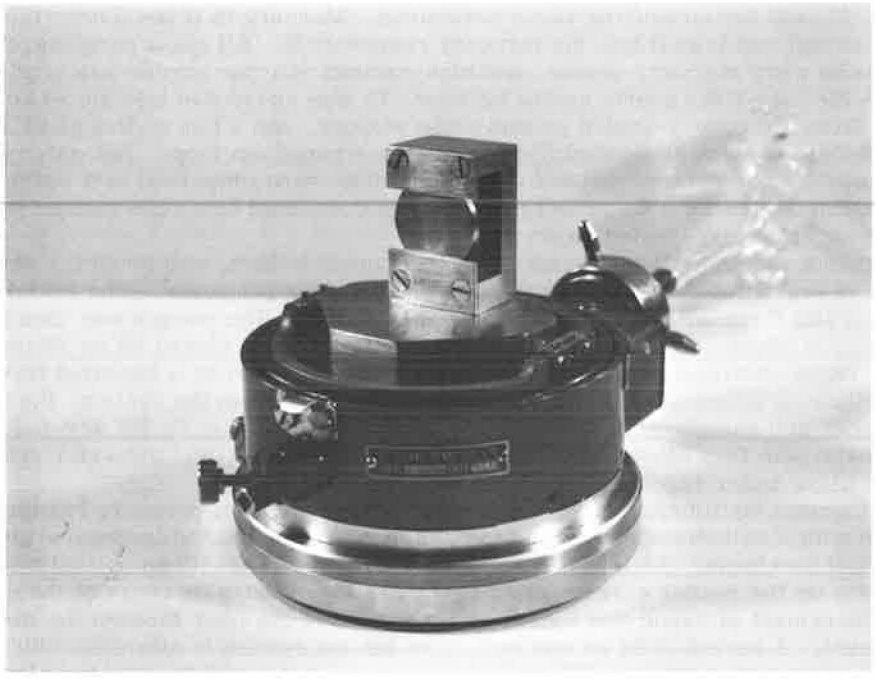

Figure 2. Sample holder for X-ray diffraction study.

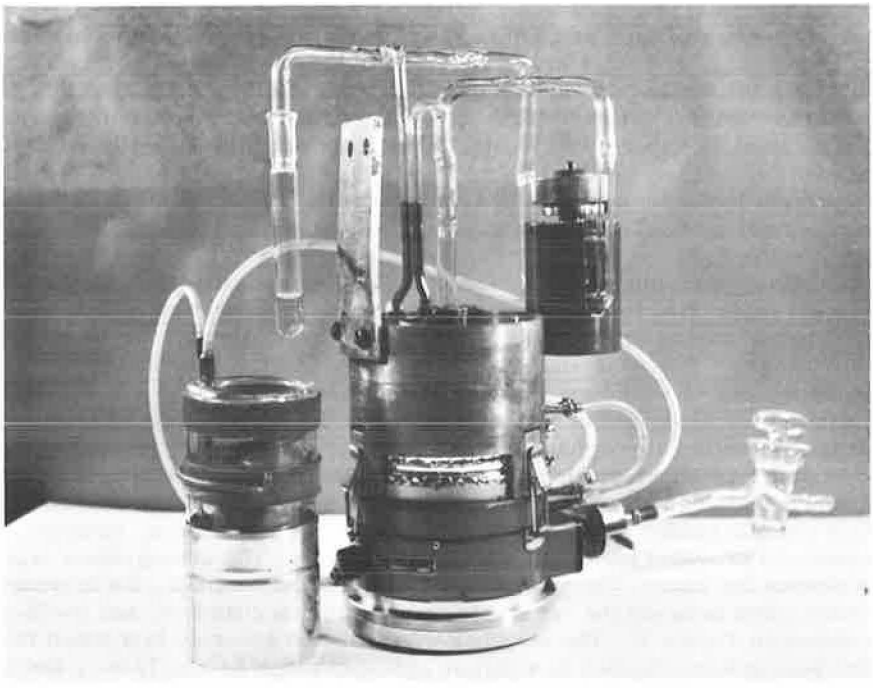

Figure 3. Apparatus for X-ray diffraction study.

The X-ray windows were made of 0.02-mm aluminum foil backed by a ½ mil Mylar polyester film. If the aluminum foil alone was used, pinhole leaks developed in the windows during the experiment.

The adsorption chamber temperature was controlled by circulating water at constant temperature through the cooling tubes provided in the top and bottom portions of the apparatus. The constant temperature water was also circulated through a cooling coil fastened in a water filled dewar flask so that, when in position, the coil surrounded the water reservoir. In Figure 3 the flask is to the left of the apparatus. The constant temperature water source was thermostatically maintained at 22.99 C. The measured temperature in the dewar flask enclosing the water reservoir was 23.2 C during all readings.

A suspension of the sodium montmorillonite was pulled, by a water aspirator, through a 30-mm diameter medium-porosity fritted glass disc so that a thin layer of the clay was deposited on the disc. The sample was dried in an evacuated desiccator containing phosphorous pentoxide. It was then placed in the sample holder and the top cover of the apparatus was positioned. The triple-distilled water in the reservoir was degassed by a repeated freezing-pumping-thawing process. The stopcock was kept closed while the sample was pumped for several days to 10^{-4} mm Hg. The connection between the adsorption chamber and the vacuum train was cut and sealed; the apparatus was connected to the constant temperature water circulation system, placed on the XRD-5 diffractometer and the sample aligned. When thermal equilibrium was attained, the sample was X-rayed with copper Kα radiation and five traces of the initial 9.82 Å 001 peak obtained. A manometer reading was taken, with a micrometer slide cathetometer reading directly to 0.001 mm, and corrected for temperature, gravity, and meniscus.

After obtaining initial peak and pressure readings, the stopcock was partially opened to allow a small increment of water vapor into the chamber. After a period of 24 hr the pressure difference and the new peak position were observed. Each new peak position was recorded five times. In this manner more and more water vapor was transferred to the chamber until the saturation pressure was reached. Desorption was accomplished by condensing vapor back into the water reservoir by cooling it with ice water until a p/p_o of 0.3 was reached, and by freezing with a dry ice-acetone mixture to a p/p_o of 0.03. The vacuum system was used to pump out the last increment.

The experimental error in determining p/p_o was calculated to range from ±0.007 at low pressures to ±0.003 near saturation.

RESULTS

X-Ray Diffraction Study

The first order basal spacings and the widths of the observed diffraction peaks obtained for two cycles of adsorption-desorption of water vapor on sodium montmorillonite are plotted against the relative pressure at which they were observed in Figure 4. The points plotted are the average of five observations for each determination. The accuracy with which individual observations could be made depended on the size of the diffraction angle and on the sharpness of the peaks obtained, which varied with the relative pressure. The average variation from the average value for five observations of the basal spacing were less than ±0.10 Å, with a maximum variation of ±0.25 Å at small angles; for line widths the variations were from ±0.01 to ±0.10 degrees. The line widths of the diffraction peaks obtained were taken as the peak width at half-maximum intensity (4).

A shift of the adsorption curve for the second cycle from the position of that for the first is shown in Figure 4. The same behavior was observed with an earlier sample used in incompleted runs. The first adsorption curve followed the present one very closely up to a p/p_o of 0.70, when a leak developed in the X-ray window. Another incomplete run with the same sample showed a shift to a position between those shown in Figure 4, somewhat closer to the curve for the second run. After solving the leakage problem, a new sample, from which the present data were obtained, was placed in the apparatus.

build up on each other by being hydrogen-bonded to the previous one. Taking 2.76 Å as the thickness of a water molecule (16, p. 464), their hypothesis results in a laminated stacking, causing a separation of 2.76 Å for each molecular layer of water.

Macey (17) noted the lattice similarities between the basal planes of ice and of clay minerals. He suggested that the ice structure develops on clay mineral surfaces with the hexagonal molecular configuration of the basal plane of ice. This structure tends to build outward from the surface. Forslind (18) suggested the same ice structure postulated by Macey, but based his argument on the Edelman-Favejee structure rather than the Hofmann-Endell-Wilm structure of montmorillonite.

Demirel (1) presented two ways in which the ice structure may develop in the interlayer regions. Using data reported in the literature and his own data for various species of homoionic montmorillonites, he found evidence to support the buildup of an ice structure in which the first hexagonal network is shared by two montmorillonite platelets, causing a separation of 2.76 Å; two hexagonal networks are stacked and held by the two silica surfaces, causing a separation of 5.52 Å; the third and fourth molecular layers of water fill in between the hexagonal networks forming tetrahedrons with the water molecules of the network. A complete unit cell of ice is formed with the entrance of the fourth molecular layer of water, causing a separation of 7.36 Å. The fifth and sixth layers of water enter between the unit cell of ice and the clay surfaces, forming hexagonal networks and causing separations of 10.12 and 12.88 Å, respectively.

Barshad (19) suggested an arrangement which becomes progressively denser with the addition of water. He postulated arrangements for water molecules that would give various increases in basal spacing for each additional molecular layer of water, depending on the position of water molecules with respect to the basal oxygens of the clay surface and to water molecules of previously adsorbed layers. The first layer would give spacing increases of 2.76 or 1.78 Å; other layers would give increases of 2.76 or 2.09 Å.

The continuity of the basal spacing vs relative pressure curve of the present study has been attributed to the simultaneous existence of clay platelets separated by various molecular layers of water. If all of the interlayer water is removed at zero relative pressure, a sharp peak is observed corresponding to the collapsed basal spacing of sodium montmorillonite, about 9.60 Å (20). As the relative pressure increases, some water begins to penetrate between some of the clay layers. If it is assumed that at low relative pressures the system consists primarily of layer spacings corresponding to zero and one molecular layers of water between platelets, i.e., that the contributions of layers separated by 2, 3 or more molecular layers of water to the observed diffraction peaks are negligible, then the system may be treated as a random interstratification of two components. At somewhat higher relative pressures the observed peaks may be treated as composite peaks from another random two-component system, one component corresponding to one molecular layer of interlayer water and the other to two layers. This may be extended to higher increments of expansion. As the relative pressure increases, the relative proportions of the two components change and the observed diffraction peaks migrate from the position of the first pure component, A, toward that of the other pure component, B. According to MacEwan, Amil and Brown (7), in a preliminary analysis there will be no great error in assuming that the peaks move linearly between the two pure component positions. When the distances from the observed peak to the A and B positions are x and y, respectively, the proportion of component A is deduced to be $y/(x + y)$. As the observed peak migrates from the A position, it first becomes diffuse and then sharper again as it approaches the B position. Taking the line width to be a function of the nonconstancy of layer separations, we would suspect that a maximum width would correspond to the most random distribution of the two layer separations, and that this would occur when the relative proportions of the two components are nearly equal. Although this conclusion may not be strictly true (7), it is felt that assuming the maximum line width corresponds to an A/B ratio of one will be in no greater error than that in assuming the peak migration to be linear.

If it is assumed that (a) the system of the present study may be treated as a random interstratification of two components; (b) peak migration between pure component positions is linear; and (c) maximum line widths occur when the relative proportions of the

TABLE 1

CALCULATED FIRST ORDER BASAL SPACINGS OF SODIUM MONTMORILLONITE

No. of Molecular Layers of Water	Laminated, Stacking Arrangement of water		Ice-like Arrangements of Water Molecules	
	Calculated Basal Spacings (Å)	Avg., Two Successive Spacings (Å)	Calculated Basal Spacings (Å)	Avg., Two Successive Spacings (Å)
0	9.60		9.60	
		10.98		10.98
1	12.39		12.36	
		13.74		13.74
2	15.12		15.12	
		16.50		13.74
3	17.88		15.12	
		19.26		16.04
4	20.64		16.96	
		22.02		18.34
5	23.40		19.72	

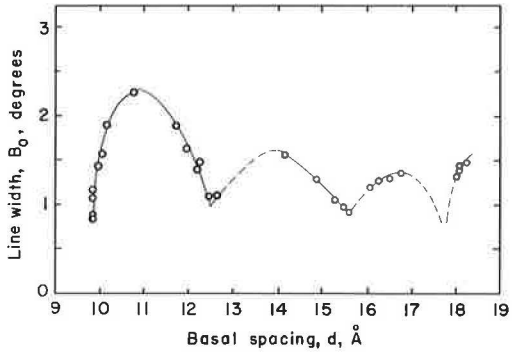

Figure 6. Variation of line widths with basal spacings of sodium montmorillonite.

two components are equal, the line width and basal spacings data of this study may be used to test possible arrangements for the interlayer water that have been postulated by others. The minimum line widths should correspond to a basal spacing near that calculated from the proposed arrangement for an integral number of molecular layers of water between clay platelets. If assumptions (b) and (c) hold, the maximum line widths should occur at a basal spacing which is the average of those calculated for two successive layers of water between platelets.

The observed basal spacing and line widths for the first adsorption run are plotted against one another in Figure 6. Using 9.60 Å as the collapsed basal spacing of sodium montmorillonite, the basal spacings for integral numbers of molecular layers of water between platelets and the averages of each two successive spacings were calculated for the various postulated interlayer water arrangements. At low pressures, the values obtained for the laminated structures and the ice-like structure of Demirel (1) showed the best agreement with experimental data; the values calculated for these arrangements are given in Table 1. The first maximum line width occurs at a basal spacing of about 11.0 Å, very near the 10.98 Å average calculated for zero and one molecular layers of water. The first minimum line width occurs at about 12.5 Å, which is close to the calculated value of 12.36 Å for one molecular layer of water. Although the observed data are scarce, the second maximum line width appears to be about 14 Å, which is reasonably near the 13.74 Å average for one and two layers of water. The second minimum line width is at about 15.5 Å, somewhat higher than the 15.12 Å calculated for two layers of water. The higher than expected basal spacings corresponding to the observed line width minima may be due to failure of the assumption of a two-component system in the region near the peak position for a pure component (all platelets at one spacing). As the peak position approaches that for a pure component, the number of platelets at the next increment of expansion increases, and probably their contributions to the observed peak are no longer negligible. Therefore, the system in

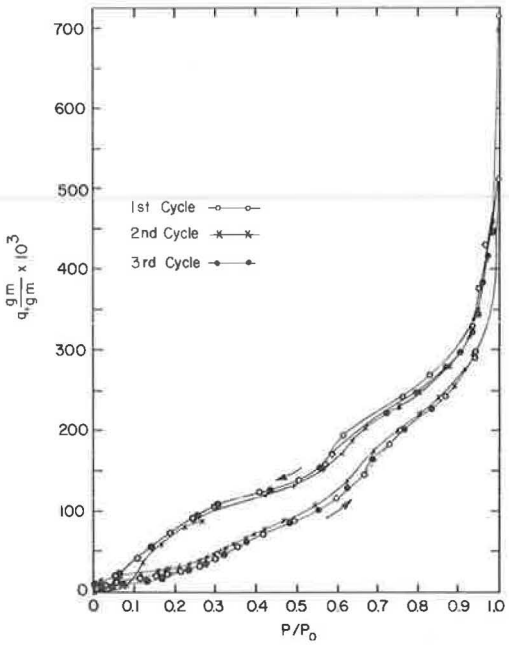

Figure 7. Adsorption and desorption isotherms of sodium montmorillonite.

this region is likely to be one of three rather than two components and the observed minimum line width may well occur at a slightly higher average basal spacing.

The rest of the data (Fig. 6) are not very conclusive. The X-ray data in this region are all in the p/p_o range of 0.97 to 1.00, and are quite crowded. However, Figure 6 does show that a probable maximum line width does occur at a basal spacing greater than about 16.7 Å. This is closer to the 16.5 Å average calculated for laminated structures than it is to the 16.04 Å average for the ice structure. The last group of points (Fig. 6) suggests than a minimum line width may occur at an average basal spacing of slightly less than 18 Å. Again, this is nearer the 17.88 Å calculated for three molecular layers of water in a laminated structure than it is to the 16.96 Å calculated for four molecular layers of water in an ice structure. More extensive data at high relative pressures are needed to draw a definite conclusion. Smaller increments of vapor transfer at high relative pressures may enhance the line width-basal spacing relationship in this region.

The data give evidence of the formation of a laminated arrangement of the interlayer water rather than an ice structure for sodium montmorillonite with up to three layers of water. The arrangement in individual layers of water cannot be ascertained from these data. More detailed studies with sodium montmorillonite, and with other materials such as calcium montmorillonite, may give more complete evidence. Also, better data on the intensity of diffraction peaks may be helpful. Other methods of investigation, such as nuclear magnetic resonance studies and heat capacity studies, may permit more definite conclusions to be drawn.

Sorption Isotherm Study

Figure 7 is a plot of the sorption isotherms for three successive adsorption-desorption cycles. The adsorption and desorption branches fall in different regions of the plot, illustrating the hysteresis expected with porous absorbents (3).

The data of the present study show that the adsorption branch is more closely reproduced on successive runs than the desorption branch. After a p/p_o value of about 0.28, the adsorption curves for the first and third cycles follow each other very closely, within the experimental error previously given. The desorption curves for these two cycles are not in as good agreement until relative pressures below 0.30 are reached. Neither the adsorption nor desorption branches for the second run, which began at a higher value of q, agree very well with those for the other cycles. If the isotherm for the second cycle is started at the origin, the agreement is much better for adsorption than for desorption. The data suggest that the adsorption branch may be the true equilibrium curve. This would be in agreement with the "ink bottle" theory of McBain (21) and the "open pore" theory of Foster (22), both of which explain the hysteresis on the basis of the shape and arrangement of the pores in which capillary condensation takes place.

Barrer and MacLeod (23) studied the adsorption of various nonpolar and polar gases and vapors, including water vapor, by a sodium-rich montmorillonite, and gave an

explanation for the hysteresis observed when polar vapors are adsorbed in the interlayer regions. When nucleation of an adsorbate-rich phase occurs around the periphery of crystallites, it must be associated with strain and interfacial free energies, which slow down the free development of the adsorbate-rich phase until the pressure has exceeded the value for true thermodynamic equilibrium between the vapor and separated montmorillonite layers with and without interlayer adsorbate. On desorption, the development of the adsorbate-poor phase in the interlayer region is delayed by strain and interfacial free energy until the pressure has fallen below that for true equilibrium, and a hysteresis loop is observed.

Hirst (24) also developed a similar explanation for hysteresis, associated with interlayer adsorption. Attractive forces between layers prevent penetration of the adsorbate until a threshold pressure is reached. These forces are then overcome by forces leading to penetration, and the layers separate to admit a layer of adsorbate. On desorption, the layers are initially separated and their attractive interaction weakened, whereas the forces tending to separate them are high. The layers cannot come together until the amount of interlayer adsorbate, and thus swelling pressure, are substantially reduced. Therefore, a hysteresis loop is observed.

According to Brunauer (3, p. 409) the adsorption process probably causes a change in the pore volume which may be either reversible or irreversible. This may result in different pore arrangements in the external surfaces of the montmorillonite, and may account for the difference in the adsorption curves prior to a relative pressure of about 0.28 for the first and third cycles. X-ray diffraction data show that at a p/p_o of about 0.28 the basal spacing begins to increase rapidly with increasing p/p_o. In this region the adsorption curves begin their agreement, suggesting that the effect of the interlayer surfaces far outweighs that of the external surfaces.

The general shape of the adsorption and desorption isotherms (Fig. 7) is very similar to those presented elsewhere (1, 13, 23, 25). Figure 4 shows that the steeper portion between p/p_o of 0.25 and 0.45 in Figure 7 corresponds to the first increment of layer separation. The steeper portion of the isotherm, beginning at a p/p_o of 0.65, corresponds to the second increment of layer separation. The argument proposed by Barrer and MacLeod explains the form of the adsorption isotherm of this study. The initial water adsorbed is mainly confined to the external surfaces of the clay. After an approximate threshold pressure is reached, the water molecules penetrate more freely between clay sheets, and cause separation. With water vapor, a second stage of interlayer adsorption occurs and is reflected by the second steeper portion of the isotherm. As p/p_o approaches 1.0, capillary condensation occurs. The X-ray data show that a third increment of layer separation also occurs at high relative pressures.

The desorption isotherms show a pronounced dip in the relative pressure range of 0.65 to 0.30. This is also shown in data of others (13, 23, 25). Barrer and MacLeod attribute the steep portion of this dip to the removal of interlayer adsorbate; this process occurs at an approximate threshold pressure below that for the adsorption curve. X-ray data of the present study show that the basal spacing remains nearly constant at 16 Å in the relative pressure range 0.65 to 0.50, corresponding to the steep portion of the dip. This would indicate that the greater portion of the water being desorbed is from the external surfaces.

Barrer and MacLeod (23) observed hysteresis loops for the adsorption-desorption of nonpolar gases and vapors on their montmorillonite. Since these adsorbates were adsorbed only on external surfaces, the reasons given for hysteresis with polar adsorbates are not applicable. They suggest that when the clay is lubricated by a film of capillary condensate some of the clay particles are drawn by surface tension forces into a thixotropic structure. This more regular array then retains capillary condensed adsorbate more firmly than would a purely random array. When the film of condensate becomes sufficiently dilute it ceases to lubricate and hold the thixotropic structure together. The array then becomes more random again, and must give up the remaining condensate. The desorption isotherm becomes steeper and, with nonpolar adsorbates, closes the hysteresis loop.

In view of the X-ray data of the present study, it is proposed that the foregoing argument may be applied to the desorption of water vapor in the relative pressure range

of 0.65 to 0.50. The steep portion of the isotherm in this range is, therefore, due to the destruction of a thixotropic structure with its accompanying release of capillary condensed water. The X-ray data show that removal of the last layer of interlayer water corresponds to a steep portion of the desorption isotherm beginning at a p/p_o of about 0.30. The hysteresis explanations of Hirst (24) and of Barrer and MacLeod (23) are applicable in this region.

Figure 7 shows that the desorption branches for the first and third cycles do not come back to the initial q value, but that the desorption branch of the second cycle does reach this value. A possible explanation for the more complete desorption for the second cycle is proposed. Figure 7 shows a break in the second desorption curve at a relative pressure of about 0.25. At this point no vapor transfers were made for a period of 18 days, after which it was observed that the sample had desorbed more water and the relative pressure had increased as shown by the shift (dashed line) to a position lower and to the right. Two more days disclosed no additional change. The next vapor transfer caused a shift down and to the left (second dashed line) in one day. Before the 18 days with no vapor transfers, it appeared that the second desorption curve was approaching the path followed in the first run and later followed in the third cycle. However, after the idle period the desorption curve became steeper and the zero value of q was attained with relative ease. On the third run, with no prolonged nonvapor-transfer period, a special effort was made to reach the initial value of q. Even with a final pumping period extending over a period of three weeks, the value of q could not be brought substantially lower than that attained on the first run. This suggests that the remaining water was trapped in external pores (such as McBain's ink bottle pores) and/or in the interlayer regions. X-ray diffraction data (Fig. 4) indicate that at a relative pressure of 0.25 the last layer of interlayer water had started to be withdrawn. This is also shown by the data of Mooney et al. (10) and of Gillery (11) reproduced in Figure 5. The prolonged period of no vapor transfer may allow for particle rearrangement and for escape of water from pores and interlayer regions which would be blocked off by contraction of the mass on further desorption.

The behavior previously discussed for a prolonged nonvapor-transfer period would indicate that equilibrium was not attained in the 24-hr period between vapor transfers, at least in that region of the desorption isotherm. There was a similar nonvapor-transfer period of 20 days, at a relative pressure of 0.70 on the desorption curve, with no significant change in the location of the position observed 24 hr after the vapor transfer, indicating equilibrium was attained in 24 hr.

No relaxation of the type described here was observed for adsorption runs; 24 hr were enough for attainment of equilibrium.

Application of BET Theory

In the low pressure region, the Brunauer, Emmett and Teller theory of multimolecular adsorption (26) predicts the adsorption equation will be

$$\frac{p}{q(p_o - p)} = \frac{1}{q_m C} + \frac{C - 1}{q_m C}\frac{p}{p_o}$$

where q_m is the mass of vapor adsorbed when solid surface is covered by a monolayer, and C is a constant approximately equal to $e^{(E_1 - E_L)/RT}$, where E_1 is the heat of adsorption of the first layer and E_L is the heat of liquefaction of the vapor.

The values of the BET function, $\frac{p}{q(p_o - p)}$, calculated from the sorption isotherm data, are plotted against p/p_o for the three sorption cycles (Fig. 8). Generally, BET plots have a straight line region only between p/p_o of 0.05 to about 0.3 (27, p. 481). A fairly straight line is obtained for the adsorption data between p/p_o of 0.05 and 0.18. Comparison with the initial adsorption curve for basal spacings (Fig. 4) shows that at p/p_o of 0.18 the first increment of interlayer separation is just beginning. Therefore,

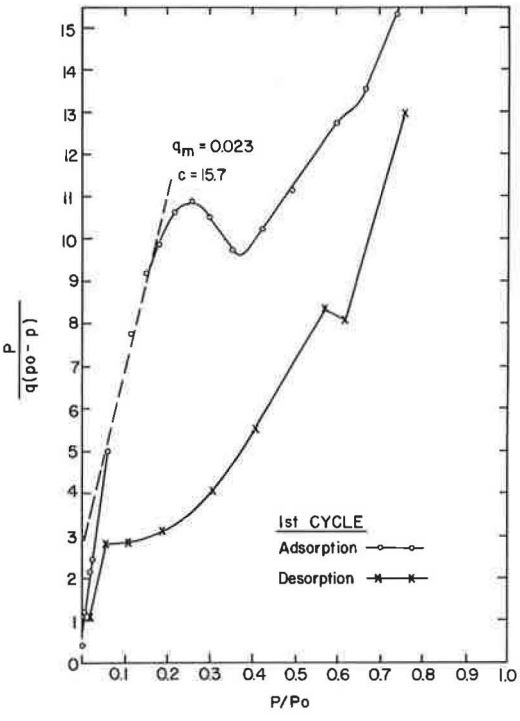

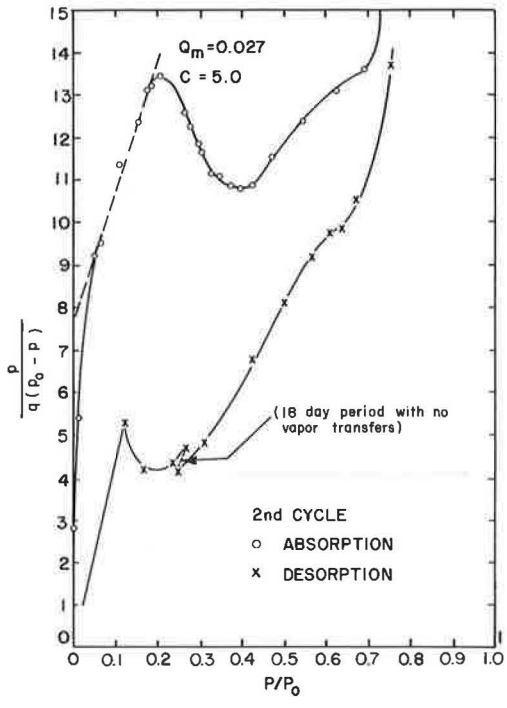

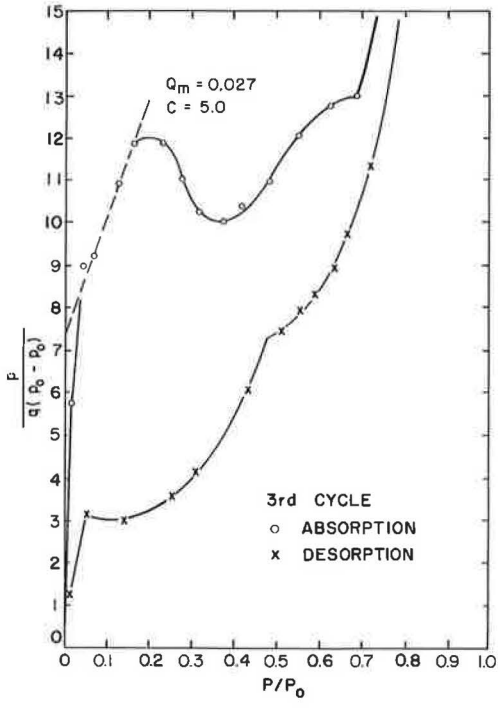

Figure 8. BET plots of sorption data for water vapor on sodium montmorillonite.

it was concluded the linear portion of the BET plot represents adsorption taking place predominantly on the external surfaces of the montmorillonite, and the BET parameters q_m and C represent the external surfaces (Fig. 8).

The present BET plots show a hump at a p/p_o of about 0.2 and another deflection point at a p/p_o of about 0.6 to 0.7. The X-ray data show that these values correspond with the initial portions of the first and second increments of expansion. Apparently this behavior is due to expansion making accessible surface areas not initially available for adsorption.

The pronounced hump at a p/p_o of 0.20 appears to be a characteristic which occurs only with sodium Wyoming montmorillonite (Volclay). The adsorption data of Hendricks et al. (6) for sodium Wyoming montmorillonite (Volclay) yield a similar hump, whereas their data for sodium Mississippi and California montmorillonites do not. The data of Johansen and Dunning for sodium Wyoming montmorillonite (Volclay) would seem to be an exception; however, their data (25, Fig. 2) show no experimental observations in the p/p_o range in which the hump occurs. Also, the q_m value of 0.056 obtained from their data is in very good agreement with values of 0.054, 0.058 and 0.055 obtained if the present BET plots in the p/p_o range of 0.4 to 0.6 are extrapolated back to low pressures. Orchiston's data for sodium Arizona montmorillonite (28) show a high point on the BET plot at a p/p_o of 0.05. This may represent a behavior similar to that observed more clearly with the present data (i.e., adsorption on external surfaces before penetration of water between clay layers) and may indicate that expansion begins at an appreciably lower relative pressure than for the Wyoming material.

External Surface Area. —If the area, s, of the adsorbent surface occupied by each water molecule of the monolayer is known, the parameter q_m could be used to determine the external surface area, A_e, per gram of montmorillonite by the expression:

$$A_e = \frac{Nq_m s}{M}$$

where N is Avogadro's constant, M is the molecular weight of the adsorbate, and q_m is expressed per gram of adsorbent. If the water molecules are in a closest packing arrangement, s is equal to 10.8 Å^2. However, other investigators have suggested other spatial geometric arrangements which result in other than closest packing for the monolayer coverage. The arrangement of Hendricks and Jefferson (5) gives an area of about 11.5 Å^2; the basal plane of ice structures of Macey (17), Forslind (18) and Demirel (1) give an area of about 17.5 Å^2. External surface areas per gram of sodium montmorillonite, A_e, were computed using each of the foregoing areas for the water molecule and the q_m values obtained from the adsorption data (Table 2). The external area increased somewhat during the first adsorption-desorption cycle; the sorption process may result in different pore shapes and volumes in the external surfaces and in different arrangements of the surfaces, thus making more area available for adsorption. The external areas obtained are larger than those reported by others as determined from nitrogen adsorption, i.e., 41 to 71 m^2/gm by Emmett et al. (29), 33 m^2/gm by Mooney

TABLE 2

EXTERNAL SURFACE AREAS PER GRAM OF SODIUM MONTMORILLONITE CALCULATED FROM WATER VAPOR ADSORPTION DATA

Cross-Sectional Area per Water Molecule, Å^2	External Surface Area, A_e (m^2/gm)		
	First Cycle q_m = 0.023	Second Cycle q_m = 0.027	Third Cycle q_m = 0.028
10.8	83.0	97.4	101.1
11.5	88.3	88.3	107.7
17.5	134.4	157.8	163.7

et al. (13), 38 m^2/gm by Johansen and Dunning (25) and 24.5 m^2/gm by Zettlemoyer et al. (30). This indicates some portions of the external surfaces are accessible to water vapor but not to nitrogen. Also, the line width data of Figure 4 show that there may be a small amount of water penetration into interlayer regions.

Heat of Adsorption. —The C parameters obtained in this study were used to calculate $E_1 - E_L$ values for the first monolayer of water adsorbed on external surfaces. The values, corrected according to Clampitt and German (31), were 3.3, 2.7 and 2.7 K cal/mole and were in good agreement with values reported elsewhere (1, 28). Calculations from the calorimetric heat of immersion data of Zettlemoyer et al. (30) yielded $E_1 - E_L$ values of 3.0 to 3.7 K cal/mole for the first monolayer on external surfaces.

The heat of adsorption curve presented by Zettlemoyer et al. (30, Fig. 4) from their heat of immersion and adsorption isotherm data does not show good agreement with isosteric heat of desorption isotherm data curve of Mooney et al. (13, Fig. 5) from desorption isotherm data. It does, however, show good agreement with the isosteric heat of adsorption data of Takizawa (32) from adsorption isotherms with Niigata bentonite. This may indicate that the adsorption isotherm is nearer the true equilibrium curve than the desorption isotherm.

Free Energy Changes

Free Energy of Wetting. —The free energy of wetting of sodium montmorillonite may be given as (1):

$$\Delta F = (\gamma_{sl} - \gamma_{so}) + \alpha\Delta V$$

where γ_{sl} is the solid-liquid interfacial tension, γ_{so} the surface tension of the solid in vacuum, α the interlayer surface area per cm^2 of total surface, and ΔV the free energy change per cm^2 of interlayer surface due to separation of layers against the force of interaction. To calculate ΔF from the adsorption isotherms, Bangham's free energy equation (33) was used; it can be expressed as:

$$-\frac{RT}{MA}\int_0^1 \frac{q}{p/p_o}\, d(p/p_o)$$

where R is the gas constant, T the absolute temperature, M the molecular weight of water, and A the specific surface of sodium montmorillonite. Figure 9 plots $q/(p/p_o)$ vs p/p_o for graphical integration of the foregoing equation. From crystallographic data, A was determined to be 748 m^2/gm for the sodium montmorillonite. The error in values of ΔF obtained was estimated to be about ±6 percent. The free energies of wetting thus determined were -40.55 ± 2.43, -36.15 ± 2.17 and -37.50 ± 2.24 ergs/cm^2 for the first, second and third adsorption runs. These values are in good agreement with that of -34.76 ± 1.91 ergs/cm^2 determined earlier for sodium montmorillonite (1).

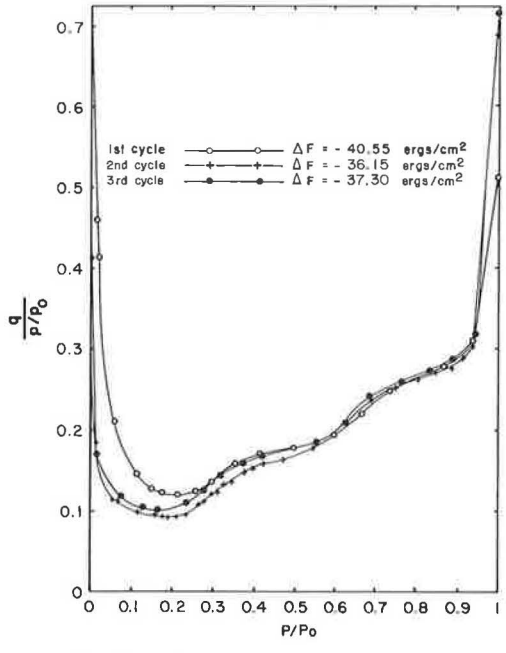

Figure 9. Plots for integration of Bangham's free energy equation for water vapor adsorption on sodium montmorillonite.

Free Energy Changes on Adsorption. —Fu and Bartell (34), in their paper on the

surface areas of porous adsorbents, evaluated the integral

$$-\frac{RT}{M}\int_0^{p/p_o}\frac{q}{p/p_o}\,d(p/p_o)$$

at various values of p/p_o for the adsorption of vapors on porous solids. When q is the mass of vapor adsorbed per gram of solid, the value obtained is the free energy change, $A\Delta F$ in ergs/gm of solid, for adsorption from a relative pressure of zero to p/p_o. When log ($A\Delta F$) was plotted against log (p/p_o), two straight-line portions were obtained.

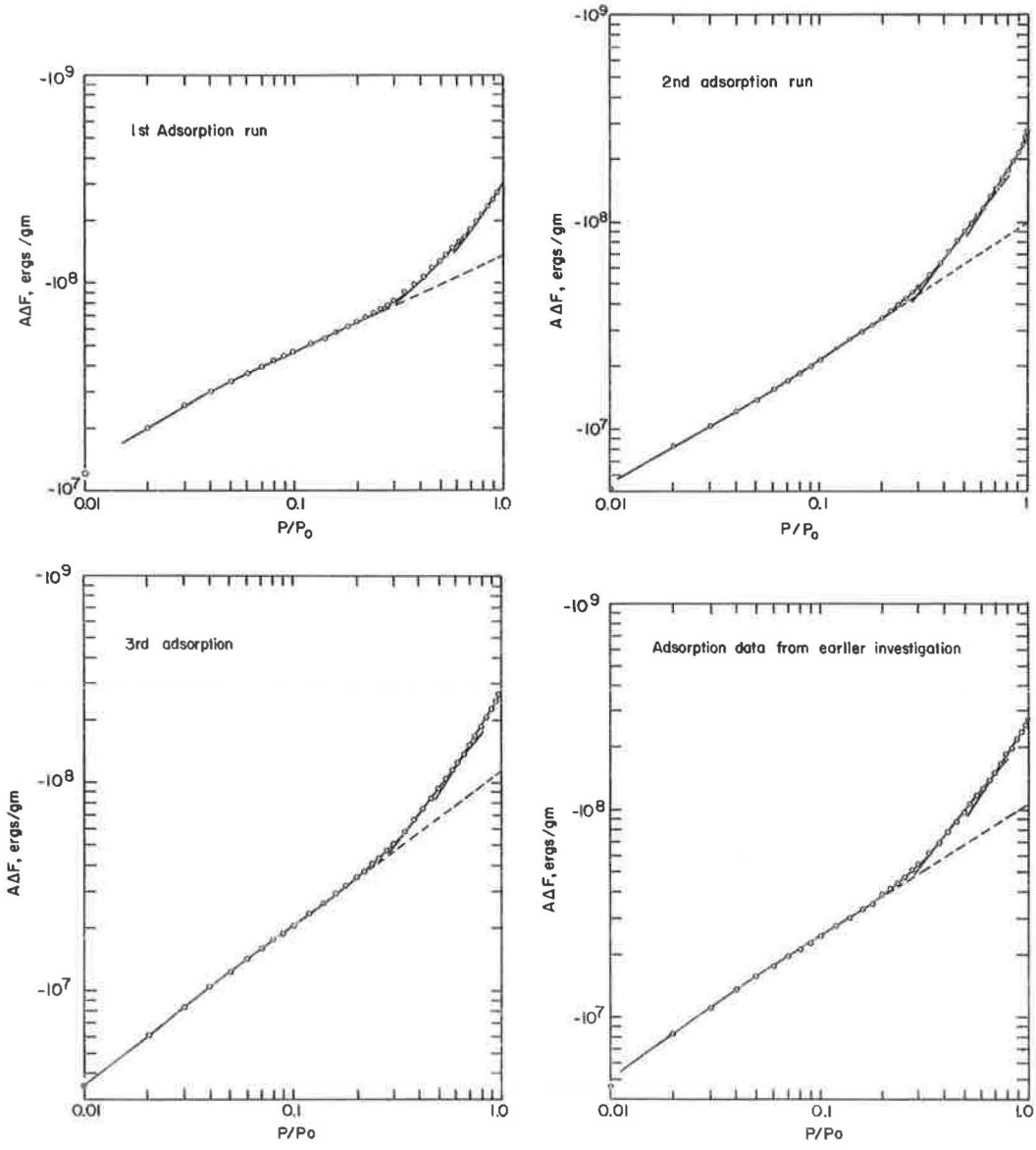

Figure 10. Log-log plots of free energy change vs relative pressure.

In discussing their method, Fu and Bartell state: "It is also conceivable that, with suitable interpretations, this method can be utilized to study the expansion or deformation of porous materials caused by the adsorption of various vapors." Sodium montmorillonite is a porous material which undergoes expansion with adsorption of water vapor; therefore, it was felt that an analysis similar to that of Fu and Bartell may be instructive. The values of the previously cited integral for increasing increments of p/p_o, up to and including the saturation point, for the adsorption data of the present study were determined by graphical integration. This was also done with the adsorption data obtained earlier for sodium montmorillonite (1). Values of the integrals, $A\Delta F$, were thus obtained for four complete adsorption runs involving two separate samples of the material.

Plots of log ($A\Delta F$) vs log (p/p_o) are shown in Figure 10 for each run. Each of the plots displays three straightline portions (implying equations of the type $A\Delta F = \alpha(p/p_o)^\beta$ for various portions) rather than the two obtained by Fu and Bartell. The portions of the plots below p/p_o of about 0.05 are not strictly linear, but show breaks in the slopes in the p/p_o range of 0.045 to 0.055. This is in agreement with the observations of Fu and Bartell, who reported nonlinearity below p/p_o of 0.05 and attributed it to the decreased accuracy in determining q values at very low pressures.

Comparison of Figure 10 with the X-ray data for the initial adsorption run reveals that the break in the log ($A\Delta F$) plot at a p/p_o of 0.16 to 0.18 corresponds closely with the beginning of an increase in the basal spacing from 9.8 Å. The break at a p/p_o of about 0.65 corresponds quite closely with the beginning of a second increment of expansion from a basal spacing of 12.5 Å; the break at a p/p_o of 0.95 corresponds closely with the beginning of the third increment of expansion from a basal spacing of about 15.5 Å. The last two breaks also correspond very well with observed minima in the line width plot of Figure 4; these minimum line widths indicate the majority of the clay platelets have the basal spacing noted. On the basis of these correlations it was concluded that the portion of the log ($A\Delta F$) vs log (p/p_o) plot below p/p_o of 0.16 to 0.18 reflects the energy changes due to adsorption on external surfaces only; at higher pressures energy changes due to adsorption on the internal surfaces are included and reflect the energy of interaction between clay platelets. The slope changes apparently reflect the differences in platelet interaction energies at increasing increments of expansion.

Fu and Bartell (34) attributed the change of slope in their plots to capillary condensation in the pores of the adsorbent. In the present system capillary condensation probably occurs in external pores in the higher relative pressure range, but its effect on the energy changes is apparently masked by those effects caused by adsorption on the internal surfaces. According to Barrer and MacLeod (23), capillary condensation of water between montmorillonite particles does not occur until the relative pressure approaches 1.0.

The relation between the free energy change and separation of clay platelets is shown in Figure 11. The values of $A\Delta F$ for the first adsorption run are plotted against platelet separation h, at the same p/p_o, obtained from the X-ray diffraction data; $A\Delta F$ data for the other adsorption runs produce similar plots. Figure 11 shows sharp breaks corresponding closely with the slope changes in Figure 10. Also, the breaks occur when h values are very nearly integral multiples of 2.8 Å, the thickness of a water molecule. This gives additional evidence that the interlayer water builds up in a laminar fashion.

Expansion Energies. —If the free energy changes could be divided into two components, one for adsorption on external surfaces and another for adsorption on internal surfaces, it would be possible to evaluate the expansion energies, i.e., the free energy change due to adsorption on, and separation of, the internal surfaces.

The free energy change brought about by the adsorption, on a solid surface, of a film at equilibrium with a vapor at some pressure, p, may be expressed as (27, p. 264)

$$\Delta F = \gamma_{SV} - \gamma_{SO} \text{ ergs/cm}^2 \qquad (1)$$

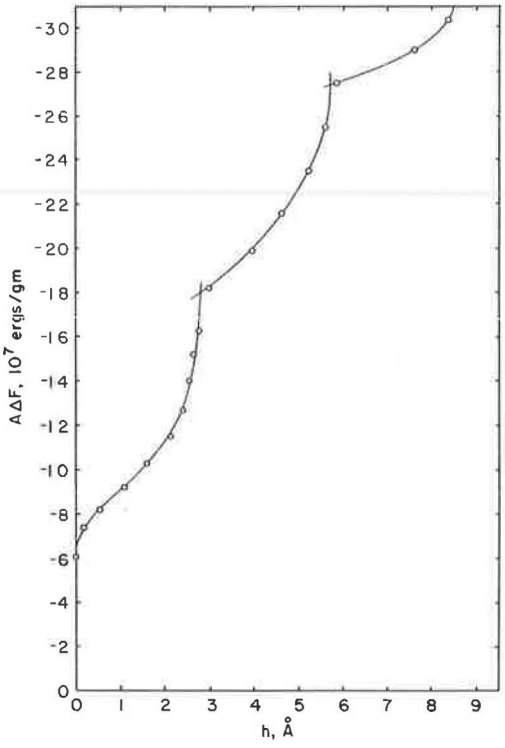

Figure 11. Plot of total free energy change vs interlayer separation, first adsorption run.

where γ_{so} is the surface free energy of the solid surface in vacuum, and γ_{sv} is that of the solid-vapor interface in equilibrium at pressure p. When the solid-vapor interface is in equilibrium with the saturated vapor, the free energy change is

$$\Delta F = \gamma_{svo} - \gamma_{so} \text{ erg/cm}^2 \qquad (2)$$

where γ_{svo} is the surface free energy of the solid-vapor interface at the saturation pressure. According to Jura and Harkins (35), when the solid is wetted by the liquid, γ_{svo} is equal to $(\gamma_{sl} + \gamma_{lv})$; γ_{sl} is the solid-liquid interfacial free energy and γ_{lv} is the surface free energy of the liquid in equilibrium with its own vapor. We have, therefore, at saturation

$$\Delta F = \gamma_{sl} - \gamma_{so} + \gamma_{lv} \text{ ergs/cm}^2 \qquad (3)$$

If capillary condensation occurs, the γ_{lv} term drops out of Eq. 3. For the present system adsorption occurs only on the external surfaces of the clay at low relative pressures. Since only external areas, A_e, are involved, the free energy change is given by

$$A_e\Delta F = A_e\ (\gamma_{sv} - \gamma_{so}) \text{ ergs/gm} \qquad (4)$$

If only the external areas were available for adsorption over the entire relative pressure range, it is proposed that the relationship $A_e\Delta F = \alpha(p/p_o)^\beta$ would continue to be obeyed. Under these circumstances, the linear portion of the log ($A\Delta F$) vs log (p/p_o) plot between p/p_o of 0.05 to 0.18 would be extended to a p/p_o of 1, as shown by the dashed lines (Fig. 10). The free energy change at saturation would be

$$A_e\Delta F = A_e\ (\gamma_{sl} - \gamma_{so} + \gamma_{lv}) \text{ ergs/gm} \qquad (5)$$

If capillary condensation were to occur (still only external surfaces available), a behavior such as that observed by Fu and Bartell (34) could be expected, and the free energy change at saturation would be reduced by $A_e\gamma_{lv}$. With the present system this probably occurs very near the saturation pressure.

On the basis of the previous discussion, the free energy changes due to adsorption on external and on internal surfaces were divided, at least to very near saturation, in Figure 10 by extending the linear portions of the plots corresponding to adsorption only on external surfaces to the saturation pressure. The difference between $A\Delta F$ and $A_e\Delta F$ gives the free energy change, $A_i\Delta F = A_i\phi$, where A_i is the internal surface area per gram and ϕ is the expansion energy per cm^2 of internal surface and given by

$$\phi = \gamma_{sv} - \gamma_{so} + \Delta V \qquad (6)$$

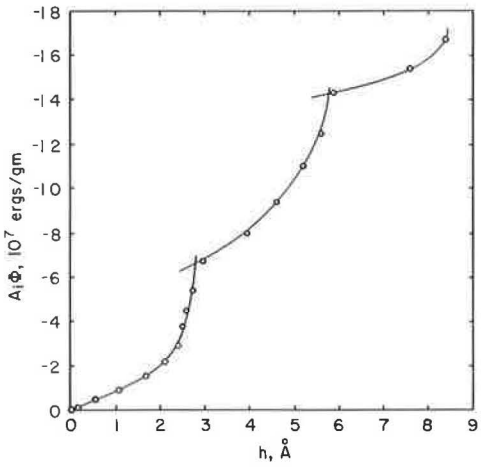

Figure 12. Plot of free energy change due to adsorption on, and separation of, internal surfaces vs interlayer separation, first adsorption run.

where ΔV is the free energy change per cm^2 of internal surface due to separation of layers against the force of interaction.

Figure 12 plots $A_i\phi$ for the first adsorption run vs platelet separation, h. Values of $A_i\phi$ obtained from data of other runs produce very similar plots. The free energy change due to adsorption of the second molecular layer of interlayer water is as great as or slightly greater than that for adsorption of the first layer. The free energy change for formation of the third layer of interlayer water is substantially less than for the other two. The term, ϕ, for adsorption of the first layer of interlayer water is the free energy change due to disappearance of a solid surface and the formation of a solid-film interface, plus that due to separation against the force of interaction between platelets. The latter term will decrease the magnitude of the free energy change. The second layer of water must penetrate between the first and the clay surface. No new surfaces are formed nor do any disappear. The free energy change is due to extension of the film thickness and to expansion against the interaction forces. The free energy change due to extension of the film thickness is probably less than that for disappearance of solid surfaces and formation of solid-film interface; however, since the platelet separation is greater, the force of interaction is less and so the free energy change for formation of the second layer may be nearly the same as that for the first. The third layer of water may penetrate between the clay surface and existing interlayer water, but most probably enters between the first and second layer. Again, no new surfaces appear or disappear. The free energy change is due to extension of the film thickness and to expansion against forces of interaction further reduced by increased platelet separation. Since the free energy change on adsorption of the third layer is considerably less than that for the second, the change due to penetration between the first and second layers of water must be less than that for penetration between the clay surface and a water layer.

Swelling Pressures. —Roderick and Demirel (2), in an earlier study, suggested that there was a correlation between free energy data and swelling pressures exerted by montmorillonites. An estimate of the pressure required to prevent separation of clay platelets due to penetration of water between layers (or the swelling pressure exerted by the clay on uptake of interlayer water) was attempted using the basal spacing and free energy data of the present study.

At constant temperature, and assuming all work to be pressure-volume work, we have for free energy:

$$dF = Vdp \tag{7}$$

where V is the molar volume and p is the external pressure. For the present system, Eq. 7 becomes:

$$A_i d\phi = Vdp$$

Assuming water is incompressible, the latter equation can be put into the following form:

$$d\phi = \frac{V}{A_i} dp = h_o\, dp \tag{8}$$

where ϕ is the expansion energy (change in free energy due to adsorption on, and separation of, interlayer surfaces) per cm^2; V is the total volume of interlayer water at saturation pressure per gram of sodium montmorillonite; h_o is the maximum platelet separation; and p is the applied pressure. From Eq. 8 we obtain

$$A_i \int_{\phi = \phi_s}^{\phi} d\phi = A_i \int_{p = 0}^{p} h_o \, dp \tag{9}$$

or

$$A_i\phi - A_i\phi_s = A_i h_o p \tag{10}$$

or

$$p = \frac{A_i\phi - A_i\phi_s}{h_o A_i} \tag{11}$$

where ϕ_s is the expansion energy when the clay is in equilibrium with saturated water vapor, p is the pressure required to prevent any platelet separation, and p = 0 is the pressure when the maximum separation is reached. The platelet separation is a function of ϕ as shown in Figure 12. The pressure required to prevent expansion beyond a certain separation h, when the sodium montmorillonite is in contact with saturated water vapor, may be obtained by determining the difference between $A_i\phi$ and $A_i\phi_s$ corresponding to separations h and h_o, respectively, and dividing the difference by maximum separation h_o. The results determined have the dimensions ergs/cm-gm, and must be divided by the internal surface area, A_i, to give the pressure in dynes/cm^2. Table 2 gives the external areas, A_e, determined for the first adsorption run by using various cross-sectional areas for the water molecule and the BET parameter q_m. Subtracting A_e from the total surface area of 748 m^2/gm (from crystallographic data) gives the

TABLE 3

EXPANSION ENERGIES AND SWELLING PRESSURES DUE TO ADSORPTION OF WATER VAPOR ON INTERLAYER SURFACES OF SODIUM MONTMORILLONITE[a]

Interlayer Water	Area Assigned to a Water Molecule (Å^2)	Internal Surface Area, A_i (m^2/gm)	Expansion Energy (ergs/cm^2)	Swelling Pressure, p (dynes/cm^2)	Swelling Pressure, p (tons/ft^2)
None present	10.8	665	—	300×10^6	313
	11.5	660	—	302×10^6	315
	17.5	614	—	325×10^6	339
One molecular layer	10.8	665	-9.8	181×10^6	190
	11.5	660	-9.8	184×10^6	192
	17.5	614	-10.6	197×10^6	206
Two molecular layers	10.8	665	-21.1	45×10^6	47
	11.5	660	-21.2	46×10^6	48
	17.5	614	-22.8	50×10^6	52
Three molecular layers	10.8	665	-24.8	—	—
	11.5	660	-25.0	—	—
	17.5	614	-26.9	—	—

[a]From the separation indicated from the maximum separation.

internal surface area A_i per gram. The values of A_i for the various water molecular areas were determined and used to calculate the swelling pressures at various interlayer spacings. The results are indicated in Table 3. Also presented are values for the expansion energy, ϕ, obtained from Figure 12. The difference in the values obtained with various internal surface areas is probably less than the error due to the approximations of the methods for evaluation of the expansion energies and swelling pressures.

The expansion energy values at saturation may be due in part to capillary condensation in external pores. This would tend to make the values given when three molecular layers of water are present somewhat larger than the actual case. The expansion energies given for the adsorption of the first two layers of water are not affected by capillary condensation because it occurs near the saturation pressure.

Since the swelling pressures were obtained from the saturation point, any capillary condensation effects would tend to make the listed values somewhat larger than those due only to adsorption on internal surfaces. This may affect the values of swelling pressure when two layers of interlayer water are present to some degree, but would probably be negligible when compared with the large swelling pressures at lower interlayer water contents. Mielenz and King (36) reported swelling pressures from 2 to 11 tons/ft^2 for sodium montmorillonite in consolidometer tests. The present data suggest the pressures they obtained were due to hydration above two layers of interlayer water.

The swelling pressures given in Table 3 are those exerted when the sodium montmorillonite is in contact with saturated water vapor; the maximum observed interlayer separation is in equilibrium with the saturated vapor. If the sodium montmorillonite were in contact with liquid water, further expansion would occur and comparatively smaller swelling pressures might develop. In this region, for separation beyond three or four molecular layers of water, the surface hydration energies are no longer important and the smaller electrical double-layer forces become the major repulsive force between platelets (37). The further expansion exerting comparatively low additional pressure may be explained by attributing it to a low energy barrier (1).

CONCLUSIONS

The sorption isotherm data and X-ray diffraction data for water vapor adsorption and desorption by sodium montmorillonite, and data from the literature, indicate the following.

1. The change in average basal spacings of sodium montmorillonite takes place in a continuous but nonuniform manner with changes in relative pressure. Continuity is due to the simultaneous existence of varying numbers of molecular layers of interlayer water. Expansion occurs in three increments. Basal spacing and line width data show that average spacings correspond with an integral number of molecular layers of water just before each increment of expansion.
2. The relationship between relative humidity and the basal spacing of sodium montmorillonite is dependent on: (a) the source and method of preparation of the sample; (b) the initial conditions of the sample at the start of tests; and (c) whether data are collected during adsorption or desorption.
3. Basal spacing, line width, and free energy change data give evidence that the interlayer water builds up in a laminar manner.
4. Adsorption isotherms are more closely reproduced on successive adsorption-desorption runs than desorption isotherms.
5. The hysteresis displayed by the sorption isotherms is due in part to the formation of a thixotropic structure at high relative pressures, and in part to attractive interaction forces between sodium montmorillonite platelets.
6. X-ray diffraction data and BET plots indicate that the BET parameter, q_m, obtained reflects adsorption only on the external surfaces of the sodium montmorillonite. Apparently sodium montmorillonite prepared from Wyoming bentonite is unique in this respect.
7. The relationship between free energy changes and relative pressure and the X-ray diffraction data for the adsorption of water vapor by sodium montmorillonite allows sep-

aration of the free energy change into two components: one due to adsorption of the external surfaces, and one due to adsorption on, and separation of, the internal surfaces.

8. Free energy data and X-ray data show that the expansion energy (free energy change due to adsorption on, and separation of, internal surfaces) during formation of the second layer of interlayer water is approximately the same as that for formation of the first layer. The change during formation of the third layer is substantially less than those for the other two.

9. Free energy data and X-ray data permit the estimation of swelling pressures exerted by sodium montmorillonite due to the uptake of interlayer water when the material is in contact with saturated vapor. The swelling pressure exerted when the platelet separation is zero is about 325 tons/ft^2. The pressure exerted when one molecular layer of water separates clay platelets is about 200 tons/ft^2. The pressure exerted when two molecular layers of water separate platelets is about 50 tons/ft^2.

ACKNOWLEDGMENTS

The research reported herein was done at the Iowa Engineering Experiment Station, Iowa State University, under Project 505-S, Chemical Stabilization and Physico-Chemical Properties of Soils. This project was sponsored by the Iowa Highway Research Board under Project HR-97 and was supported with funds from the Iowa State Highway Commission and the U. S. Bureau of Public Roads.

REFERENCES

1. Demirel, T. Adsorption of Water Vapor by Sodium and Calcium Montmorillonite. Unpublished Ph. D. thesis, Iowa State Univ. of Sci. and Tech., 1962.
2. Roderick, G. L., and Demirel, T. Expansion of Montmorillonite Due to Adsorption of Water Vapor. Iowa Acad. of Sci. Proc. 70, pp. 280-289, 1963.
3. Brunauer, S. The Adsorption of Gases and Vapors. Physical Adsorption. Princeton, N. J., Princeton Univ. Press, 1943.
4. Klug, H. P., and Alexander, L. E. X-ray Diffraction Procedures for Polycrystalline and Amorphous Materials. New York, John Wiley and Sons, Inc., 1954.
5. Hendricks, S. B., and Jefferson, M. E. Structure of Kaolin and Talc-Pyrophyllite Hydrates and Their Bearing on Water Sorption of Clays. American Mineralogist Vol. 23, pp. 863-875, 1938.
6. Hendricks, S. B., Nelson, R. A., and Alexander, L. T. Hydration Mechanism of the Clay Mineral Montmorillonite Saturated with Various Cations. American Chem. Soc. Jour. Vol. 62, pp. 1457-1464, 1940.
7. MacEwan, D. M. C., Amil, A. R., and Brown, G. Interstratified Clay Minerals. In Brown, G., ed., The X-ray Identification and Crystal Structures of Clay Minerals. London, Mineralogical Soc., pp. 393-445, 1961.
8. Johns, W. D., Grim, R. E., and Bradley, W. F. Quantitative Estimations of Clay Minerals by Diffraction Methods. Jour. of Sedimentary Petrology, Vol. 24, pp. 242-251, 1954.
9. Milne, I. H., and Warshaw, C. M. Methods of Preparation and Control of Clay Mineral Specimens in X-ray Diffraction Analysis. National Conf. on Clays and Clay Minerals, Proc. 4, pp. 22-30, 1956.
10. Mooney, R. W., Keenan, A. G., and Wood, L. A. Adsorption of Water Vapor by Montmorillonite. II—Effect of Exchangeable Ions and Lattice Swelling as Measured by X-ray Diffraction. Amer. Chemical Soc. Jour. Vol. 74, pp. 1371-1374, 1952.
11. Gillery, G. H. Adsorption-Desorption Characteristics of Synthetic Montmorilonoids in Humid Atmospheres. Amer. Mineralogist Vol. 44, pp. 806-818, 1959.
12. Messina, M. L. Expansion of Fractional Montmorillonites Under Various Relative Humidities. Clays and Clay Minerals, Vol. 19, pp. 617-632, 1964.
13. Mooney, R. W., Keenan, A. G., and Wood, L. A. Adsorption of Water Vapor by Montmorillonite. I—Heat of Desorption and Application of BET Theory. Amer. Chem. Soc. Jour. 74, pp. 1367-1371, 1952.
14. Grim. R. E. Clay Mineraology. New York, McGraw-Hill, 1953.

15. Winterkorn, H. F. The Science of Soil Stabilization. Highway Research Board Bull. 108, pp. 1-24, 1955.
16. Pauling, L. The Nature of the Chemical Bond. Ithaca, N. Y., Cornell Univ. Press, 1960.
17. Macey, H. H. Clay-Water Relationships and the Internal Mechanism of Drying. Ceramic Soc. Trans. 41, pp. 73-121, 1942.
18. Forslind, E. Crystal Structure and Water Adsorption of Clay Minerals. Swedish Cement and Concrete Res. Inst. Bull. 11, pp. 1-20, 1948.
19. Barshad, I. The Nature of Lattice Expansion and Its Relation to Hydration in Montmorillonite and Vermiculite. Amer. Mineralogist 34, pp. 675-684, 1949.
20. Brindley, G. W. X-ray Diffraction by Layer Lattices with Random Layer Displacements. In Brown, G., ed. The X-ray Identification and Crystal Structures of Clay Minerals, London, Mineralogical Soc., pp. 446-466, 1961.
21. McBain, J. W. An Explanation of Hysteresis in the Hydration and Dehydration of Gels. American Chem. Soc. Jour., Vol. 57, pp. 699-700, 1935.
22. Foster, A. G. The Sorption of Condensible Vapors by Porous Solids. I—The Applicability of the Capillary Theory. Faraday Soc. Trans. 28, pp. 645-657, 1932.
23. Barrer, R. M., and MacLeod, D. M. Intercalation and Sorption by Montmorillonite. Faraday Soc. Trans. 50, pp. 980-989, 1954.
24. Hirst, W. The Mechanical Interaction Between Mobile Insoluble Adsorbed Films, Capillary Condensed Liquid and Fine-Structured Solids. Faraday Soc. Discussions 3, pp. 22-28, 1948.
25. Johansen, R. T., and Dunning, H. N. Water-Vapor Adsorption on Clays. National Conf. on Clays and Clay Minerals, Proc. 6, pp. 249-258, 1959.
26. Brunauer, S., Emmett, P. H., and Teller, E. Adsorption of Gases in Multimolecular Layers. Amer. Chem. Soc. Jour. 60, pp. 309-319, 1938.
27. Adamson, A. W. Physical Chemistry of Surfaces. New York, Intersci. Pub., Inc, 1960.
28. Orchiston, H. D. Adsorption of Water Vapor. III—Homoionic Montmorillonites at 25° C. Soil Sci. 79, pp. 71-78, 1955.
29. Emmett, P. H., Brunauer, S., and Love, K. S. The Measurement of Surface Area of Soils and Soil Colloids by the Use of Low Temperature van der Waals Adsorption Isotherms. Soil Sci. 45, pp. 57-65, 1938.
30. Zettlemoyer, A. C., Young, G. J., and Chessick, J. J. Studies of the Surface Chemistry of Silicate Minerals. Jour. of Physical Chem., Vol. 59, pp. 962-966, 1955.
31. Clampitt, B. H., and German, D. E. Heat of Vaporization of Molecules at Liquid Vapor Interfaces. Jour. of Physical Chem., Vol. 62, pp. 438-440, 1958.
32. Takizawa, M. Mechanism of Water Vapor Adsorption on Bentonite. Tokyo Inst. of Physical and Chem. Res. Sci. Papers Vol. 54, pp. 313-322, 1960.
33. Bangham. D. H. The Gibbs Adsorption Equation and Adsorption on Solids. Faraday Soc. Trans. 33, pp. 805-811, 1937.
34. Fu, Y., and Bartell, F. E. Surface Area of Porous Adsorbents. Jour. of Physical and Colloid Chem. 55, pp. 662-675, 1951.
35. Jura, G., and Harkins, W. E. Determination of the Decrease of Free Surface Energy of a Solid by an Adsorbed Film. American Chem. Soc. Jour. 66, pp. 1356-1362, 1944.
36. Mielenz, R. C., and King, M. E. Physical-Chemical Properties and Engineering Performance of Clays. State of California Dept. of Natural Res., Div. of Mines Bull. 169, pp. 196-254, 1955.
37. van Olphen, H. An Introduction to Clay Colloid Chemistry. New York, Intersci. Publ., 1963.

Behavior of Soil-Cement in Repeated Compression and Flexure

CHIH-KANG SHEN, Assistant Professor of Civil Engineering, Loyola University of Los Angeles*; and
JAMES K. MITCHELL, Associate Professor of Civil Engineering and Associate Research Engineer, Institute of Transportation and Traffic Engineering, University of California, Berkeley

•RECENT field evaluations (7, 10) have shown consistently that flexible pavements containing cement-treated layers give better performance under traffic loads than untreated gravel bases of the same thickness. Nussbaum and Larsen (14) established from the results of plate load tests that untreated granular bases may deflect from 1.5 to 3.3 times as much under a given load as an equal thickness of soil-cement. In rigid pavements cement-treated bases reduce the hazardous effect of pumping at the joints. In addition, Childs (3) has shown that for constant edge deflection an 8-in. concrete slab bonded to a 5-in. cement-treated base was able to support 200 percent of the load carried by the 8-in. slab on a 5-in. gravel subbase.

The quality design (i.e., treatment level, compaction conditions, etc.) of stabilized soils is usually based on tests such as unconfined compression, California bearing ratio, and the Hveem stabilometer for strength; and wet-dry and freeze-thaw for durability. Strength evaluations of this type all make use of static loading conditions. There is very little knowledge of the behavior of stabilized soils under dynamic loading conditions. It is well known, however, that the properties of most materials can be significantly altered, and, in fact, failure due to fatigue may result under the action of repeated subfailure stresses with intensities less than the static strength of the material.

Although investigations of the resilience characteristics of compacted subgrade soils under triaxial repeated loading tests have been reported by Seed et al. (16, 17, 18, 19, 22, and 23) and Ahmed and Larew (1), among others, and the resilient characteristics of unbound granular base courses have been investigated by Mitry (13), Biarez (2), Trollope, Lee and Morris (24), and others, knowledge of the resilience characteristics of cement-stabilized soils is limited. (In accordance with the terminology introduced by Hveem (11), recoverable deformations are referred to in this paper as resilient deformations, and the corresponding moduli as resilient moduli.)

Recent advances in the application of Burmister's three layer elastic theory to problems of pavement analysis and design (4, 5, 12, and 15) make knowledge of the elastic properties of cement-stabilized soils all the more important. Values of properties as determined by dynamic tests may be quite different from those determined by conventional static tests. Layered-theory approaches deal primarily, however, with stresses and strains generated in the pavement structure under the action of moving loads. Thus there is need for additional information concerning soil-cement behavior under the action of repeated dynamic stresses.

This paper presents the results of an investigation of the behavior of soil-cement subjected to repeated loads of subfailure magnitude in both compression and flexure and of the resultant effects on strength and deformation properties.

---

*Formerly Assistant Specialist, Institute of Transportation and Traffic Engineering, University of California, Berkeley.

Paper sponsored by Committee on Soil-Portland Cement Stabilization and presented at the 45th Annual Meeting.

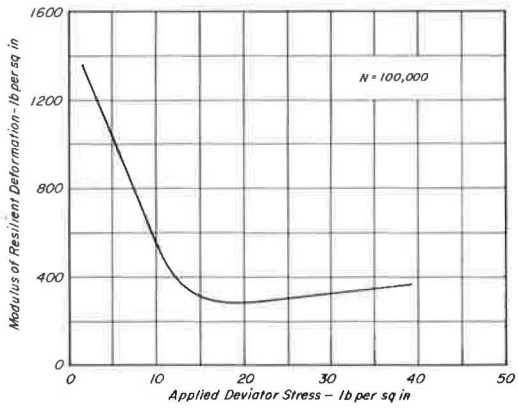

Figure 1. Effect of stress intensity on resilience characteristics, AASHO Road Test subgrade soil (23).

PREVIOUS WORK

Previous studies of untreated soils and base-course materials under the action of repeated compressive stresses have shown that such factors as stress history, frequency and intensity of repeated stress, and number of load repetitions may influence the properties significantly. In a detailed investigation of the resilience characteristics of compacted subgrade soils Seed, Chan, and Lee (23) established the importance of the following factors.

1. Number of load applications. The resilient deformation varied with the number of load applications, and the greatest value occurred between one and 5,000 applications, depending on the initial conditions of the soil.

2. Applied repeated loading stress intensity. The resilient deformation of compacted clay varies with the magnitude of the applied deviator stress intensity. At low stress intensities the resilient modulus of AASHO Road Test subgrade soil decreased rapidly with increasing values of the deviator stress (Fig. 1). At deviator stresses greater than 15 psi, the resilient modulus increased slightly with increasing deviator stress. This increase of modulus with increased stress was attributed to the densification of the sample under high repeated loading stress intensities.

3. Method of compaction. Samples compacted wet of optimum water content using a method producing a dispersed structure (e.g., kneading) showed larger resilient deformations and lower moduli than samples compacted using a method producing a flocculent structure (e.g., static).

In the case of cohesionless soils, confining pressure may influence resilient modulus significantly. Trollope et al. (24) observed that the modulus of resilient deformation increased with an increase in confining pressure, and was independent of the applied stress level for a sand subjected to slow repeated cyclic loads.

Mitry (13) found, from triaxial repeated loading tests on dry granular material, that the modulus of resilient deformation varied with the effective confining pressure according to the equation, $E = K \cdot \sigma_3^n$, where K and n are constants, depending on the material investigated, and σ_3 is the effective confining pressure, in psi. He found K = 12,500 and n = 0.35 for Monterey sand and K = 7,000 and n = 0.55 for gravel.

The properties of cement-stabilized soils under static loading conditions and a limited amount of information concerning the elastic properties and dynamic moduli are given in Reference 9. Dunn (6) reported the results of a study in which specially prepared sand-clay mixtures stabilized with portland cement were tested under dynamic conditions. Cylindrical specimens were subjected to a 40-psi compressive stress at a frequency of 106 cpm. This repeated loading had little effect on the physical properties, and it was concluded that this was due to the fact that the repeated load stress was small in relation to the strength of the material (2 to 10% of the compressive strength).

Dunn also determined the dynamic modulus from sonic velocity measurements on beams, and obtained values about two times greater than those determined as a secant modulus in compression tests. This was probably because the dynamic test deals primarily with elastic effects, and soil-cement exhibits time-dependent deformation properties which influence static test results.

Whittle and Larew (27) studied the effects of repeated loads on elastic micaceous soils stabilized with 5 percent type III portland cement. Results showed that the ultimate strength as determined from a repeated load stress-strain curve was considerably

less than the ultimate strength obtained from identical samples using conventional loading. The strain at failure, however, remained nearly the same under both types of loading. They concluded that specimens would fail under repeated loading when the magnitude of the repeated load stress is greater than 60 percent of the ultimate compressive strength.

EXPERIMENTAL PROGRAM

Notation

N = number of repeated loading applications,
w/c = molding water content,
γ_d = dry density,
$\sigma_{max\ c}$ = unconfined compressive strength,
$\Delta\sigma_{max\ c}$ = change of unconfined compressive strength in percentage,
S_{max} = modulus of rupture in flexure test,
σ_c = applied repeated compressive stress,
σ_T = applied repeated tensile stress,
ϵ_{RC} = resilient strain in compression test,
ϵ_{RF} = resilient strain in flexure test,
ϵ_{TC} = total strain in compression test,
ϵ_{TF} = total strain in flexure test,
ϵ_{fc} = strain at failure in compression test,
ϵ_{fF} = strain at failure in flexure test,
M_{RC} = modulus of resilient deformation in compression test,
M_{RF} = modulus of resilient deformation in flexure test,
E_{SC} = tangent modulus in compression test, and
E_{SF} = tangent modulus in flexure test.

Materials

The two soils chosen for this study are similar to materials used in the field for soil-cement stabilization. They were silty clay from Vicksburg, Miss., and a river sand with added fines from Eliot, Calif. The Vicksburg silty clay (VSC) represented a typical subgrade material, and the Eliot sand mixture (ESM) represented a typical stabilized base course material. A gradation curve of the ESM indicated its adequacy to meet base course specifications (AASHO E grading, designation M147-57). It was composed of, by weight, 80 percent Eliot sand, 10 percent kaolinite (grain size finer than 2μ), 5 percent No. 84 Ottawa sand and 5 percent silica flour (passing No. 325 sieve but coarser than 2μ).

Figure 2 shows the grain-size distribution curve of ESM and the range of AASHO E grading material, as well as the particle-size distribution curve for VSC. The physical properties of the untreated soils are given in Table 1.

According to the AASHO soil classification system, VSC is an A-6 soil, and the ESM is an A-2-4 soil.

Cement Treatment Level

The amount of cement used in each of the two soils was determined using freeze-thaw (ASTM D560-44) and wet-dry (ASTM D559-44) tests on specimens compacted to maximum density at optimum moisture content using standard AASHO compaction.

TABLE 1

PHYSICAL PROPERTIES OF VICKSBURG SILTY CLAY AND ELIOT SAND MIXTURE

Soil	L. L. (%)	P. L. (%)	P. I. (%)	Sp. Gr.	Mineral Comp. of -2μ Fraction
VSC	37-39	23-24	14	2.72	Mont., illite, quartz
ESM	20.6	15.4	5.2	2.70	Kaolinite

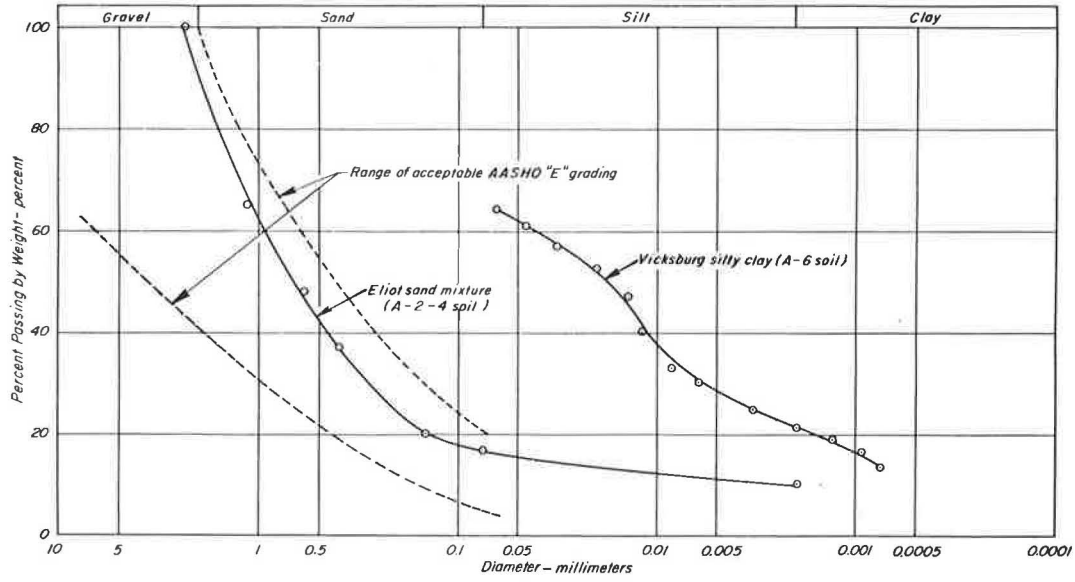

Figure 2. Grain-size distribution curves.

Results from these tests indicated that the cement requirements were 13 percent by weight for VSC and 7 percent by weight for ESM. Type I commercial portland cement was used.

Types of Tests and Selection of Stress Intensities

Both triaxial compression tests on cylindrical specimens and flexural tests on beam specimens were conducted. Appropriate ranges of repeated loading stress intensities were selected on the basis of computations using three-layer elastic theory for highway and airfield loading conditions, assuming the VSC to be a stabilized subgrade material and the ESM to be a stabilized base course. In tests where applied stress intensity was not considered as a variable, stress intensities of 50 and 100 psi were used for ESM in compression and 50 psi in flexure; 20 and 40 psi were applied to VSC in compression, and 20 psi in flexure.

Mixing

Soil and the appropriate amount of cement were first mixed in an air-dry condition, then the necessary amount of water was added to the air-dry mixture and thoroughly

mixed for about 3 min. Inasmuch as delaying compaction after mixing reduces the dry density and strength of a compacted specimen (26), the time lapse between mixing and compaction was kept constant for all samples. The amount of water-cement-soil mixture mixed each time was enough for two cylindrical specimens or for one beam specimen; and the time lapse from after mixing to the completion of compaction was approximately 10 min.

Sample Compaction

Cylindrical Samples. —Compaction was performed using a modified Harvard Miniature kneading compactor. Samples were compacted in 1.4-in. diameter molds to an approximately 3.5-in. trimmed height. The sample was placed between a lucite cap and base, enclosed in two rubber membranes (with a thin film of silicone grease in between), sealed top and bottom by O-rings, and stored under water for curing.

Beam Samples. —Beam samples were compacted using the Triaxial Institute kneading compactor (25) with a rectangular tamping foot $2\frac{2}{3}$ by 2 in. in plan. A steel mold 12 in. long 3 in. wide and $2\frac{1}{2}$ in. deep was used. The finished sample was extruded from the mold and wrapped with Saran sheet for curing.

Curing

All samples, except those used for the study of the effects of curing time were cured for 7 days. Some samples were soaked unconfined for a period of 24 hr after 7 days of curing.

Repeated Loading Apparatus

The repeated loading equipment was the same as that used for a number of years in the soil mechanics laboratory at the University of California (20).

In both compression and flexure tests the load applications were 20/min, the average duration of a load application was 0.1 sec, and the load rise time was about 0.01 sec. Figure 3 is a typical load vs time trace.

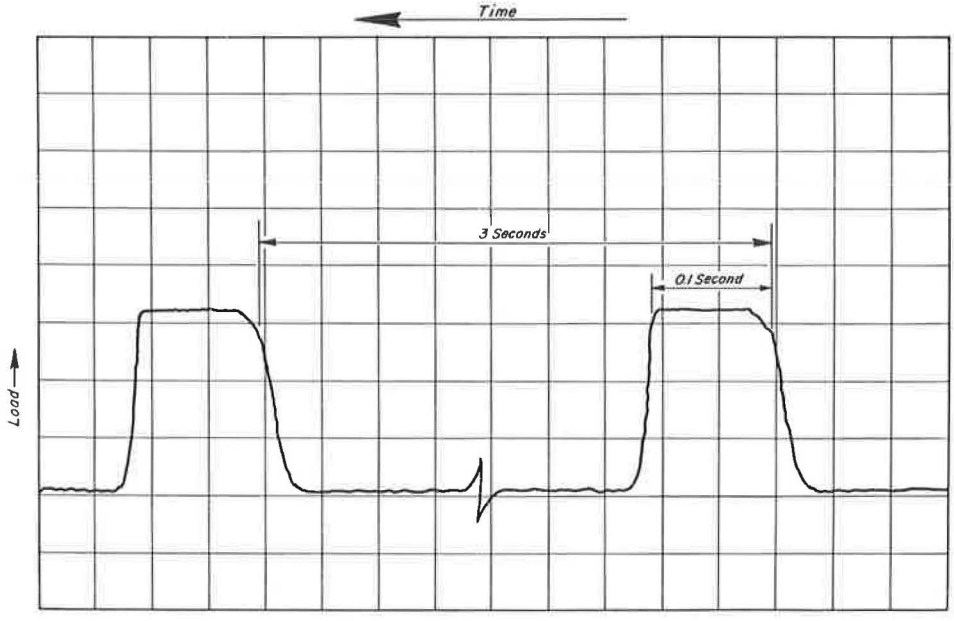

Figure 3. Repeated loading time vs load trace.

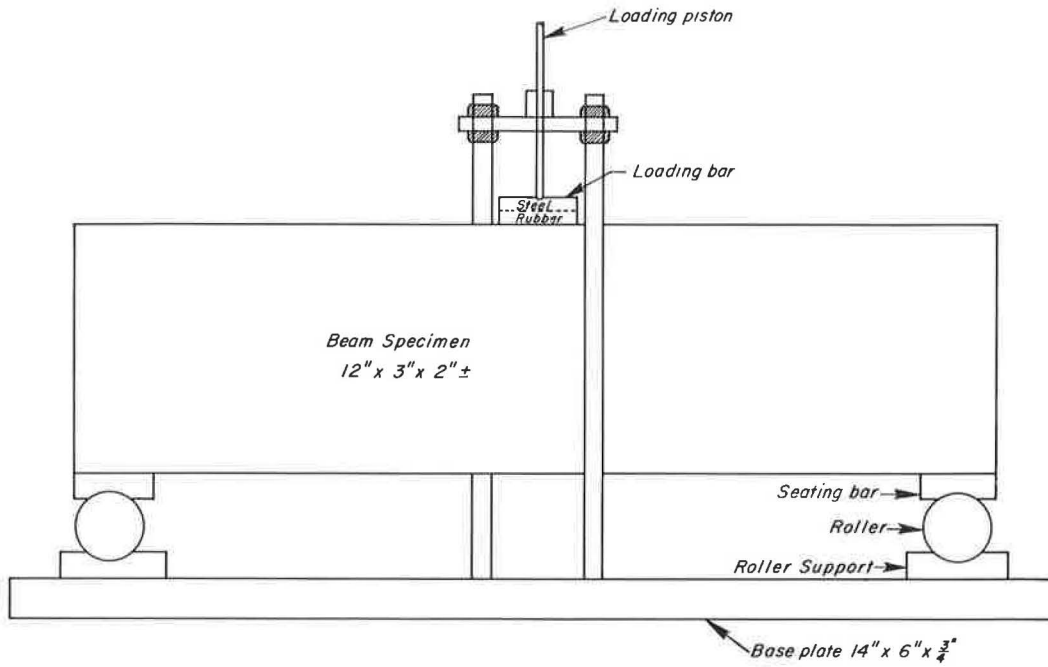

Figure 4. Flexural test apparatus.

Repeated loading compression tests were carried out inside triaxial compression cells. No confining pressure was used. All samples were tested undrained, and no pore pressure measurements were attempted.

A simple apparatus was used for flexural tests (Fig. 4). One of the two roller supports was fixed on the 14- by 6- by $^3/_4$-in. steel base plate; the other was free to move, thus giving simple support conditions. Load was applied using a loading piston and was transmitted to the beam by a two-layered loading bar, which was seated on the top of the midspan of the beam. This loading bar was made of a plate of steel sealed to a layer of hard rubber. Approximate simple-beam elastic theory could be used for stress-deflection analysis of the results obtained.

Measuring and Recording Systems

Since the soil-cement specimens, especially the ESM, were very stiff in relation to untreated soils, accurate measurement of deformation was difficult. The amount of deformation under repeated loading was of the order of only 1×10^{-5} in./in. or less in some cases, and could not be accurately measured using a dial gage. Moreover, the magnitudes of the applied repeated loads were comparatively high, ranging from 40 to about 250 lb. Thus the elastic deformation of the apparatus was appreciable. Therefore, a measuring technique independent of apparatus deflections was needed for this research.

A technique for measuring the relative deformation of compression specimens which made use of Schaevitz type 100M-L linear variable differential transformers (LVDT's) was found successful. Dual LVDT's were connected in parallel to increase the sensitivity of the measuring system and to give representative average values of deformation. They were mounted directly on the specimens by means of two small aluminum alloy clamps (Fig. 5). One clamp held the transformer coil assembly; the other the adjustable core rod.

Bonded-wire strain gages were used to measure the deflection of ESM beam specimens under repeated loading. A four-arm Wheatstone bridge was formed by connecting

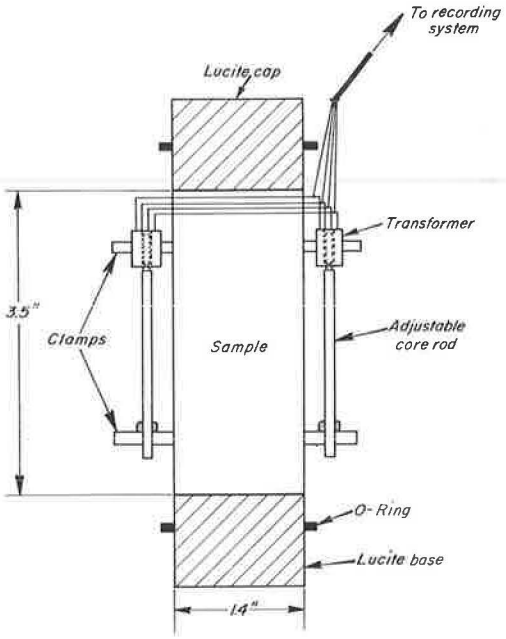

Figure 5. Linear variable differential transformer assembly for deflection measurements on cylindrical sample.

two active and two compensation strain gages. Strain gages could not be securely bonded to the smooth, moist surfaces of VSC beam specimens; therefore, LVDT's were used. Measurements were taken both at the middle and the ends of the span. The adjustable core rod was connected to the beam at mid-height (neutral axis), and the transformer coil assembly was fixed on a stationary rod screwed into the base plate (Fig. 6).

Both the transformers and the strain gages were wired to model 150-1100AS Sanborn carrier preamplifiers, which were in turn wired to a model 152-100BP, two-channel, direct-writing Sanborn recorder. Calibration curves were established before testing. Occasional checks were made to insure that accuracy was consistently maintained.

Conventional Strength Tests

After being subjected to a specific number of repeated loading applications (generally 24,000), all samples, except for those which failed during the course of repeated loading tests, were tested using

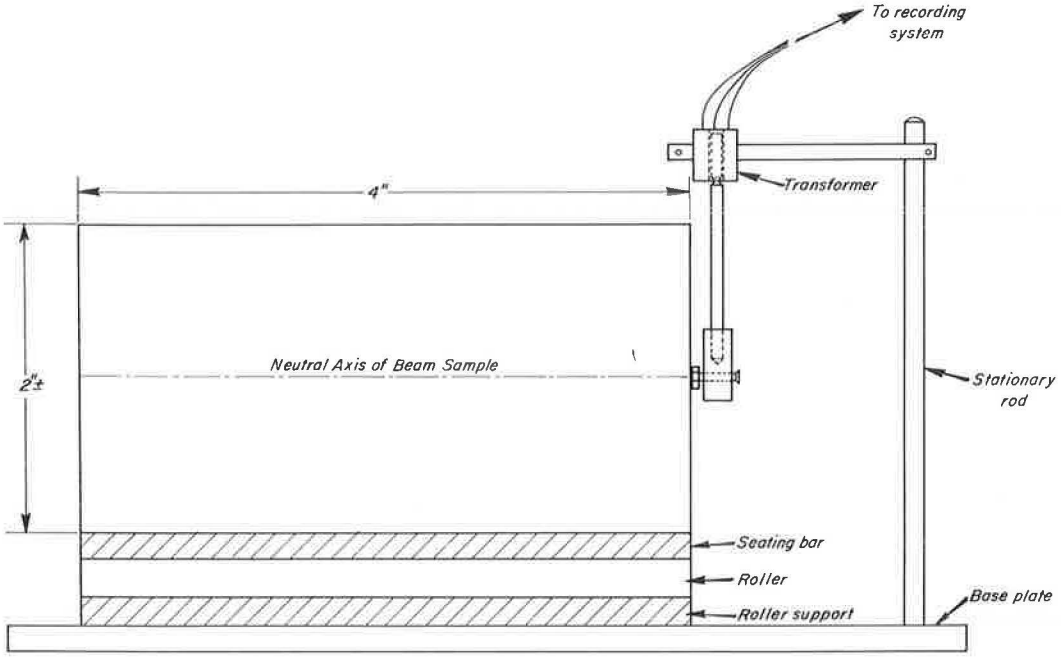

Figure 6. Linear variable differential transformer assembly for deflection measurements on beam samples.

conventional compression or flexural strength tests. A dummy sample of the same age as the corresponding repeated loading sample was also tested to determine the effect of repeated load application on the mechanical properties.

RESULTS

Repeated Load Compression Tests

Effect of Density and Moisture Content. —The effects of moisture content and density on behavior under repeated compressive loading were determined using specimens compacted along three curves (Figs. 7 and 8). Six identical samples were prepared at each point on the curves. All samples were cured for 7 days following compaction. Four specimens were then soaked for 24 hr. Repeated loading tests were carried out on two

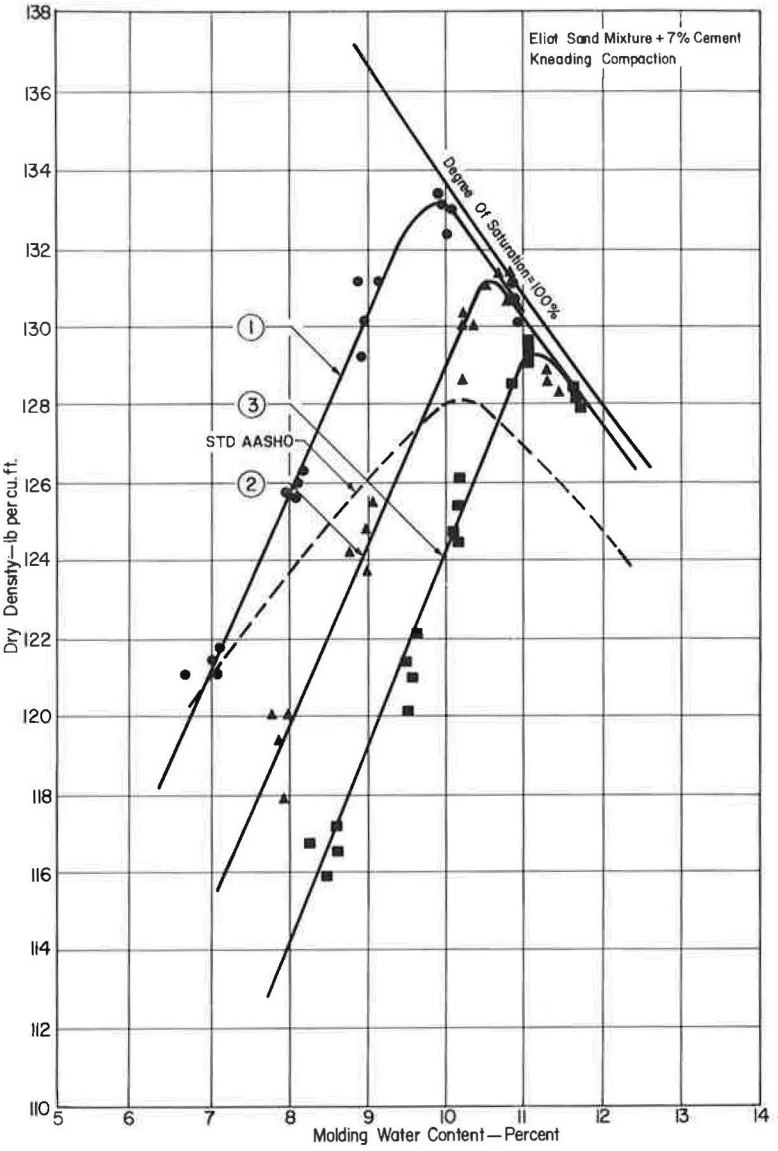

Figure 7. Compaction curves, Eliot sand mixture-cement.

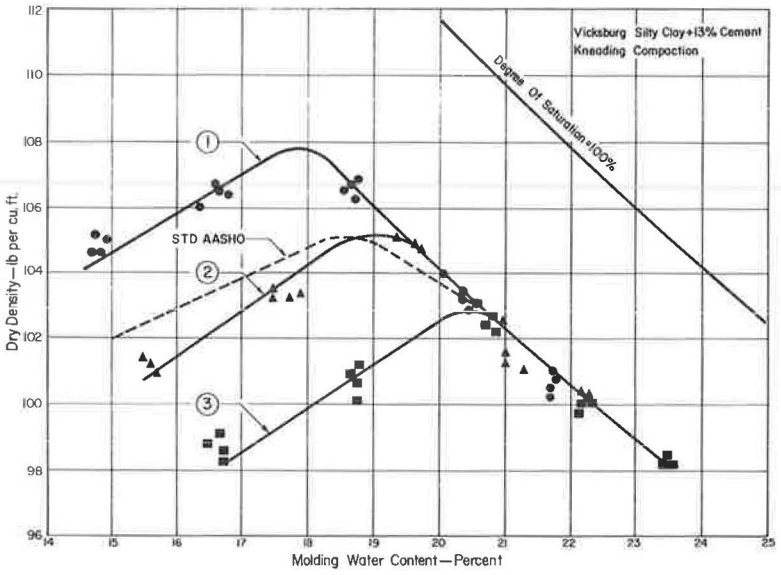

Figure 8. Compaction curves, Vicksburg silty clay-cement.

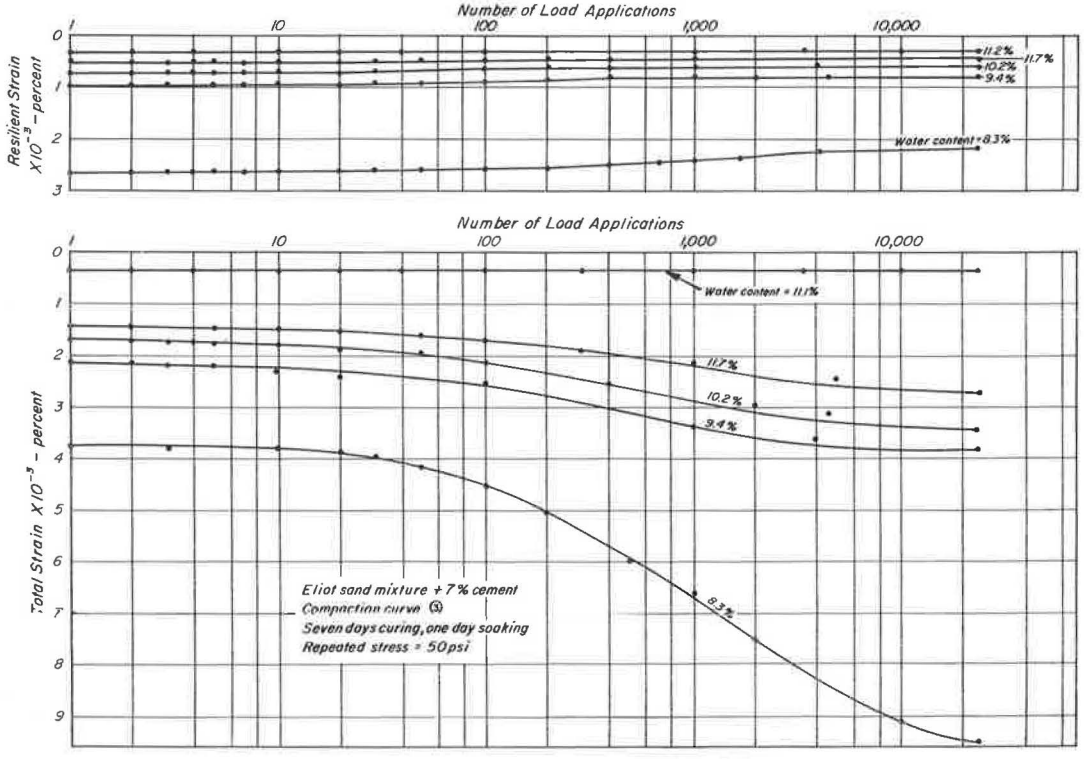

Figure 9. Deformation of Eliot sand mixture-cement samples in repeated compression tests.

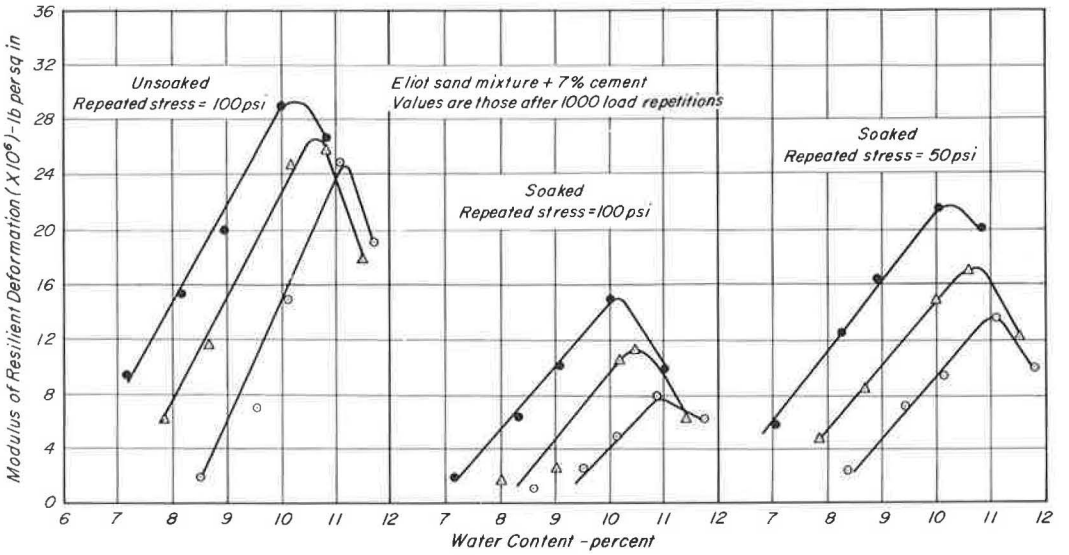

Figure 10. Relationship between water content and modulus of resilient deformation in compression for Eliot sand mixture-cement.

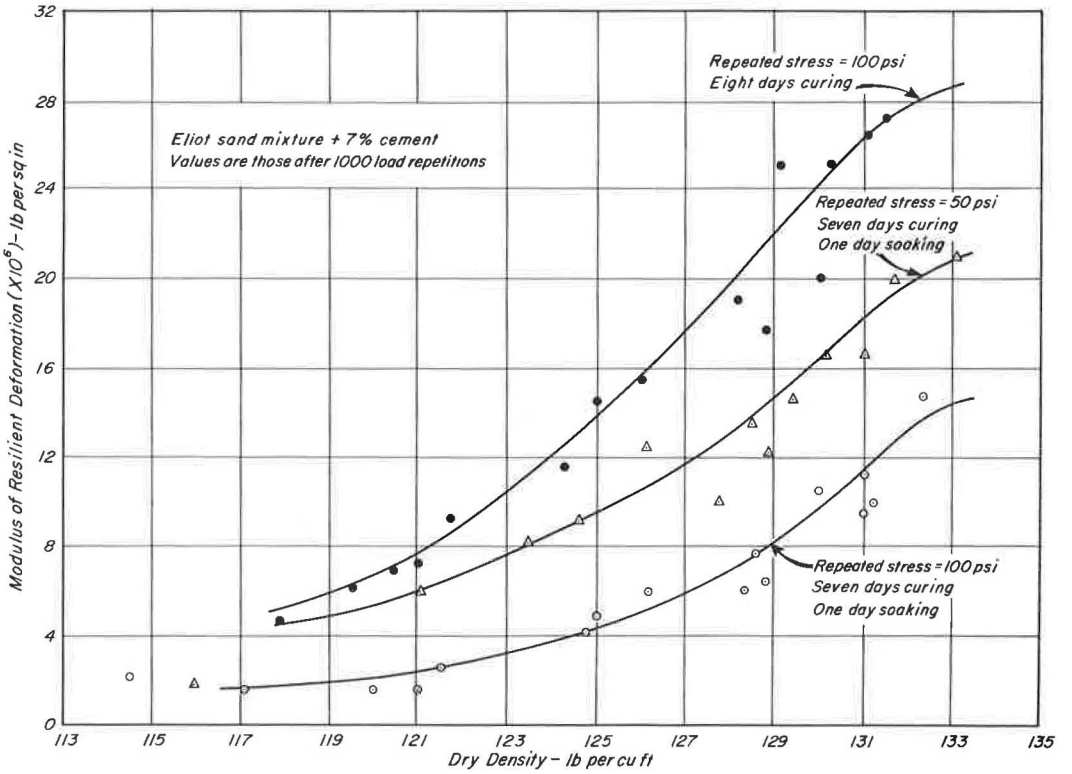

Figure 11. Relationship between dry density and modulus of resilient deformation in compression for Eliot sand mixture-cement.

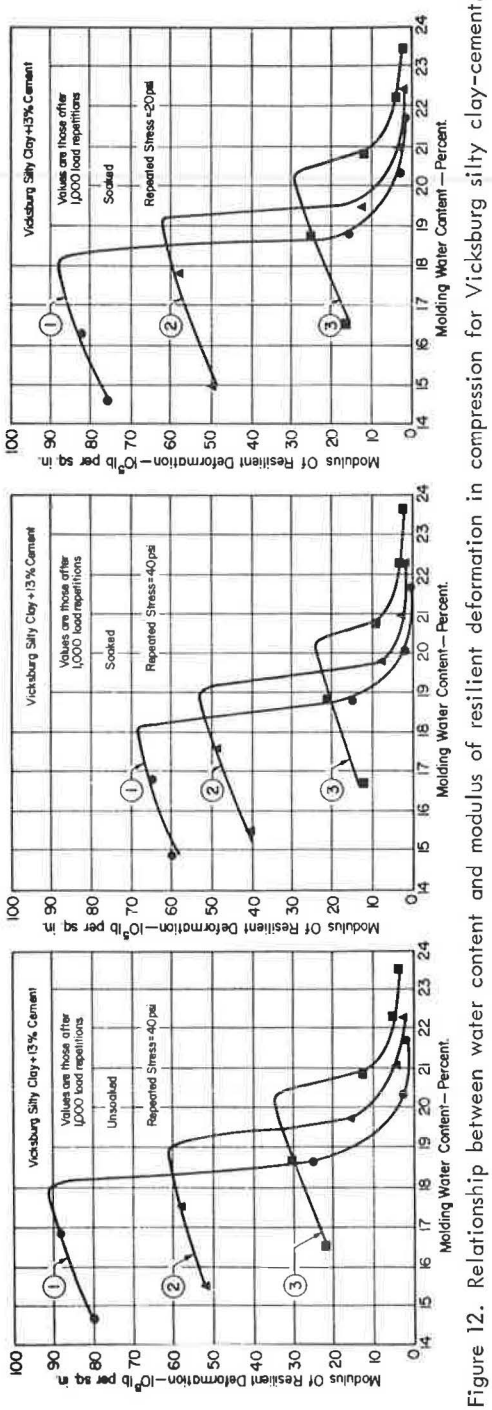

Figure 12. Relationship between water content and modulus of resilient deformation in compression for Vicksburg silty clay-cement.

soaked samples and one unsoaked sample on the eighth day after compaction. Tests were stopped after approximately 24,000 repeated load applications, and the specimens were subjected to unconfined compression tests. The strengths of dummy samples which had not been subjected to repeated loading were also determined.

Figure 9 shows typical plots of the variation of resilient (ϵ_{RC}) and total (ϵ_{TC}) compressive strains with the number of load applications (N) for ESM-cement. At the comparatively low (but realistic in relation to traffic-induced stresses) applied repreated load stress intensities (less than 30 percent of the initial strength for VSC-cement and 40 percent for ESM-cement) both the resilient and total strains are small. There is little variation in resilient strain with increase in number of load applications.

The variation of modulus of resilient deformation (M_{RC}) in compression, after 1,000 load repetitions, with molding water content, is shown in Figure 10 for the ESM. Both the stress intensity and soaking affect the values of M_{RC}. The maximum values of M_{RC} for soaked specimens were only about half of the corresponding values for unsoaked specimens under the same stress intensity. Figure 10 suggests that for the ESM-cement the modulus is related primarily to dry density for given conditions of curing and applied stress. Figure 11 bears out this relationship, indicating that M_{RC} is uniquely related to density without influence of molding water content.

The variation of M_{RC} with molding water content for the VSC-cement specimens is shown in Figure 12. Sharp reductions in moduli values occur at or near optimum water content, and no unique correlation with density appears to exist. The results show further that both soaking and applied stress intensity influence the results.

Figure 13 shows the relationship between water content and unconfined compressive strength for VSC-cement. Essentially, the same pattern as shown in Figure 12 is indicated. Thus for specimens prepared wet of optimum using

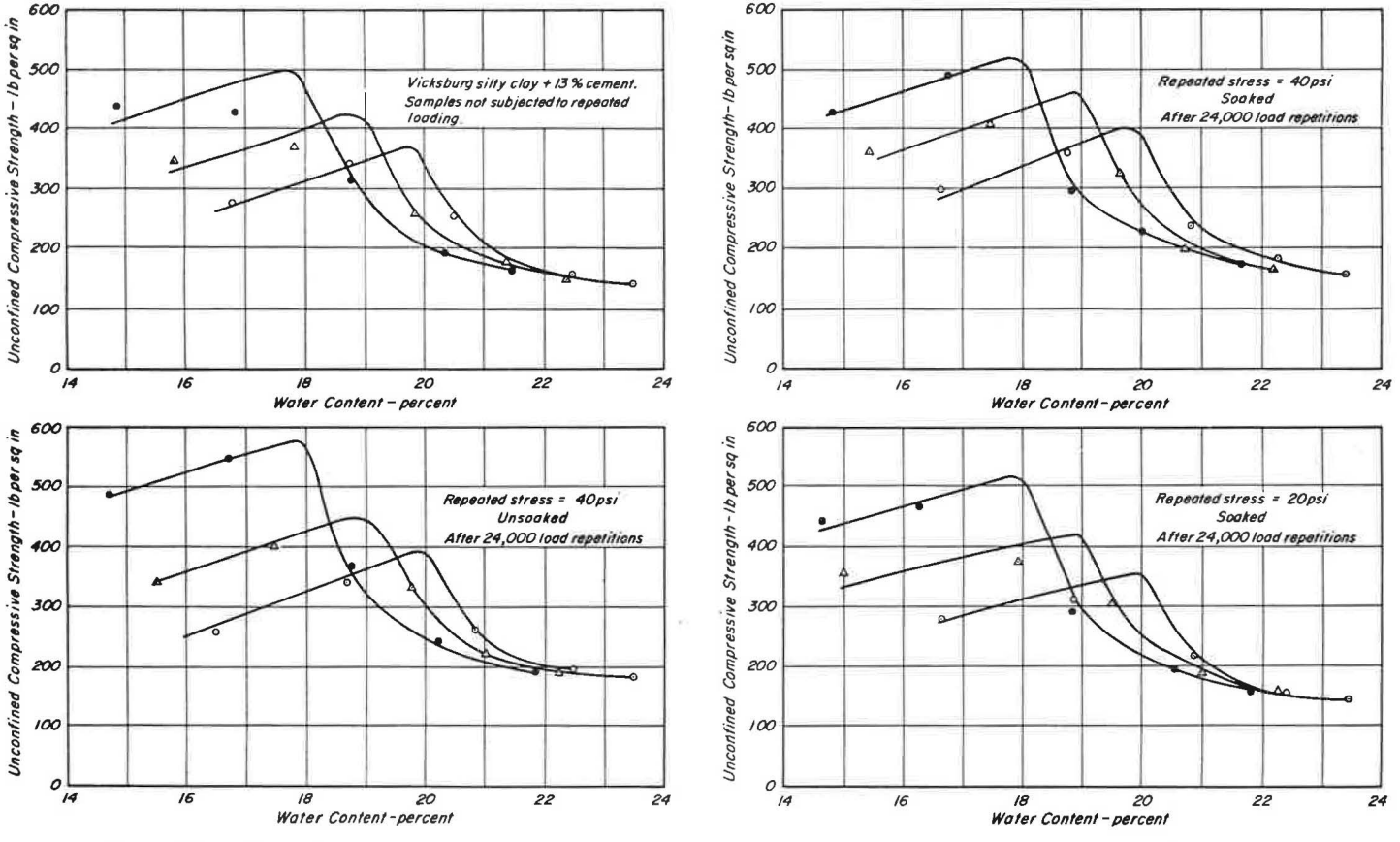

Figure 13. Relationship between water content and unconfined compressive strength for Vicksburg silty clay-cement.

kneading compaction, a higher compactive effort may result in lower modulus and strength. This type of behavior was observed by Seed and Chan (21) for untreated VSC, and could be explained in terms of the more dispersed structure induced at high kneading compactive efforts. It appears that even in the presence of cement, which should tend to flocculate the clay particles before hydration, the silty clay remains structure-sensitive, and density alone cannot be taken as a criterion of behavior.

Further evidence of this structure-sensitivity was obtained by Groves (8), who investigated the effect of method of compaction on the strength of the silty clay-cement. His results showed that samples compacted wet of optimum by static compaction were stronger than those compacted to the same density by kneading compaction. Static compaction does not induce significant shear strain, thus the soil structure retains a flocculent character, whereas kneading compaction disperses and weakens the structure. These effects of compaction method are similar to those reported by Seed and Chan for the untreated silty clay.

Finally, it appears from Figure 13 that 24,000 repetitions of compressive stress had little fatigue effect on the VSC-cement specimens, because the strengths are little different and in some cases greater than those of specimens of the same age not subjected to repeated loading. Similar behavior was observed for the ESM-cement. As previously noted, however, the repeated stress intensities were only of the order of 10 to 40 percent of the ultimate strength.

Contours of equal values of M_{RC} taken at 1,000 load applications are shown in Figures 14 and 15 for VSC-cement and ESM-cement, respectively. In the case of VSC-cement, the modulus of resilient deformation varies with compactive effort, molding water content, and dry density; whereas parallel horizontal contours of M_{RC} for ESM-cement indicate that molding water content and compactive effort have little influence on the values of modulus of resilient deformation, and the higher the compaction density the higher the modulus.

Effect of Stress Intensity. —The studies of moisture content and density effects suggested that M_{RC} varies with the applied repeated loading stress intensity. Tests were conducted to investigate this variation in more detail and to study the effect of the magnitude of the applied repeated loading stress on other properties of soil-cement.

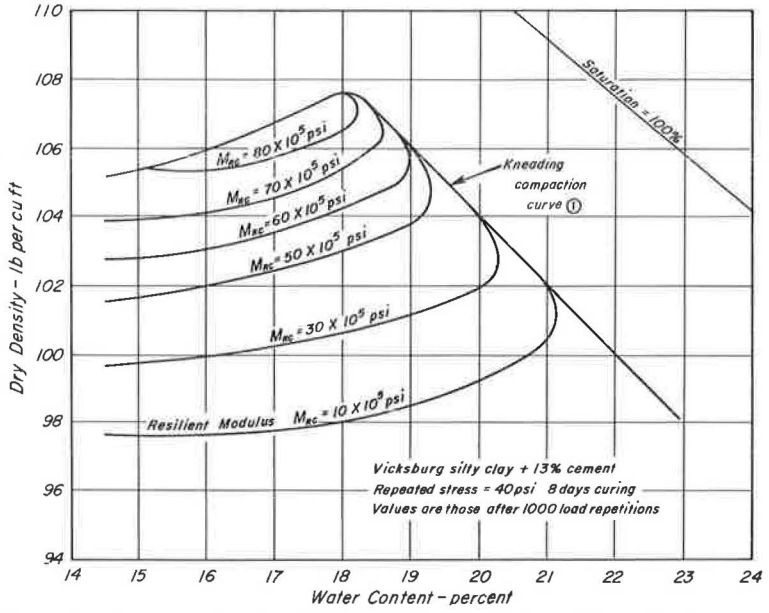

Figure 14. Relationship between dry density, water content and modulus of resilient deformation in compression for Vicksburg silty clay-cement.

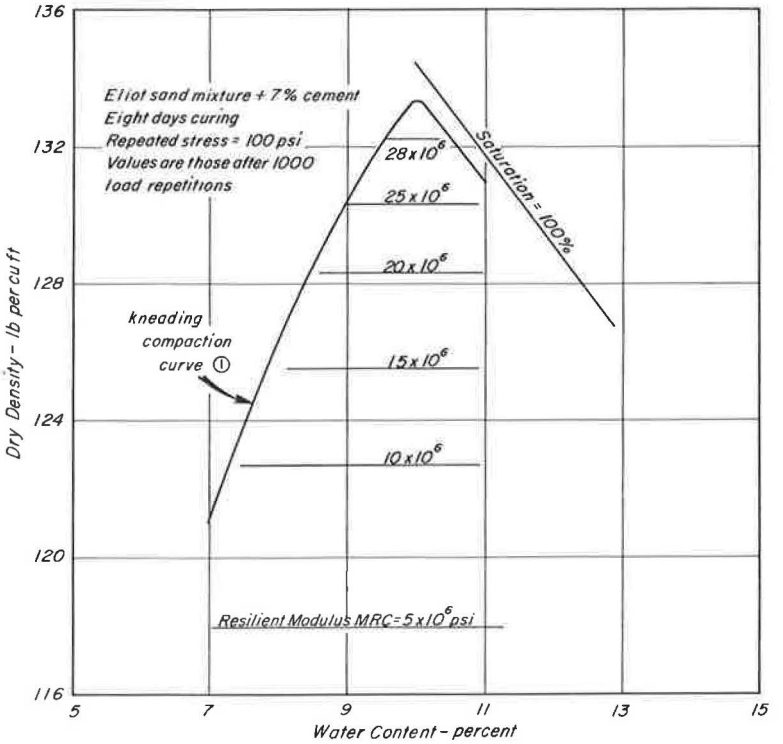

Figure 15. Relationship between dry density, water content and modulus of resilient deformation in compression for Eliot sand mixture-cement.

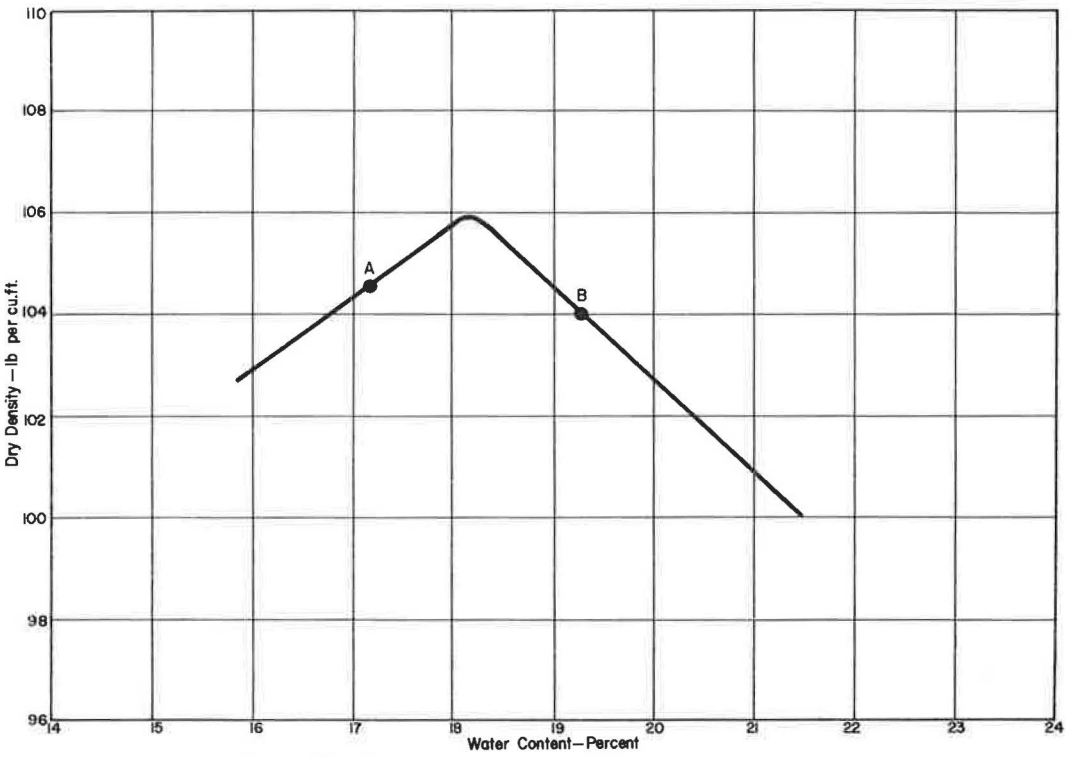

Figure 16. Compaction curve, Vicksburg silty clay-cement.

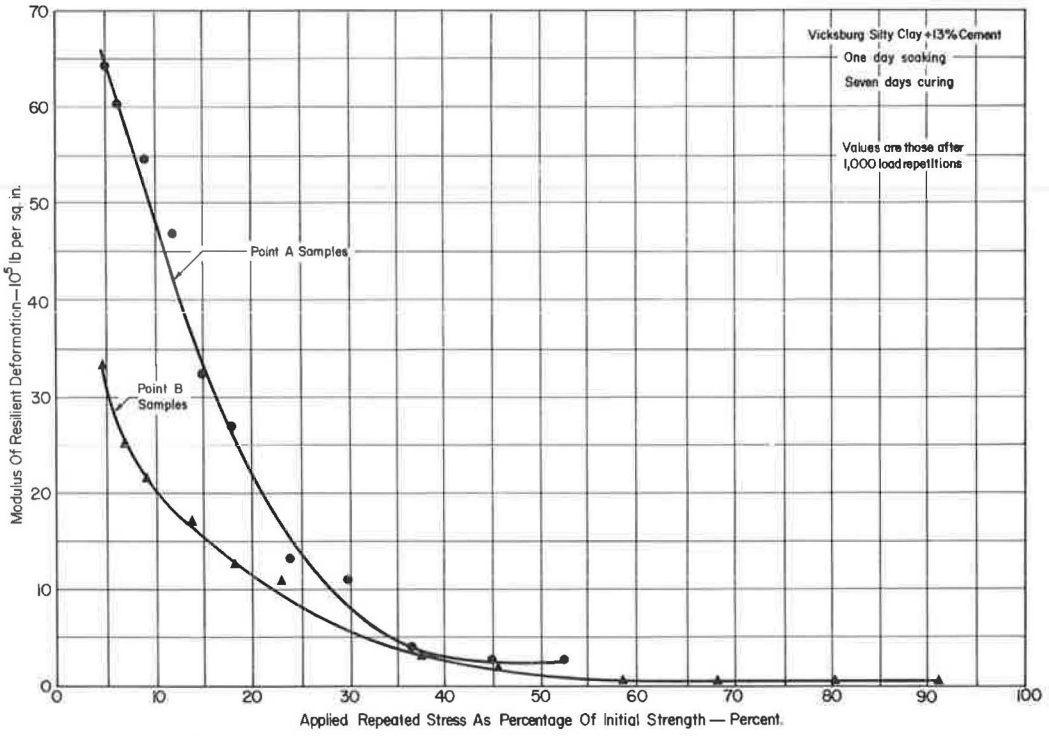

Figure 17. Effect of stress level on resilient modulus in compression for Vicksburg silty clay-cement.

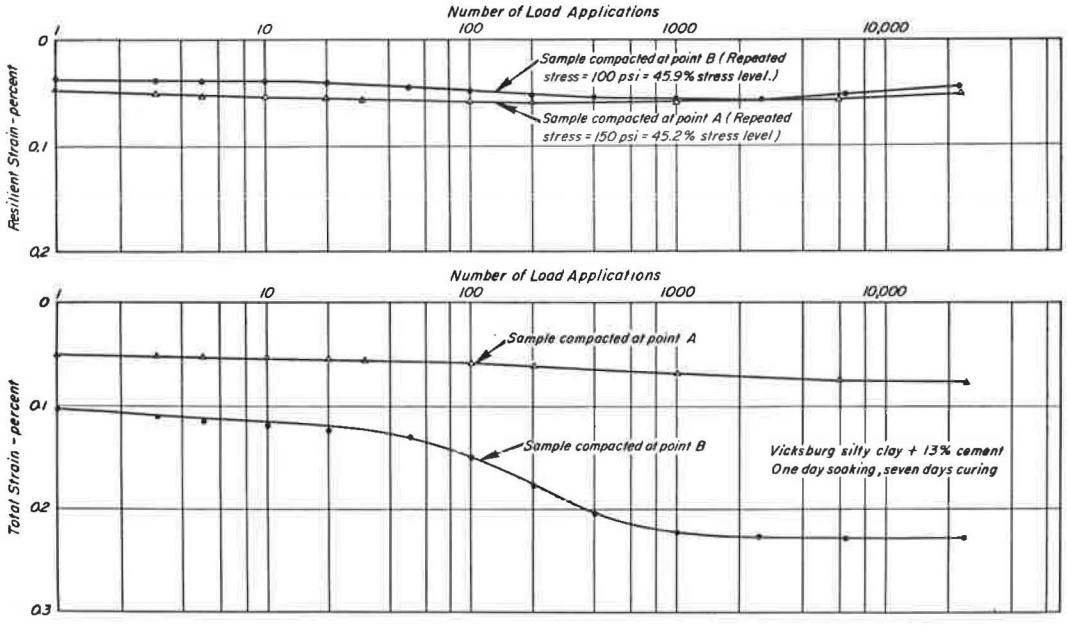

Figure 18. Resilient and total strains vs number of load applications curves in repeated compression for Vicksburg silty clay-cement.

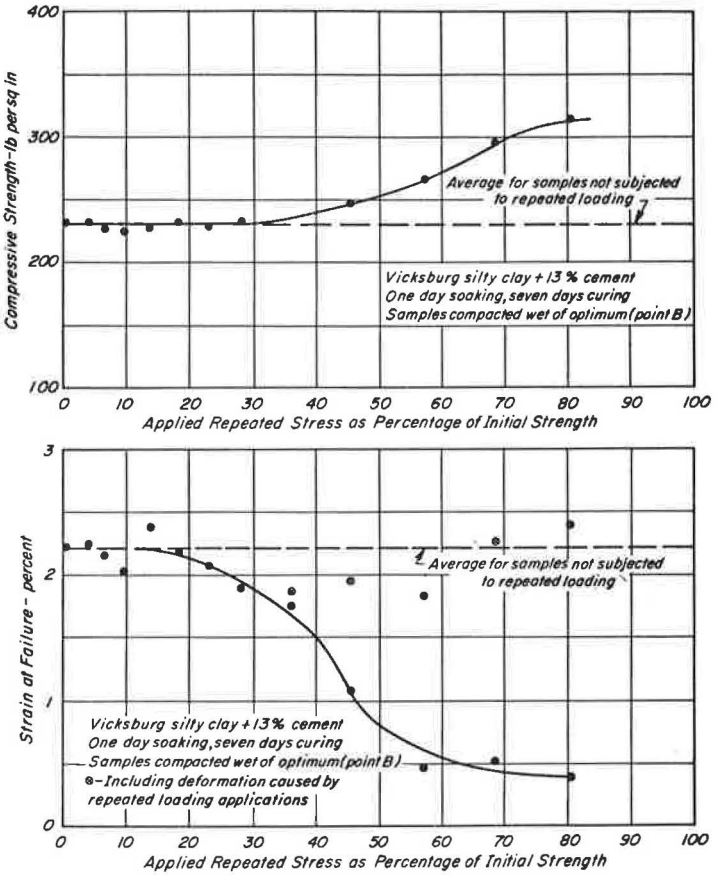

Figure 19. Effect of repeated stress intensity on properties of Vicksburg silty clay-cement in compression.

VSC-cement samples were compacted at two water contents (Fig. 16). Point A samples were compacted dry of optimum water content, whereas samples at point B were at the same dry density wet of optimum. Only soaked samples were used for this study.

The variation of the modulus of resilient deformation with applied stress intensity is shown in Figure 17. For each curve the resilient modulus, determined at N = 1,000, varies greatly at low stress intensities; the smaller the applied stress intensity, the higher the modulus. For stress intensities greater than about 40 percent of the initial strength, however, M_{RC} remains almost constant.

No fatigue failures were observed in point A samples, which were subjected to applied repeated loading stress intensities up to about 53 percent of the initial strength. One sample at point B, however, when subjected to 200-psi repeated loading stress intensity (corresponding to 92% of the initial strength) failed after 188 load applications.

A comparison was made of a dry-side sample VSD 37, at a water content of 17.5 percent, and a wet-side sample VSWC 6, at a water content of 19.1 percent, both subjected to repeated loading stress intensities of about 45 percent of their individual initial strengths (150 psi for VSD 37 and 100 psi for VSWC 6). In this case the resilient strains of the two samples were essentially the same (Fig. 18). The modulus of resilient deformation of the dry-side sample, however, was about 1.5 times greater than that of the wet-side sample because the applied repeated loading stress intensities were in that ratio; and conversely, the total strain of the former was less than one-half that of the latter.

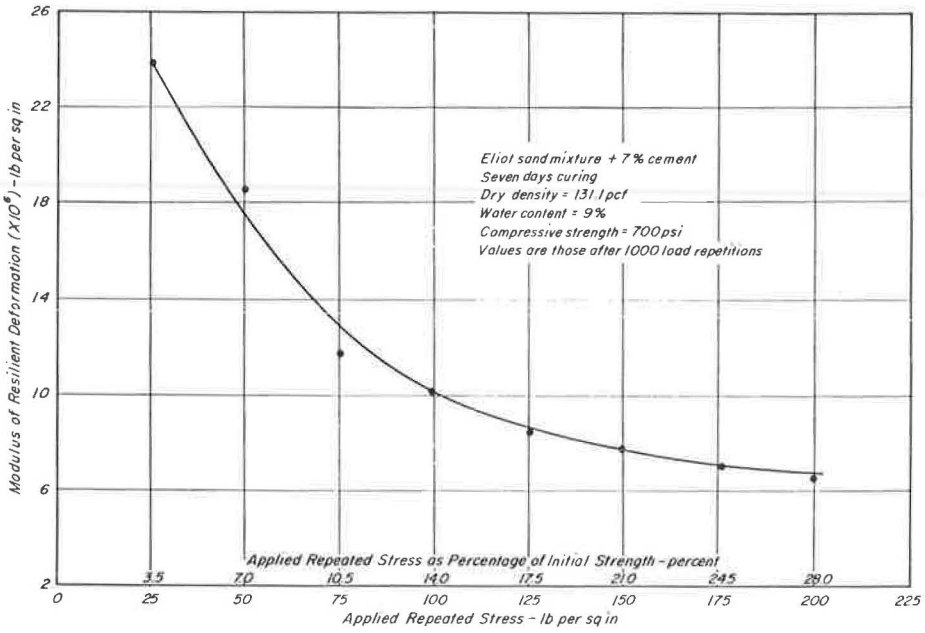

Figure 20. Effect of stress intensity on resilience characteristics in repeated compression tests for Eliot sand mixture-cement.

For point A samples, with repeated loading compressive stresses up to about 53 percent of the initial strength, no significant change of mechanical properties was noticed at the end of 24,000 repetitions. Point B samples, however, when subjected to repeated loading stresses of 50 percent or more of their initial strengths became stronger and stiffer, as indicated by the unconfined compressive strength and strain at failure values shown in Figure 19. If the amount of axial strain which occurred during repeated loading applications was included in the calculations, all samples when compacted under the same condition would tend to fail at about the same strain whether or not previously subjected to repeated loading. The strengthening effect at high repeated stress intensities may have resulted from densification during the test.

Figure 20 shows the variation of modulus of resilient deformation after 1,000 repetitions with respect to the magnitude of applied repeated loading stress for ESM-cement. Within the range of the repeated loading stresses applied, M_{RC} decreased as the magnitude of the applied repeated loading stress increased. No fatigue failures were observed. Measurements using higher repeated loading stress intensities would have been desirable; such measurements could not be made, however, because of the limited capacity of the repeated loading apparatus.

Effect of Number of Load Repetitions. —Identical samples of VSC-cement were compacted wet of optimum at a water content of 19.2 percent and a dry density of 105.5 pcf. All samples were cured for 7 days and soaked for 24 hr before testing. The average initial strength of these samples was about 260 psi. Specimens were subjected to a repeated loading stress of 170 psi, which corresponded to about 65 percent of the initial strength, for 1,000, 5,000, 10,000, 50,000, and 100,000 applications. After being subjected to the designated number of applications, the samples were tested to failure in unconfined compression tests.

Figure 21 shows the variation of resilient and total deformations with the number of load applications for each sample. The maximum resilient deformation occurred between about 1 and 500 load applications. The value of resilient strain at N = 100,000 was only about one-fifth to one-fourth of the maximum value. Figure 22 shows the

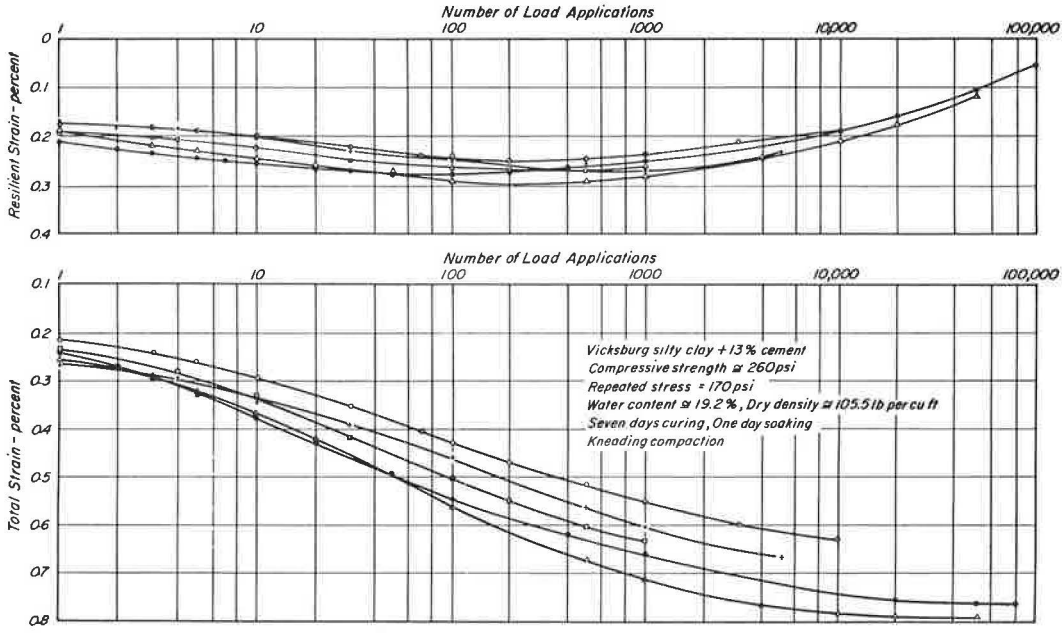

Figure 21. Relationship between deformation and number of load applications for Vicksburg silty clay-cement samples in repeated compression tests.

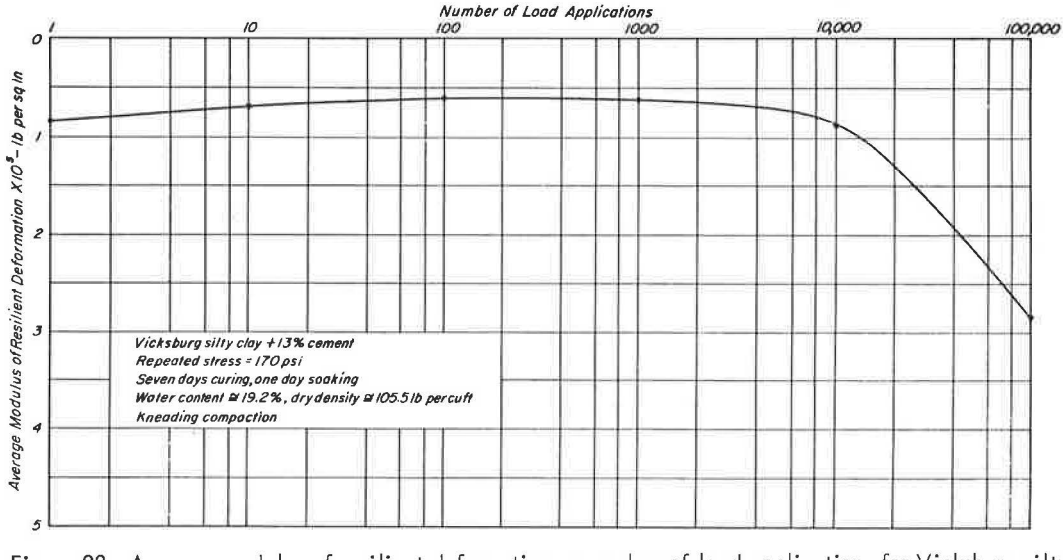

Figure 22. Average modulus of resilient deformation vs number of load applications for Vicksburg silty clay-cement samples in compression.

variation of the average resilient modulus for all samples with the number of load applications. The results also indicated that within the range of the number of repetitions studied, the greater the number of load applications, the greater the increase in unconfined compressive strength in relation to dummy samples of the same age.

The ESM-cement samples were studied in the same way as the VSC-cement samples. The initial strength of samples was about 700 psi with a dry density of 131.5 pcf and a

water content of 9.1 percent. A repeated loading stress intensity of 100 psi was used. There was no significant change in values of resilient strain with respect to the numbers of the load applications at this relatively low stress intensity. An increase of 5 to 10 percent, however, was attained in unconfined compressive strength as a result of repeated loading.

Influence of Time of Curing. —Some of the early test results for silty clay-cement showed that the properties of samples subjected to high repeated loading stress intensities varied greatly with the number of load applications. A series of tests was carried out to determine whether this behavior was true for samples of all ages or only for samples cured for short periods. Samples were compacted at a water content of 20.2 percent and a dry density of 102 pcf, and cured for 1, 3, 5, 14, 29, 49, and 70 days. Samples were soaked for a period of 24 hr before testing. Repeated loading stresses of 60 percent of the respective initial strengths at each age were used, and the samples were subjected to 24,000 load applications. Initial strength values of samples of different ages are shown in Figure 23.

Figure 24 shows the variation of resilient and total strains with the number of load applications for samples of different ages. The resilient strains increased to a maximum in all samples at different numbers of load applications, and as the number of load applications increased, the resilient strain decreased. The occurrence of the maximum resilient strain value depended on the age of the sample at the start of the test. The younger the sample, the smaller was the number of load applications required to reach this point (Fig. 25). This behavior reflects the composite effects of the structural breakdown caused by the repeated stress applications and the greater strengths associated with longer curing periods. Figure 26 shows the minimum value of resilient modulus with respect to time of curing, indicating that the minimum modulus of resilient deformation of the sample cured for 70 days was about nine times as high as that of the sample cured for 1 day. Thus it can be concluded that the duration of curing period can have a significant influence on the modulus of resilient deformation in compression.

The change in strength as a result of repeated loading is shown in Figure 27. The strengths of the samples cured for 7 weeks or more were not affected by repeated loading applications at a stress level of 60 percent. In would appear, however, that

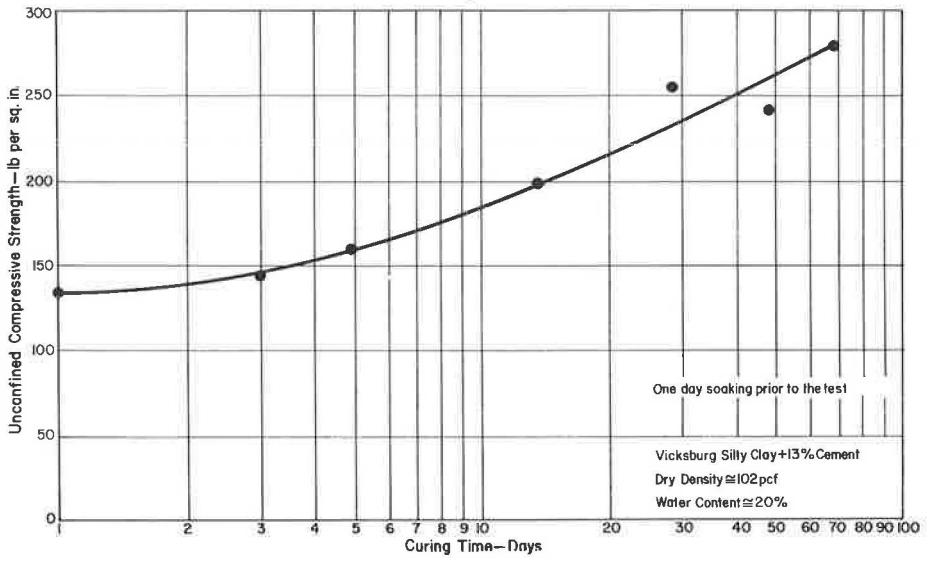

Figure 23. Relationship between curing time and unconfined compressive strength for Vicksburg silty clay-cement.

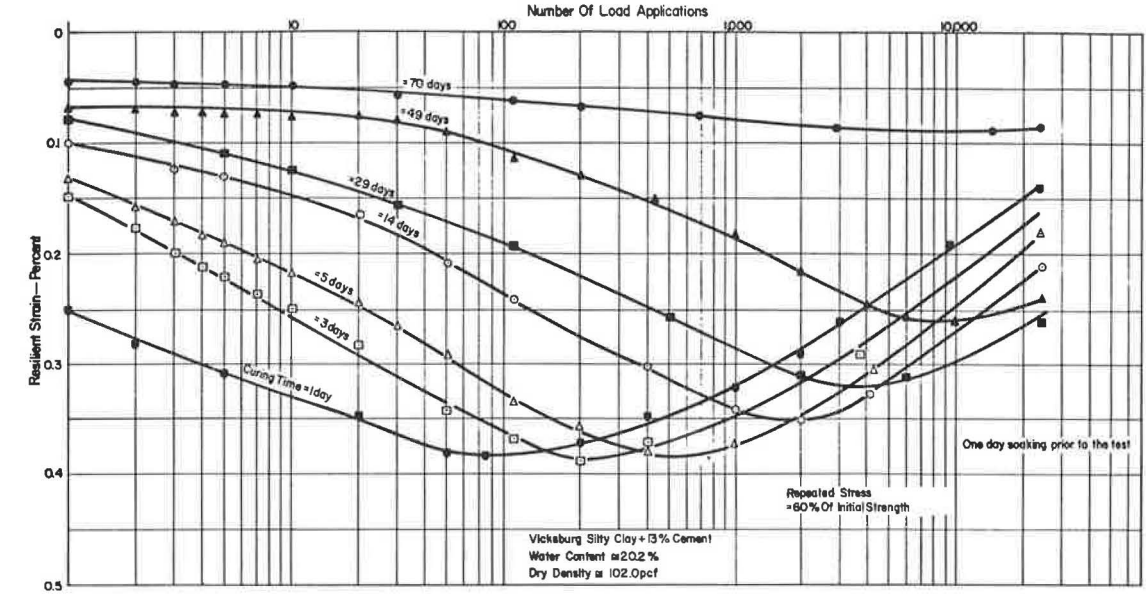

(a)

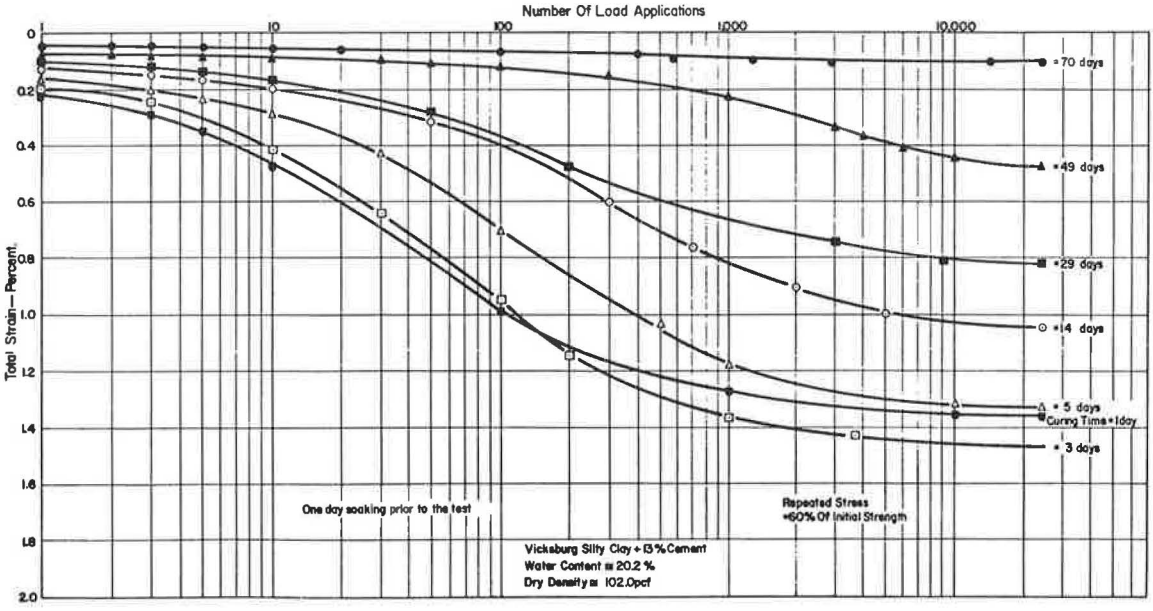

(b)

Figure 24. Effect of curing time on (a) resilient deformation of Vicksburg silty clay-cement in compression and (b) total deformation of Vicksburg silty clay-cement in compression.

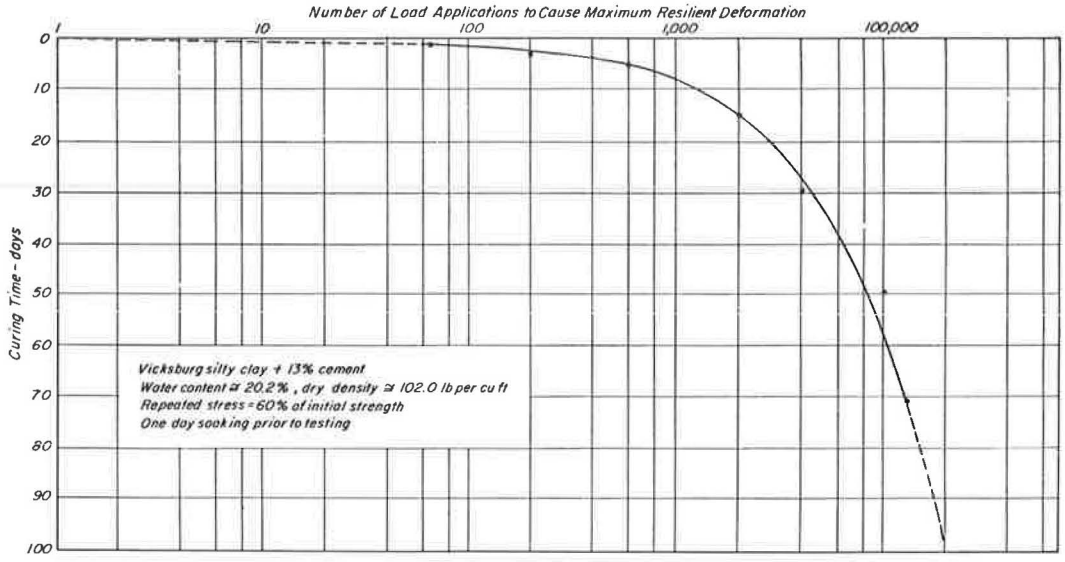

Figure 25. Effect of curing period on number of load applications to cause maximum resilient deformation in compression for Vicksburg silty clay-cement.

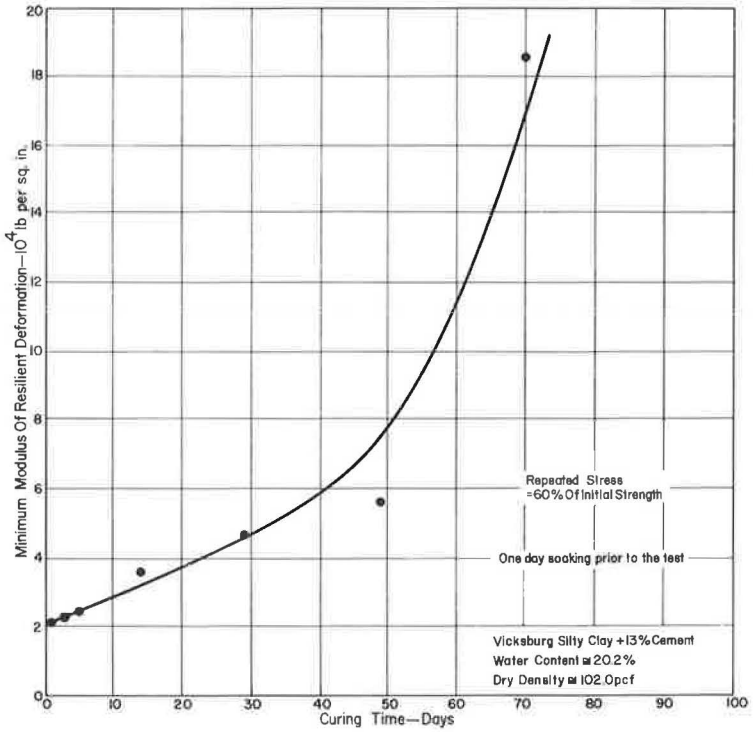

Figure 26. Minimum modulus of resilient deformation in compression as a function of curing time for Vicksburg silty clay-cement.

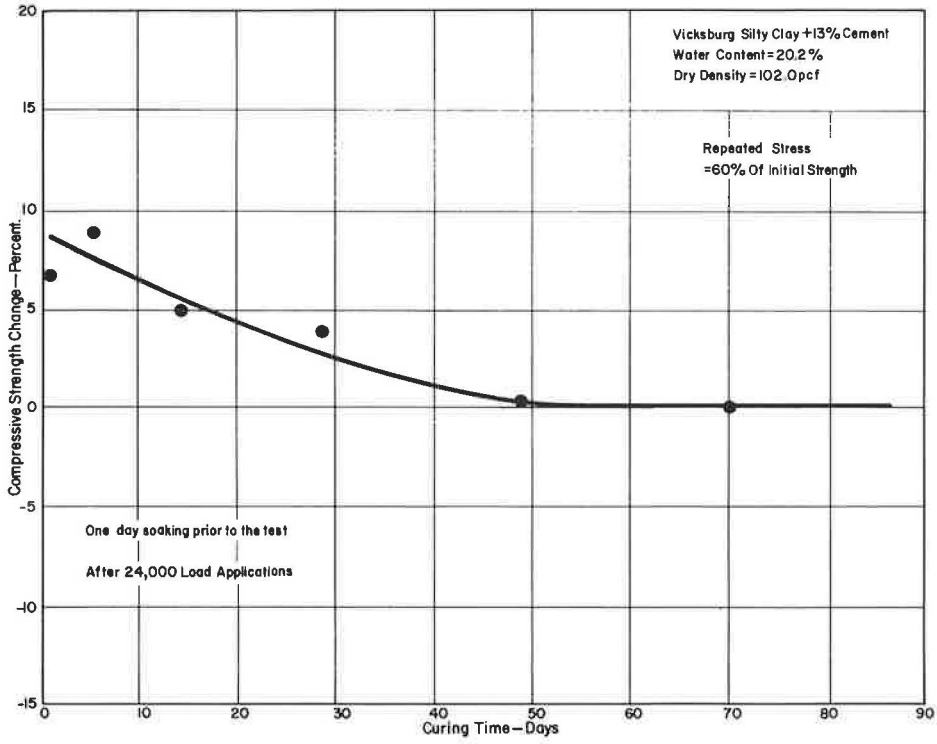

Figure 27. Change in strength caused by repeated loading as a function of curing time for Vicksburg silty clay-cement.

repeated loading in compression tends to strengthen samples cured less than 7 weeks. This is probably because at earlier ages the specimens are still sufficiently deformable that the repeated stresses can cause further densification and decreases of particle spacing at contact points.

Repeated Load Flexure Tests

Effect of Density and Moisture Content. —For each soil-cement, ten samples were compacted at five different water contents along the compaction curves shown in Figure 28. Samples were cured for 8 days after compaction and were not soaked before testing. Repeated loads were applied so as to give a tensile stress of 20 psi in VSC-cement samples and 50 psi in ESM-cement samples. All tests were carried to 24,000 applications. Very little variation of resilient modulus in flexure (ϵ_{RF}) was observed throughout the test period. The effect of repeated loading on the flexural properties of beam samples was minor (Figs. 29 and 30). A typical maximum deflection vs load curve for a sample of silty clay-cement from a conventional flexural test is shown in Figure 31. A straightline relationship up to the failure point is observed, thus making possible the application of elastic beam theory.

Effect of Repeated Stress Intensity. —VSC-cement samples were compacted at a water content of 18 percent and a dry density of 106.8 pcf. Repeated tensile stresses of 10, 30, 50, 75, 100, 120, and 135 psi were applied. One sample failed in fatigue after 600 load applications of a repeated loading stress intensity of about 90 percent of the initial modulus of rupture. Otherwise, the flexural properties of the beam samples were not affected by the high stress intensity repeated loading applications. Figure 32 shows the variation of resilient flexural strain, ϵ_{RF} at N = 1,000, with different applied repeated tensile stress intensities. This straightline relationship indicates that the

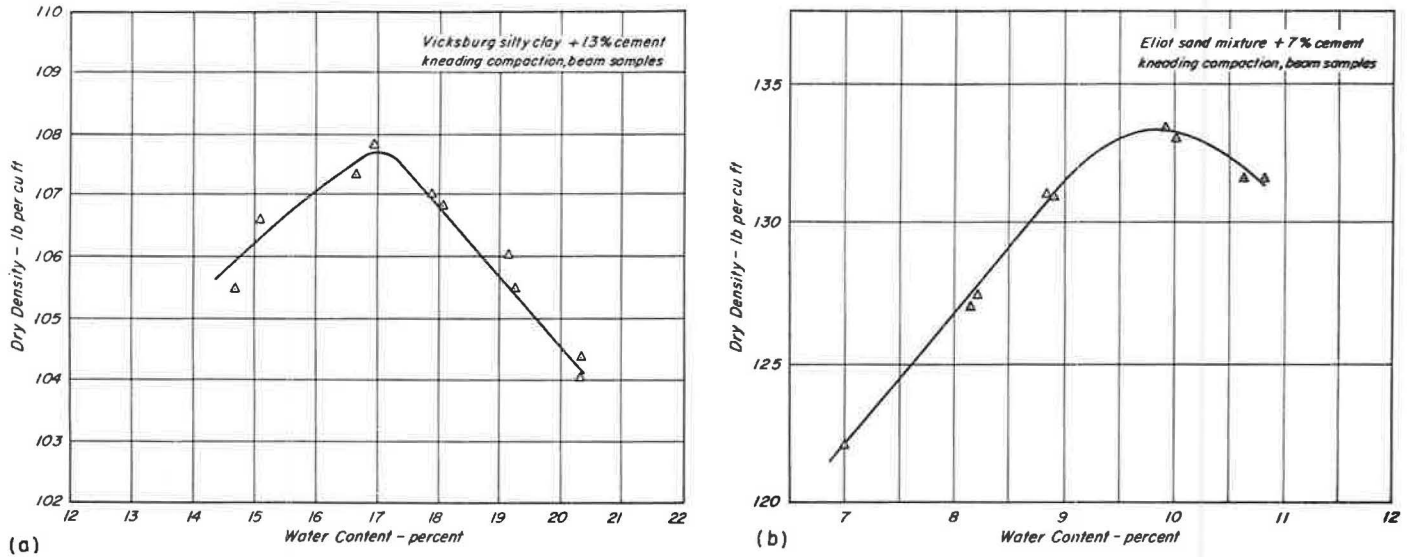

Figure 28. Compaction curves for (a) Vicksburg silty clay-cement beam samples; (b) Eliot sand mixture-cement beam samples.

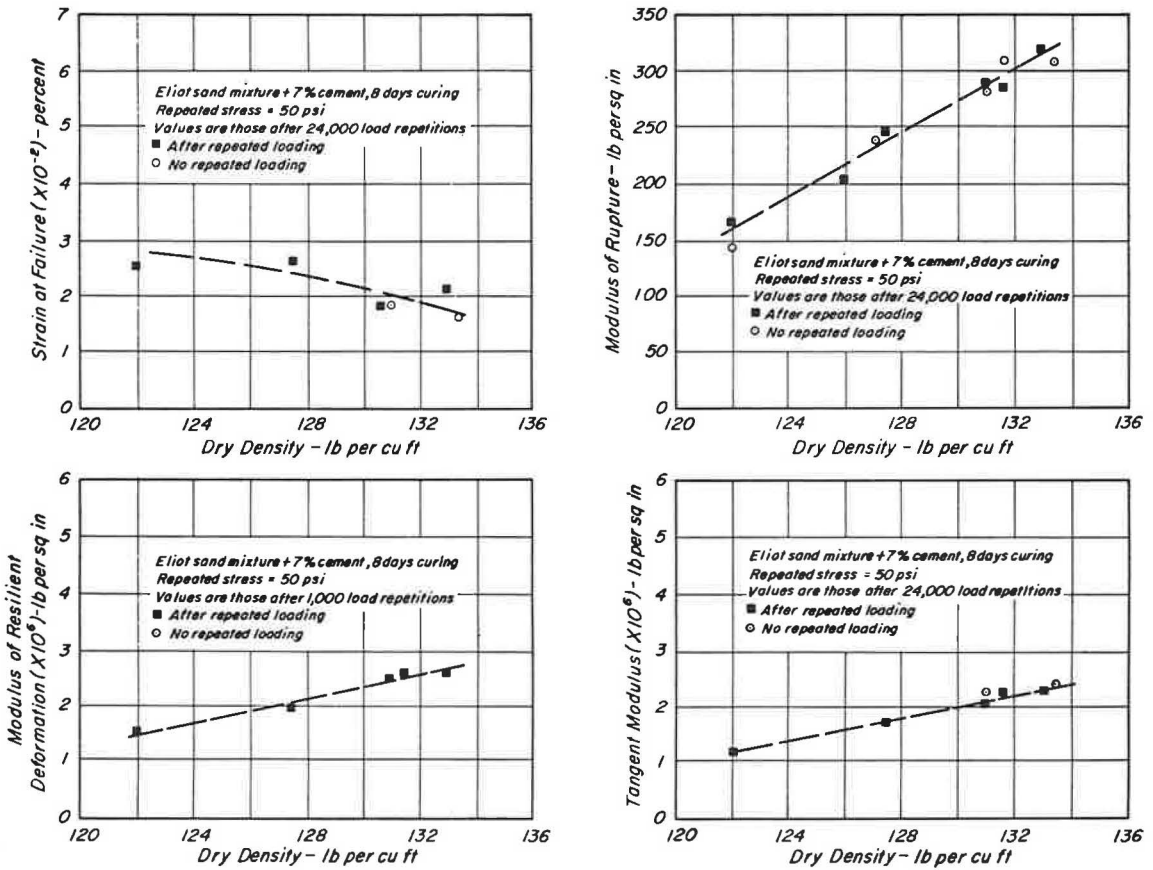

Figure 29. Effect of repeated flexural stress on the properties of Eliot sand mixture-cement.

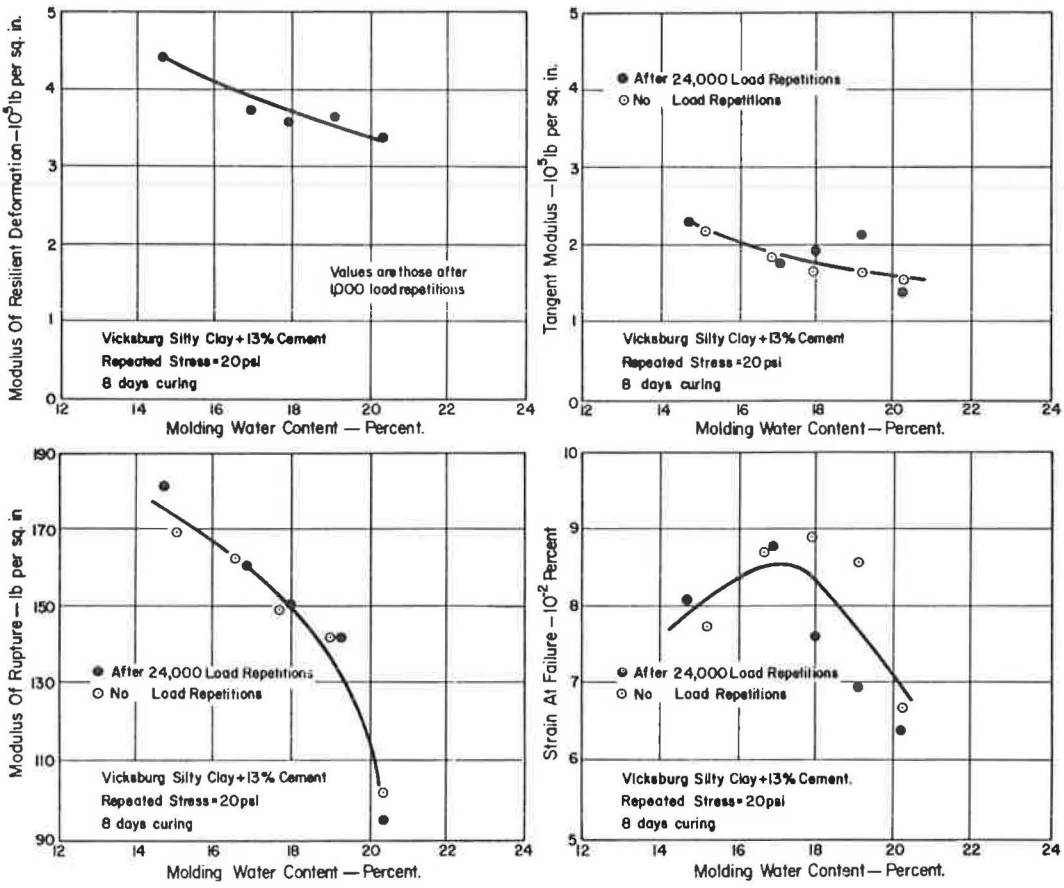

Figure 30. Effect of repeated flexural stress on the properties of Vicksburg silty clay-cement.

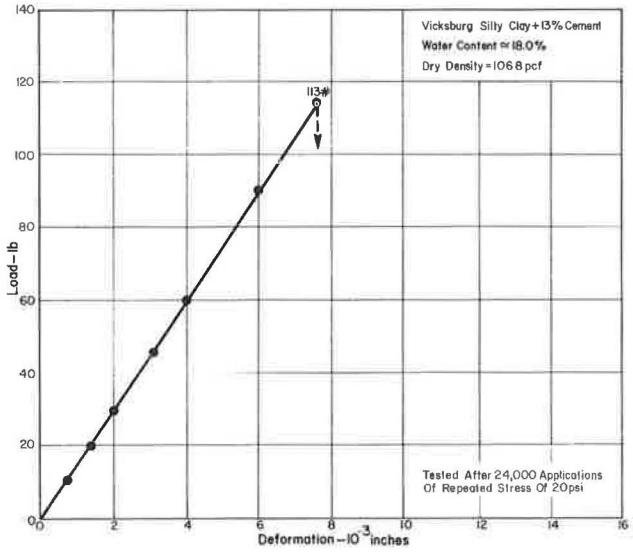

Figure 31. Load-deformation curve for Vicksburg silty clay-cement in flexure.

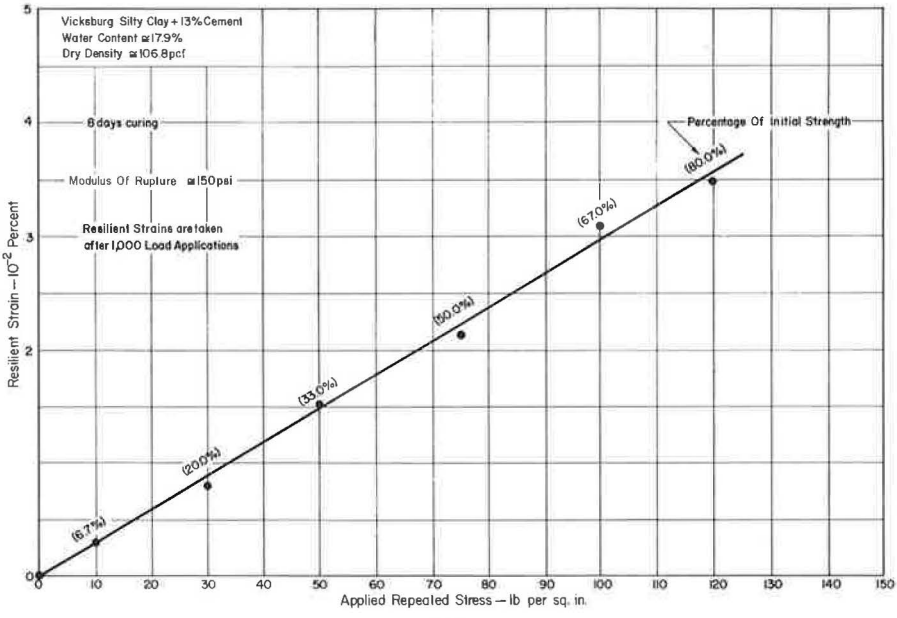

Figure 32. Effect of stress intensity on resilient deformation of Vicksburg silty clay-cement.

modulus of resilient deformation in flexure is independent of the magnitude of applied repeated stress.

ESM-cement samples were compacted at a water content of 9.1 percent and a dry density of 132.0 pcf. Repeated flexural tensile stresses of 15, 30, 70, 100, 125, 150, 200, and 225 psi were applied. Different magnitudes of repeated loading stresses had no significant influence on properties. One sample failed during the course of repeated loading under a stress of 225 psi, which corresponded to about 75 percent of the initial modulus of rupture of the sample.

Variations in number of load applications up to 100,000 had little effect on the properties of VSC-cement and ESM-cement subjected to repeated stress intensities of 20 and 50 psi, respectively.

COMPARISON OF BEHAVIOR IN COMPRESSION AND IN FLEXURE

In the analysis of pavement structures, it is important to ascertain whether properties such as resilient modulus and strength are the same in tension and compression. A comparison of these properties under the two types of loading may be made using the test results obtained in this investigation.

Vicksburg Silty Clay-Cement

1. The modulus of resilient deformation in compression varies greatly with compaction conditions, applied stress intensity, curing period, and number of load applications at high intensities, thus indicating that the stress-strain relationship of cylindrical samples under loading is not linear. Similar results were found by Seed et al. (23) for compacted clay samples. In flexure tests, however, the modulus of resilient deformation varies little with compaction conditions and is almost invariant with both the applied stress intensity and the number of load applications up to 100,000.

Figure 33a shows values of modulus of resilient deformation with respect to molding water content both in compression and in flexure. The modulus of a dry-side sample in compression could be as much as 30 times that in flexure. This difference decreases as the molding water content increases. Essentially the same values of modulus are recorded for both types of tests at a molding water content of 20 percent or more.

2. Figure 33b compares the tangent modulus as determined by static compression and flexure tests. In this case, greater values were observed in flexure tests.

3. In flexure tests, the values of the modulus of resilient deformation are about two times greater than the tangent modulus values. On the other hand, values of the tangent modulus in compression tests are only about 2 to 10 percent of the modulus of resilient deformation. These differences are believed to be caused by the fact that the stress-strain curve obtained from a static test, which is the basis for the static modulus calculation, includes the effects of both elastic and plastic strains. The time of loading in the repeated loading tests is so short that little opportunity is provided for plastic deformation to develop. The greater variation between resilient and static values in compression tests than in flexural tests probably reflects the fact that the specimens were much more brittle in flexure.

4. Fatigue failure occurred in both types of tests at a repeated loading stress intensity of about 90 percent of the initial strengths.

5. The values of the modulus of rupture in flexure tests ranged from one-fourth to one-half of the strength in unconfined compression tests (Fig. 34a). This result agrees with the values in HRB Bulletin 292 (9).

6. The strains at failure in flexure tests range from 3 to 14 percent of the values for compression tests. The largest difference appears wet of optimum water content (Fig. 34b). A very low strain at failure in flexure may be one of the important factors governing the failure of soil-cement layers in pavement structure.

Eliot Sand Mixture-Cement

1. Moduli of resilient deformation in both compression and flexure increase significantly with dry density. Figure 35a shows that the modulus of resilient deformation in compression is about 4 to 10 times greater than in flexure.

2. Figure 35b shows a comparison of the tangent modulus from both types of static tests. Values in flexure are about 10 times greater than those in compression.

3. In flexure the values of the modulus of resilient deformation are about equal to the values of the tangent modulus. In compression, however, values of the modulus of resilient deformation are 10 to 100 times greater than the values of the tangent modulus.

4. The values of modulus of rupture in flexure range from one-third to one-half of the strength in unconfined compression (Fig. 36a).

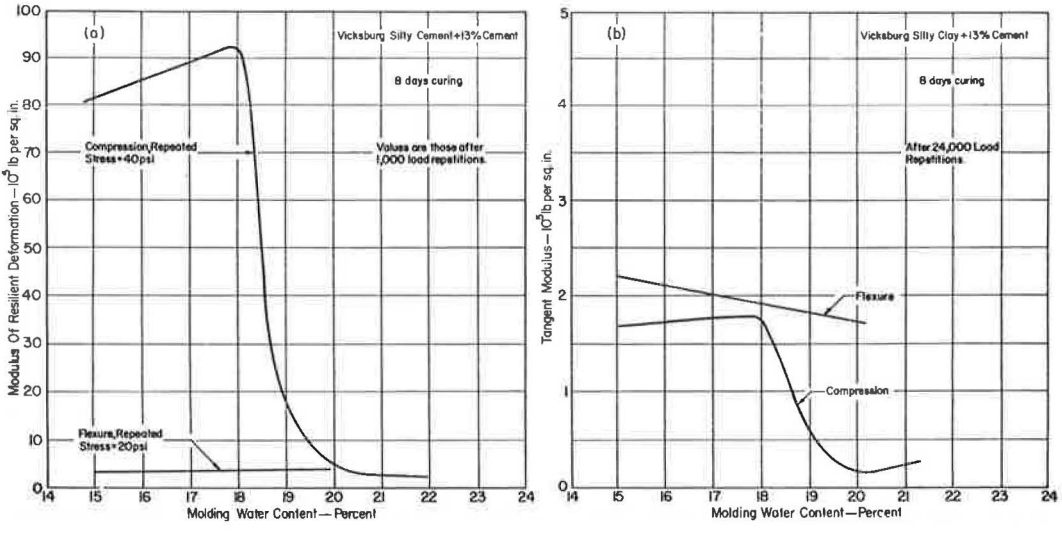

Figure 33. Comparison of the properties of Vicksburg silty clay-cement samples in compression and flexure.

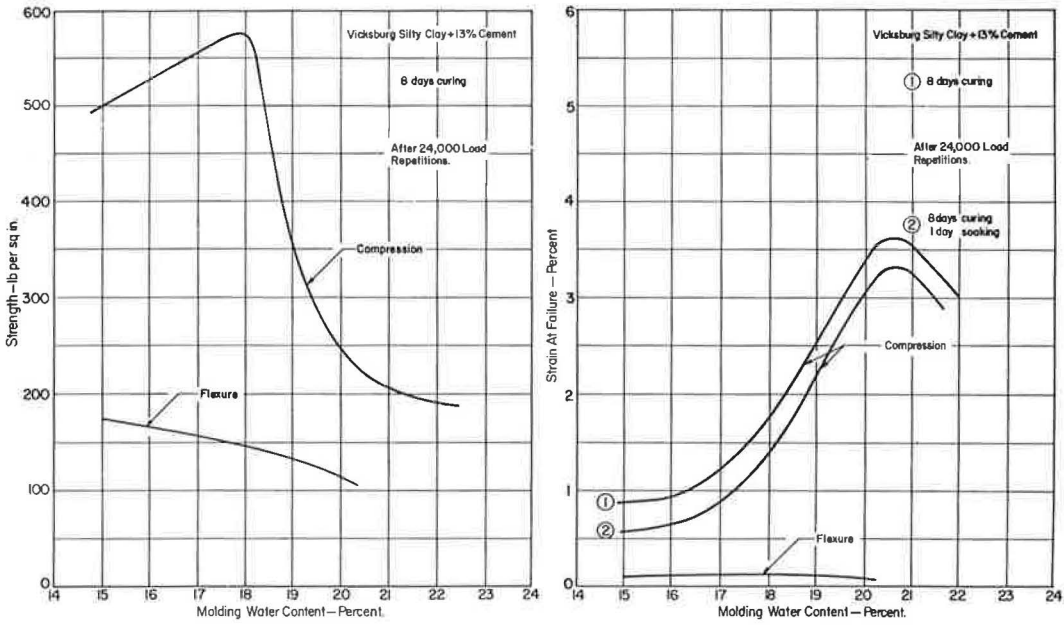

Figure 34. Comparison of the properties of Vicksburg silty clay-cement samples in compression and flexure.

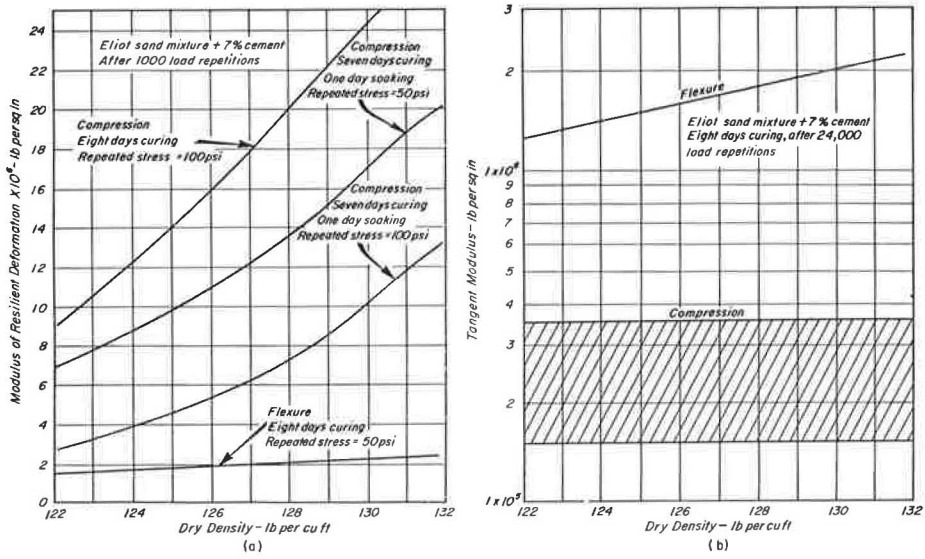

Figure 35. Comparison of the properties of Eliot sand mixture-cement samples in compression and flexure.

5. The strain at failure in flexure is only 5 percent that of the values in compression (Fig. 36b).

Table 2 summarizes the ranges of the foregoing values. Table 3 summarizes a few of the most significant differences in the behavior of soil-cement samples subjected to

TABLE 2

EXPERIMENTAL VALUES OF THE ELASTIC AND STRENGTH PROPERTIES OF SOIL-CEMENT

Material	Type of Loading	Water Content (%)	Dry Density (pcf)	Strength[a] (psi)	Resilient Modulus (psi)	Static Modulus (psi)	Strain at Failure (%)	Remarks
VSC-cement	Compression	14.5		570	90×10^5	1.8×10^5	0.8	M_{RC} varies with compaction conditions, curing period, N, and applied stress. Fatigue failure occurred at R. L. stress level of 90 percent. Kneading compaction causes dispersed soil structure on wet side of optimum.
		↓	–	↓	↓	↓	↓	
		22		200	2×10^5	0.2×10^5	3.5	
	Flexure	15		175	4.4×10^5	2.3×10^5	0.09	M_{RF} varies little with compaction conditions. No variation with N and applied stress. Fatigue failure occurred at R. L. stress level of 90 percent.
		↓	–	↓	↓	↓	↓	
		22		100	3.4×10^5	1.7×10^5	0.07	
ESM-cement	Compression	7	122	400	8×10^6	1.5×10^5	0.38	M_{RC} varies with γ_d, N, applied stress, and treatment condition.
		↓	↓	↓	↓	↓	↓	
		12	132	750	24×10^6	3.0×10^5	0.46	
	Flexure	7	122	160	1.5×10^6	1.2×10^6	0.03	M_{RF} varies with γ_d, no variation with N and applied stress. Fatigue failure occurred at R. L. stress level of 75 percent.
		↓	↓	↓	↓	↓	↓	
		11	132	320	2.7×10^6	2.4×10^6	0.02	

[a]Compressive strength or modulus or rupture.

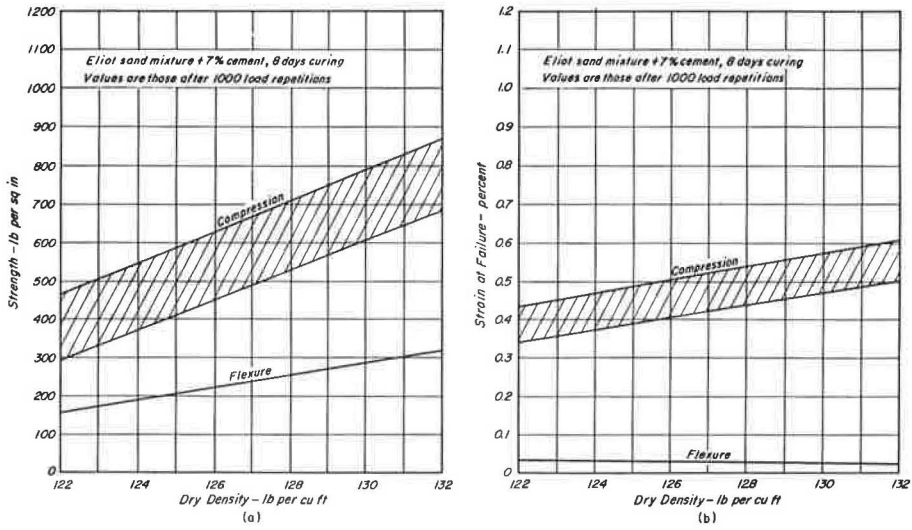

Figure 36. Comparison of the properties of Eliot sand mixture-cement samples in compression and in flexure.

TABLE 3

DIFFERENCES IN THE BEHAVIOR OF SOIL-CEMENT SUBJECTED TO REPEATED STRESSES IN COMPRESSION AND FLEXURE

Behavior	Compression	Flexure
Modulus of resilient deformation	High (varies with applied stress intensity)	Low (independent of applied stress intensity)
Fatigue failure occurred at about	90 percent R. L. stress level (VSC-cement)	90 percent R. L. stress level (VSC-cement) 75 percent R. L. stress level (ESM-cement)
Strain at failure	High	Low
Effect of repeated loading on properties	Large	Small

repeated compressive and flexural stresses as derived from this study. These results clearly indicate that consideration must be given to the type of loading when selecting values of soil-cement properties for use in analysis.

CONCLUSIONS

This study has been concerned with the investigation of the dynamic properties, the resilience characteristics, and the fatigue behavior of two types of soil-cement (a silty clay and a sand) under the action of both repeated compressive and flexural stresses. Major conclusions from this study may be summarized as follows.

1. Under constant repeated stress, the modulus of resilient deformation in both compression and flexure at a given number of load applications is directly related to dry density for ESM-cement samples. The higher the dry density, the greater is the modulus. In the case of VSC-cement, the modulus of resilient deformation in flexure of beam samples decreases as molding water content increases. For cylindrical

samples the resilient modulus in compression is greatly influenced by dry density, molding water content, and compactive effort. This is due to the structure-sensitive character of specimens compacted wet of optimum moisture content. In both materials, the ranges of modulus variation are greater in compression than in flexure.

2. The modulus of resilient deformation of soil-cement in repeated compression is greatly affected by the magnitude of the stress intensity. The resilient modulus decreases rapidly with increasing applied stress intensity at low stress levels. There is, however, only very little change in resilient modulus with change in stress at applied stress intensities greater than 30 to 40 percent of the initial strength of the sample.

The unconfined compressive strengths of the ESM-cement samples are increased by about 10 percent of their initial values after being subjected to 24,000 low stress intensity repeated loadings (stress intensity of 15 percent of the strength). In VSC-cement, however, increase of strength was only noticed in the samples subjected to higher stress intensities (up to 80 percent of the strength). An increase in strength of 8 to 35 percent was recorded at these stress levels.

The relationships between resilient modulus and applied stress intensity and the relationship between strength variation and applied stress intensity in repeated flexure tests do not parallel those in compression tests. In flexure tests both the resilient modulus and the strength are virtually unaffected by the magnitude of the applied repeated stress intensity.

3. Results from the repeated flexure tests have indicated that the resilient deformation remains almost unchanged with respect to number of load applications, even at applied stress intensities very close to the limiting value which causes fatigue failure. Results from the repeated compression tests have shown that only at applied stress levels of less than about 30 to 40 percent of the initial strength is the magnitude of resilient deformation not affected by the number of load applications. At higher applied stress intensities, resilient deformations vary with the number of load applications, with the maximum values occurring between about 1 and 500 load applications. The resilient deformation at N = 100,000 may be only about one-fifth to one-fourth of the maximum value.

4. The longer the curing period before the start of repeated compression, the greater the minimum resilient modulus for a repeated loading stress equal to a given percentage of the initial strength.

5. Soaked samples yield smaller values of resilient modulus than unsoaked samples when subjected to the same magnitude of repeated loading stress.

6. The values of modulus of resilient deformation are several times greater in compression than in flexure, except in VSC-cement samples compacted wet of optimum where essentially the same values of modulus are recorded in both types of tests.

7. The values of modulus of rupture range from one-fourth to one-half of the values of unconfined compressive strength.

8. The strain at failure in flexure is only about 5 to 15 percent of that in compression.

9. The tangent modulus as determined by static tests is greater in flexure than in compression. In ESM-cement, the difference is as much as 10 times.

10. The minimum stress intensity required to cause fatigue failure in VSC-cement samples is about 90 percent of the strength of the sample both in compression and in flexure, whereas in ESM-cement samples the minimum stress intensity is around 75 percent of the strength in flexure. No fatigue failures developed in cylindrical ESM-cement samples, because of the limited capacity of the repeated loading piston and the high strength of the ESM-cement.

The results of this study provide information that can be used in the analysis of pavement structures containing soil-cement layers. It is believed that the repeated loading test may provide a realistic means of assessing soil-cement properties in the laboratory for predicting field behavior under repetitive traffic loads. Inasmuch as the results indicate that values for moduli may be considerably different when evaluated under static loading rather than repeated loading conditions, it is particularly important that consideration be given to the type of test for selection of property values.

Furthermore, consideration must be given to the fact that properties in compression and flexure differ.

Finally, it should be emphasized that all results are for samples prepared and tested in the laboratory. Field tests are needed to verify many of the findings, and careful consideration must be given to the effects of shrinkage and temperature cracking that might develop in the field, but which did not affect the laboratory specimens.

ACKNOWLEDGMENTS

These studies were supported in part by the Institute of Transportation and Traffic Engineering, University of California, Berkeley, and in part by the U. S. Army Engineer Waterways Experiment Station, Army Materiel Command Project No. 1-T-0-21701-A-046-05.

Valuable suggestions and helpful criticisms were provided by Carl L. Monismith; Clarence K. Chan provided assistance in instrumentation for the experimental work; George Dierking and J. P. Singh prepared the figures; and Mian-Chang Wang Assisted with the experimental work.

REFERENCES

1. Ahmed, S. B., and Larew, H. G. A Study of the Repeated Load Strength Moduli of Soils. Proc. Internat. Conf. on the Structural Design of Asphalt Pavements, Univ. of Michigan, 1962.
2. Biarez, J. Analysis of Flexible Airfield Pavements by Surface Plate-Loading. Proc. Internat. Conf. on the Structural Design of Asphalt Pavements, Univ. of Michigan, 1962.
3. Childs, L. D. Tests of Concrete Pavement Slabs on Cement-Treated Subbase. Res. and Dev. Lab., Portland Cement Assoc., 1964.
4. Dormon, G. R. The Extension to Practice of a Fundamental Procedure for the Design of Flexible Pavements. Proc. Internat. Conf. on the Structural Design of Asphalt Pavements, Univ. of Michigan, 1962.
5. Dormon, G. R., and Metcalf, C. T. Design Curves for Flexible Pavements Based on Layered System Theory. Highway Research Record 71, pp. 69-84, 1965.
6. Dunn, F. P. The Effect of Sustained and Repeated Loads on Soil-Cement; and An Analysis of Its Viscoelastic Behavior. C. E. Res. Experiment Sta., Ohio State Univ., 1960.
7. Federal Aviation Agency. Thickness Design Procedure for Airfields Containing Stabilized Pavement Components. U. S. Department of Commerce, Office of Tech. Services, 1964.
8. Groves, B. A. The Influence of Method of Compaction on Soil-Cement Strength Properties. Res. Rept., Univ. of California, 1964.
9. Soil Stabilization with Portland Cement. Highway Research Board Bull. 292, 1961.
10. Highway Research Board. The AASHO Road Test: Report 7—Summary Report. Spec. Rept 61G, 1962.
11. Hveem, F. N. Pavement Deflections and Fatigue Failures. Highway Research Board Bull. 114, pp. 43-73, 83-87, 1955.
12. Jones, A. Tables of Stresses in Three-Layer Elastic Systems. Highway Research Board Bull. 342, pp. 176-214, 1962.
13. Mitry, F. G. Determination of the Modulus of Resilient Deformation of Untreated Base Course Materials, Ph.D. thesis, Univ. of California, 1964.
14. Nussbaum, P. J., and Larsen, T. J. Load-Deflection Characteristics of Soil-Cement Pavements. Highway Research Record 86, pp. 1-14, 1965.
15. Peattie, K. P. A Fundamental Approach to the Design of Flexible Pavements. Proc. Internat. Conf. on the Structural Design of Asphalt Pavements, Univ. of Michigan, 1962.
16. Seed, H. B., Chan, C. K., and Monismith, C. L. Effect of Repeated Loading on the Strength and Deformation of Compacted Clay. Proc. Highway Research Board, Vol. 34, pp. 541-558, 1955.

17. Seed, H. B., and McNeill, R. L. Soil Deformations in Normal Compression and Repeated Loading Tests. Highway Research Board Bull. 141, pp. 44-53, 1956.
18. Seed, H. B., McNeill, R. L., and deGuenin, J. Increased Resistance to Deformation of Clay Caused by Repeated Loading. ASCE Proc. Paper 1645, 1958.
19. Seed, H. B., and Chan, C. K. Effect of Stress History and Frequency of Stress Application on Deformation of Clay Subgrades Under Repeated Loading. Proc. Highway Research Board, Vol. 37, pp. 555-575, 1958.
20. Seed, H. B., and Fead, J. W. N. Apparatus for Repeated Load Tests on Soils. ASTM Spec. Tech. Publ. No. 254, 1959.
21. Seed, H. B., and Chan, C. K. Structure and Strength Characteristics of Compacted Clays. ASCE Proc. Paper 2216, ASCE Jour. Soil Mech. and Found. Div., Vol. 85, No. SM5, 1959.
22. Seed, H. B., and Chan, C. K. Effect of Duration of Stress Application on Soil Deformation Under Repeated Loading. Proc. 5th Internat. Conf. on Soil Mech. and Found. Eng., Vol. 1, 1961.
23. Seed, H. B., Chan, C. K., and Lee, C. E. Resilience Characteristics of Subgrade Soils and Their Relation to Fatigue Failure on Asphalt Pavements. Proc. Internat. Conf. on the Structural Design of Asphalt Pavements, Univ. of Michigan, 1962.
24. Trollope, D. H., Lee, I. K., and Morris, J. Stresses and Deformation in Two Layer Pavement Structures Under Slow Repeated Loading. Proc. Australian Road Res. Board, Vol. 1, Pt. 2, 1962.
25. Vallerga, B. A. Recent Laboratory Compaction Studies of Bituminous Paving Mixtures. Proc. Assoc. Asphalt Paving Technologists, Vol. 20, 1951.
26. West, G. A Laboratory Investigation into the Effect of Elapsed Time After Mixing on the Compaction and Strength of Soil-Cement. Geotechnique, March 1959.
27. Whittle, J. P., and Larew, H. G. Effects of Repeated Loads on Elastic Micaceous Soils Stabilized with Portland Cement. Highway Research Record 86, pp. 28-38, 1965.

Measurement of Elastic and Strength Properties of Cemented Materials in Road Bases

R. JONES, Road Research Laboratory, Department of Scientific and Industrial Research, Great Britain

•MEASUREMENTS of the elastic properties of lean concrete and cement-stabilized materials, i.e., cemented materials in the bases or subbases of flexible roads, are useful for three main reasons.

1. A knowledge of the elastic properties and the thicknesses of the constituent layers of a road permits calculation of the stresses arising in the road from traffic loading (1).
2. There is usually an empirical relationship between the modulus of elasticity and the strength of a cemented material (2). Thus, in situ measurements of the elastic properties of a cemented base or subbase can provide an estimate of its strength and give an indication of whether the material is likely to fail under the stresses previously cited.
3. Changes in the elastic properties of cemented layers of a road with time and traffic indicate whether or not severe deterioration has occurred (3).

The considerably reduced value of the elastic modulus obtained from measurements on roads having badly cracked cemented bases has permitted more realistic computations (1) to be made of the stresses which will develop in other parts of the road when the design criteria allow cracking to occur.

This paper gives the results of measurements of the dynamic elastic properties and the compressive and flexural strengths of laboratory specimens of cemented materials of the type used in road bases and subbases.

A surface wave propagation method is described for measuring the in situ modulus of elasticity of cemented layers of a road. Estimates of the strength of the uncracked materials are made from empirical relations of the type discussed in the next section.

The paper discusses repetitive measurements at the surface of a road by the surface-wave propagation method to study the changes in the elastic properties of cemented bases. The influence of the results of these measurements on design criteria for cemented layers of a road is discussed briefly later.

LABORATORY EXPERIMENTS ON TEST SPECIMENS

Experimental Procedure

Resonance and pulse methods (2) are used to obtain the dynamic Young's modulus and Poisson's ratio of test specimens that are subsequently broken to give the compressive or flexural strength of the material. The measurements of the longitudinal resonant frequency and pulse velocity are made by techniques which are now widely used for test specimens of normal concrete and which are fully described elsewhere (2).

The fundamental resonant frequency (n_o) of a cylinder or prism in its longitudinal mode of vibration is related to the dynamic Young's modulus (E) of the material by the relation:

$$\left(\frac{gE}{\rho}\right)^{1/2} = 2\, n_o\, l\, T_\ell \qquad (1)$$

Paper sponsored by Committee on Soil-Portland Cement Stabilization and presented at the 45th Annual Meeting.

where

ρ = bulk density of specimen,
g = acceleration due to gravity,
l = length of specimen, and
T_ℓ = a factor to correct for finite cross-section of specimen (2). (In the present experiments T_ℓ has a maximum value of about 1.05.)

Eq. 1 allows E to be calculated when ρ, n_o, l and T_ℓ are known. When a comparison is made with in situ tests on road bases, it is more convenient to work with the parameter $(gE/\rho)^{1/2}$ as explained later.

The pulse velocity α in the specimen is related to the elastic moduli by the relation:

$$\left(\frac{gE}{\rho}\right)^{1/2} = \alpha\left[\frac{(1+\nu)\ (1-2\nu)}{1-\nu}\right] \qquad (2)$$

where ν is Poisson's ratio calculated from Eqs. 1 and 2 and n_o, l, T_ℓ and α are known.

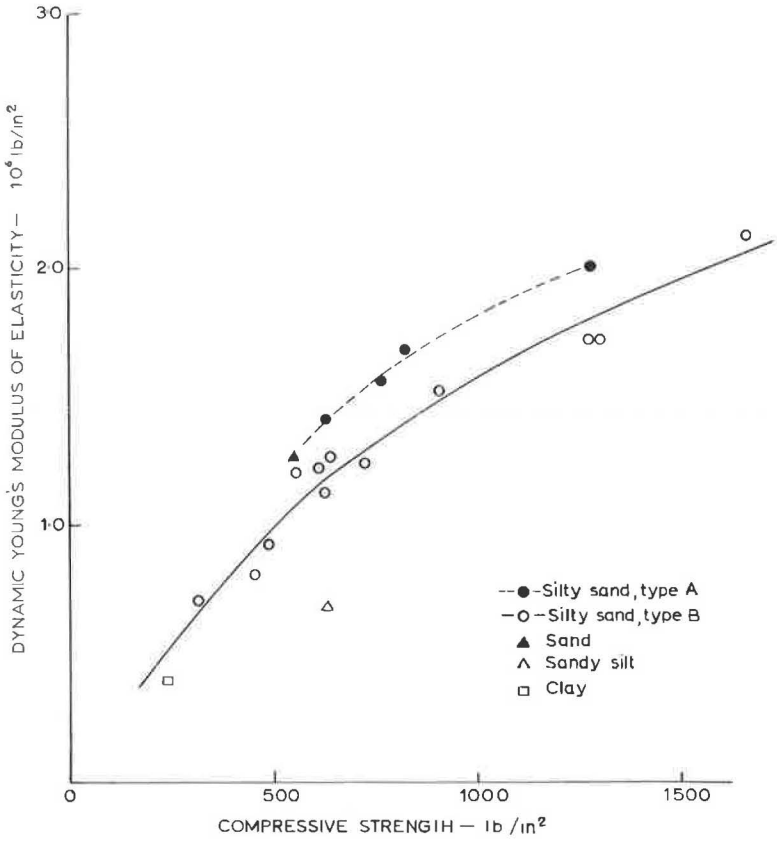

Figure 1. Relation between dynamic Young's modulus and compressive strength of different types of soil cement (fine-grained soils).

TABLE 1

CHARACTERISTICS OF SOILS USED IN INVESTIGATION FOR FIGURES 1 AND 2

Soil Type	Casagrande Class.	Particle Size Distribution				Index Tests			British Standard Compaction Test (B. S. 1377:1948)	
		Gravel (%)	Sand (%)	Silt (%)	Clay (%)	L. L. (%)	P. L. (%)	P. I. (%)	Max. Dry Density (pcf)	Opt. Moist. Content (%)
Sandy gravel	GF	52	28	13	7		Nonplastic		128	10
Sand	SU	—	95	2	3		Nonplastic		113	12
Silty sand (A)	CL	6	57	29	8	21	15	6	126	10
Silty sand (B)	CL	—	56	31	13	26	15	11	119	12
Sand silt	CL	—	25	60	15	31	18	13	113	15
Clay	CH	—	30	23	47	65	20	45	92	24

Results

The relation between the dynamic Young's modulus and the compressive strength of soil-cement containing fine-grained soils is shown in Figure 1; details of the various soils are given in Table 1. The relation between the dynamic Young's modulus and the flexural strength of the soil cements is shown in Figure 2. The results show that the

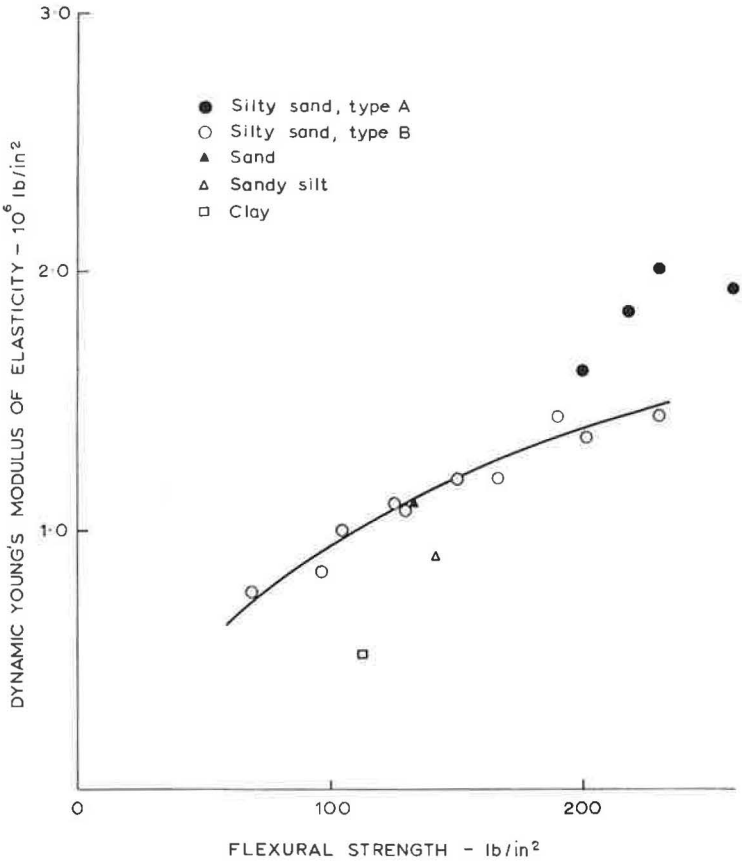

Figure 2. Relation between dynamic Young's modulus and flexural strength of different types of soil cement (fine-grained soils).

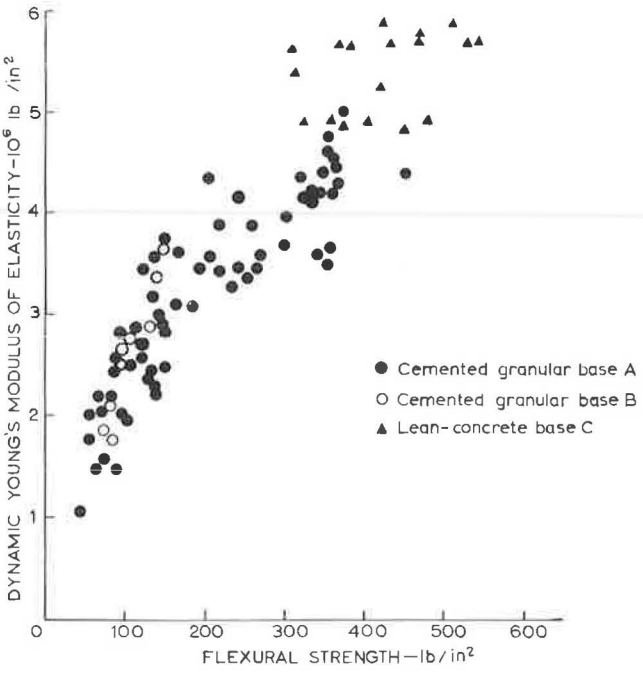

Figure 3. Relation between dynamic Young's modulus of elasticity and flexural strength of cemented base materials.

dynamic modulus varied between about 0.5×10^6 psi and 2.0×10^6 psi; in the case of soil-cement made from silty sand, type B, the variations were produced by changing the dry density, cement content, moisture content and age of test. Figures 1 and 2 show that the relations between dynamic modulus of elasticity and either compressive or flexural strength for the soil-cement containing silty sand, type B, were relatively insensitive to the variations in composition or age of test; changes in soil type often produced significant deviations from these relations.

Results obtained for the dynamic Young's modulus of elasticity and the flexural strength of cemented base materials containing gravel aggregate to a maximum size of about 1½ in. are shown in Figure 3. Bases A and B contained "as-dug" aggregate and conformed to an outdated specification for cement-bound granular base material, whereas base C contained washed and graded aggregate, and the material conformed to the specification for lean concrete given later. The results (Fig. 3) were obtained on beams cut from the bases, and there is an approximate relation between the dynamic modulus and flexural strength applicable to all three base materials. The significance of these results in the design criteria for cemented bases is discussed later.

Poisson's ratio for all the materials tested in the foregoing investigations was within the range 0.25 to 0.40.

MEASUREMENTS OF ELASTIC AND STRENGTH PROPERTIES

Experimental Procedure

Measurements of the wavelength and velocity of surface vibrations generated at frequencies between about 500 and 25,000 cps were made at the surface of the bases. The experimental technique (3) and interpretation of the results (4) have been given elsewhere, and only essential details are given here.

When the velocity of surface waves exceeds the velocity of compressional waves in the medium below the base layer, the wave propagation becomes approximately independent of the underlying medium (4). Flexural waves are propagated in the base layer

TABLE 2

THEORETICAL RELATION BETWEEN c AND λ FOR SURFACE WAVES ALONG A BASE LAYER OF THICKNESS, H

c/γ	$(\lambda/H)\ \nu = \frac{1}{4}$	$(\lambda/H)\ \nu = \frac{1}{3}$
1.00	0	0
0.80	2.20	2.30
0.70	3.05	3.20
0.60	4.15	4.30
0.50	5.40	5.65

and there is a relation between velocity c and wavelength λ of the surface waves. This is given in Table 2 for values of Poisson's ratio ¼ and ⅓; the graphical form of this relation will be called branch A.

In Table 2, γ is the velocity of Rayleigh waves in the base material, and is found either by extrapolating the experimental results to zero wavelength or (by means of Table 2) from the known value of H and the measured values of c and λ. The first procedure gives a value for γ which is determined mainly by the properties of the material near the surface of the base, whereas the second procedure, applied at the longer wavelengths, provides a better average value for a base of variable properties with depth. The γ-wave velocity is related to the parameter $(gE/\rho)^{1/2}$ by a factor which changes by less than 4 percent for the range of Poisson's ratio, 0.25 to 0.40, found for cemented materials.

When ν is unknown, an assumed value of ⅓ will enable $(gE/\rho)^{1/2}$ to be calculated from γ with an error of less than ±2 percent by the relation:

$$\gamma = 0.571 \left(\frac{gE}{\rho}\right)^{1/2} \tag{3}$$

Thus $(gE/\rho)^{1/2}$ is a useful parameter for comparing the elastic properties of bases with those of laboratory test specimens tested in resonance. The dynamic modulus (E) required in stress distribution computation can be found from γ when the density (ρ) is known.

Results on Sand-Cement and Lean-Concrete Bases

Figure 4 shows experimental results from branch A of the relation between the velocity and wavelength of surface waves on sand-cement bases 3, 6 and 9 in. thick. The sand-cement base consisted of closely graded sand mixed with 8 percent portland cement and 14 percent water; the bases were tested at an age of 15 days, before being surfaced with rolled asphalt. Results are also shown in Figure 4 for a lean-concrete base, 6 in. thick, tested at an age of 24 days; the lean concrete was of the same composition as base C in Figure 3 and contained graded aggregate complying with B. S. 882, 1½-in. maximum-size mixed with portland cement in the ratio of 1 part cement to 15 parts aggregate by weight to which 5 percent of water was added.

The measurements were made on a test length of approximately 50 ft, along the inner wheelpath of vehicles in the inside lane, where maximum traffic loading occurs. Subsequent measurements were made along a corresponding test length at the surface of the added bituminous wearing course.

Theoretical curves for branch A have been deduced from Table 2 and fitted to the experimental results of Figure 4; nominal construction thicknesses were assumed and Poisson's ratio ν was calculated from resonance and pulse velocity experiments on test specimens. The curves (Fig. 4) were computed theoretically and are intended to provide the best correlation with the experimental points at the higher velocities so as to give a reliable extrapolation to zero wavelength γ. The experimental results deviate below the theoretical curves at the longer wavelengths in all except the tests on the 3-in. sand-cement base, suggesting that either the construction thicknesses were slightly less than the nominal value (though within the limit of the specification) or, as is more likely, that there was a decrease in compaction towards the bottom of the 6- and 9-in. thick bases.

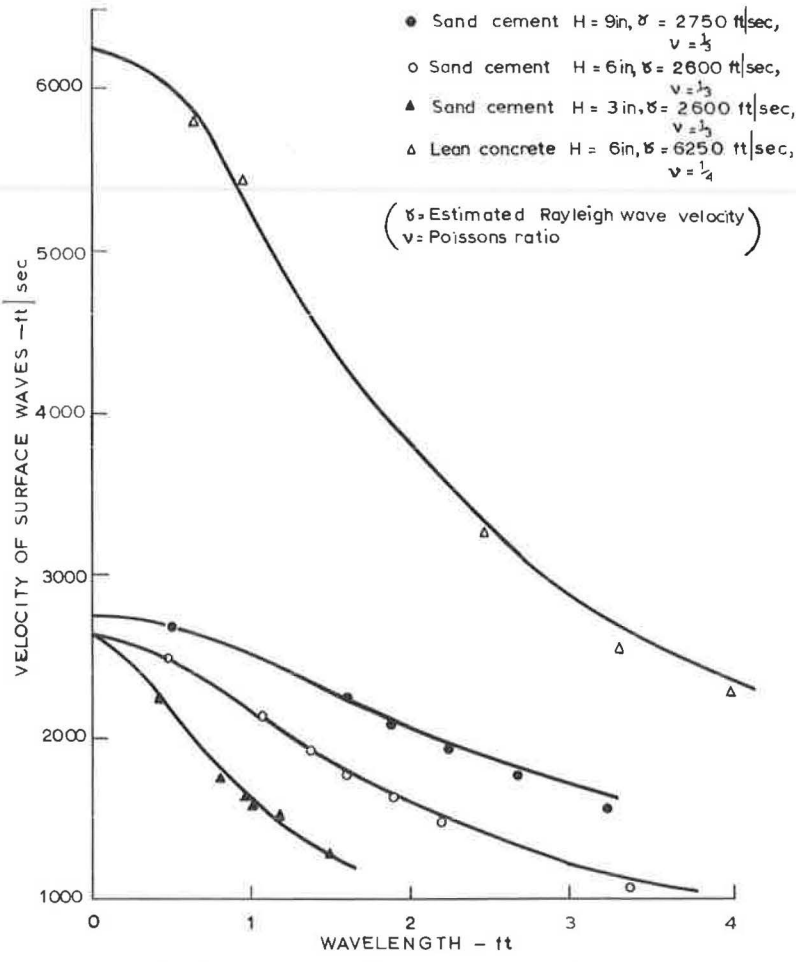

Figure 4. Experimental results obtained from surface wave propagation on cemented bases of different nominal thicknesses (H).

Estimates of $(gE/\rho)^{1/2}$ obtained from γ are compared in Table 3 with the corresponding parameter deduced from laboratory experiments on test specimens at an age of 28 days and cores drilled from the bases. The estimated value of $(gE/\rho)^{1/2}$ at 28 days on the bases was 6 to 20 percent below the same parameter measured on test specimens for both the sand-cement and lean concrete. This is not unusual because it is rarely

TABLE 3

COMPARISON OF RESULTS OBTAINED ON BASES AND TEST SPECIMENS

Type and Thickness of Base	Age (days)	γ (ft/sec)	E ($\times 10^6$ psi)	$(gE/\rho)^{1/2}$ (ft/sec)	Estimated $(gE/\rho)^{1/2}$ (ft/sec)	Test Specimens at 28 Days $(gE/\rho)^{1/2}$ (ft/sec)	Cores at 28 Days
Sand-cement (3 and 6 in.)	15	2,600	0.50	4,550	4,950	5,500	5,200
Sand-cement (9 in.)	15	2,750	0.50	4,800	5,200		5,300
Lean concrete (6 in.)	24	6,250	3.5	10,750	10,900	13,200	—

possible to produce such good compaction in the bases as in the test specimens. The cores taken from the soil-cement bases gave a slightly higher value of $(gE/\rho)^{1/2}$ than was derived from in situ measurements on the bases, but the discrepancy would have arisen because the cores were not from the full depth of the bases and probably represented the stronger material in the base.

TESTS ON ROADS HAVING CEMENTED BASES

Experimental Procedure

The experimental procedure is essentially the same as that described previously except that the experiments are made at the surface of the road. The relation between velocity and wavelength corresponding to branch A is modified by the presence of the extra surface layer which usually has a Young's modulus of elasticity comparable with

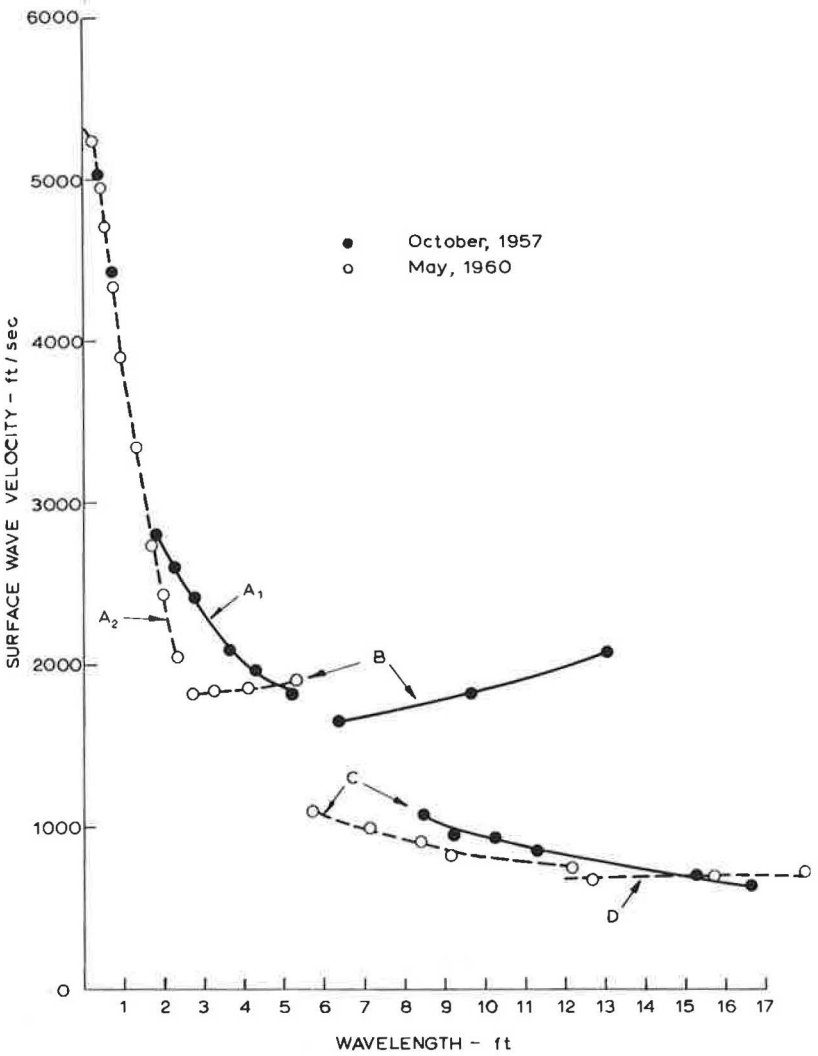

Figure 5. Changes in relation between velocity and wavelength of surface wave on section having 4-in. rolled-asphalt surfacing, 9-in. sand-cement base, 7½-in. sand subbase and clay subgrade.

the cemented base. In such cases, the relation corresponding to branch A can be constructed by adding the wavelengths from branch A of the separate layers at each velocity (4). This procedure provides a reliable approximation at velocities below the γ-wave velocity in the layer with the lowest modulus of elasticity and for ratios of moduli of less than 2:1. Lower velocity branches of the relation between velocity and wavelength become important during the breakup of cemented bases, and these are discussed later.

Results

The experimental results for flexural waves in a composite layer formed by a 4-in. rolled-asphalt surfacing and the 9-in. thick sand-cement layer, are shown in Figure 5 as branch A_1; these results were obtained in 1957, immediately after the road was constructed, before it was opened to traffic. In 1960, the experimental results fell on curve A_2 which represents propagation in the asphalt surfacing only and indicated that the sand-cement base was no longer a continuous material.

Branch B (Fig. 5) can be explained by the compressional wave velocity in the clay subgrade being higher than the compressional wave velocity in the sand subbase (4). The theory indicates that branch B approaches the velocity of compressional waves in the sand subbase at short wavelengths, and the increase in velocities along branch B between 1957 and 1960 reflects the compaction that occurred in the subbase under traffic (3).

Branch C (Fig. 5) depends on the overall stiffness of the road. The value of the parameter $c^2\lambda$ for this branch is a useful indication of the stiffness of the road and approximately related to the inverse of the deflection of the surface in deflection beam experiments (3). The parameter $c^2\lambda$ decreased from about 90 units in 1957 to about 70 in 1960, showing that the decrease in stiffness due to breakup of the base more than offsets the increase in stiffness of the subbase.

Branch D is connected with the shear elastic properties of the broken base layer (3) and gave a value for the dynamic Young's modulus of approximately 4×10^4 psi in 1960 compared with the original value of 6×10^5 psi in sound material.

There were even more spectacular changes in the relation between velocity and wavelength of surface waves associated with the breakup of the 6-in. lean-concrete base discussed previously. This base was on a sand subbase and clay subgrade but was surfaced with 4-in. bitumen macadam. Branch A (Fig. 6) represents flexural waves in the composite layer of surfacing plus base obtained in 1957 before the road was opened to traffic. Eighteen months later, there was no contribution to branch A from the base layer and branch A_2 refers solely to vibrations in the bitumen macadam. Complete results for all experimentally observed branches of the relation between velocity and wavelength of surface waves in 1957 and 1960 were compared (Fig. 6). Corrections have been applied to the results obtained in 1960 to allow for the effect of a different test temperature on the elastic properties of the bitumen-macadam layer.

Branch B gives the increase in compressional wave velocity in the sand subbase associated with the compaction occurring between 1957 and 1960. In spite of the increased stiffness of the subbase, the overall stiffness has decreased considerably between 1957 and 1960 and $c^2\lambda$ for branch C fell from about 140 units to 60 units.

Branch D gives an approximate value for the shear wave velocity in the disintegrated lean concrete of 760 ft/sec. The effective dynamic Young's modulus of elasticity was about 6×10^4 psi compared with the original value of 3.5×10^6 psi. The final value in 1960 was equivalent to that which has been obtained on well-compacted crushed-stone bases (3).

Branch E gives a shear wave velocity of 610 ft/sec in the compacted sand subbase. The effective dynamic Young's modulus was 28,000 psi compared with 9,000 psi measured directly on the subbase (3). The sand in the subbase was of the same type as was used in the sand-cement subbase and the results suggest that, in its compacted state, it attained an elastic modulus (28,000 psi) comparable with the badly broken sand-cement base (40,000 psi).

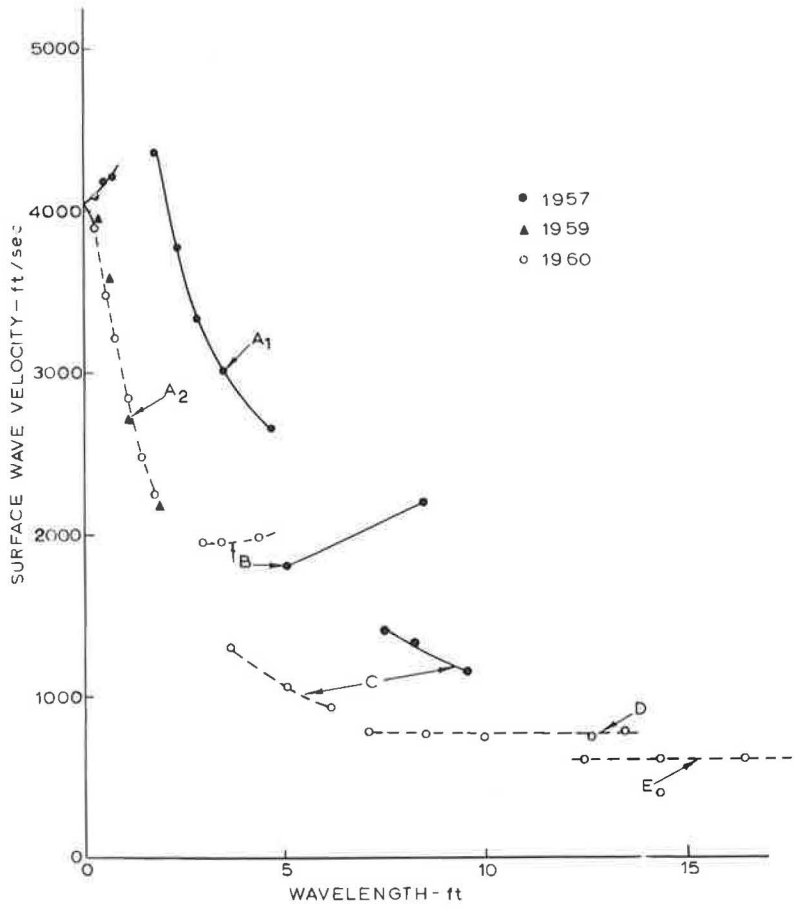

Figure 6. Change in relation between surface wave velocity and wavelength on a road having 4-in. bitumen-macadam surfacing, 6-in. lean-concrete base, 9-in. sand subbase on clay subgrade.

Discussion

The foregoing technique can be used to provide information on tensile stresses developed in cemented road bases and caused by the passage of traffic. It permits an estimate to be made as to whether the base will develop cracks from these stresses.

Figure 7 shows the computed tensile stresses at the bottom of two thicknesses of bases, 6 and 9 in., where Young's modulus of elasticity varied between 0.5 to 6.0 × 10^6 psi. The foundation material had a Young's modulus of 3 × 10^4 psi (CBR about 17 percent). The cemented bases were each covered by a rolled-asphalt surfacing, 4-in. thick, having a Young's modulus of 10^5 psi; the asphalt has this modulus when the surface temperature is about 35 C. The wheel load for this calculation was 14,000 lb. These conditions represent the passage of a very heavy wheel load at normal traffic speeds and correspond to a heavier load than the maximum legal loading for British roads. The mean relation between the Young's modulus and flexural strength of cemented and lean-concrete bases (Fig. 4) is also reproduced in Figure 7.

Only materials having a flexural strength of over 300 psi for a 6-in. base, or over 150 psi for a 9-in. base, would be likely to survive even a single traverse of a 14,000-lb wheel load in this construction without cracking (Fig. 7). The flexural strength

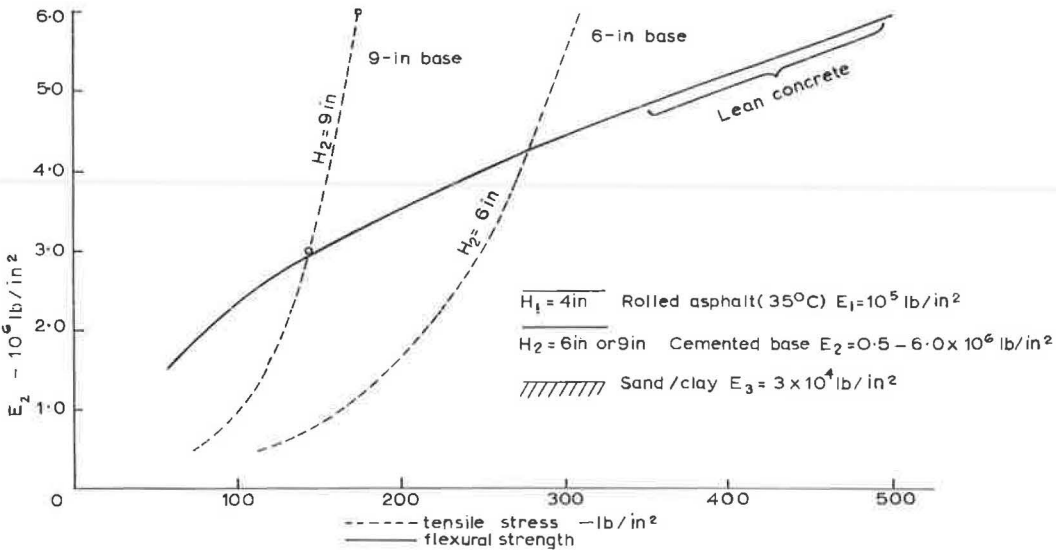

Figure 7. Computed tensile stresses at bottom surfaces of 6- and 9-in. cemented bases of different moduli of elasticity compared with flexural strength.

measured on beams is, however, no guide to the behavior of the actual bases, and it is likely to give a very conservative estimate of the resistance of the base to flexural failure for the following reasons.

1. Additional stresses from causes other than traffic are likely to be present, i.e., those due to temperature or moisture gradient.
2. The fatigue strength is lower than the flexural strength derived from a single loading.
3. Cemented materials obey the "weak link" theory and failure will occur at lower stresses in the larger volume of the base than in relatively small test specimens.

At present, deficiencies in our knowledge of the physical properties of these types of material, and particularly of their fatigue failure under appropriate stress conditions, make it impossible to make reliable use of the calculations of stresses and displacements for design purposes. A very approximate idea of the overestimation of the failure condition by the flexural strength may be obtained by comparing the results of Figure 7 with the road performance of lean-concrete bases in comparable road structures. After 5 years of mixed traffic containing between 2 and 3 percent vehicles with half-axle loads (i.e., wheel or wheel units) between 10,000 and 20,000 lb, tests on the lean-concrete bases indicated appreciable cracking of the 6-in. base and intermittent cracking of the 9-in. base. This suggests that the flexural strength measured on beams is perhaps 2 or 3 times the failure strength of the in situ material. Once a crack forms in the base there is stress relief in the adjacent material and the frequency of occurrence of cracks depends on the redistribution of stress in relation to the failure strength of the material (6). The stronger the material, the greater is the distance between cracks, but in the absence of reinforcement there is also a tendency for the cracks to widen giving poor transference of shear stresses and producing reflection cracks in the surfacing.

For the weaker cemented materials, it has been suggested (6) that the material breaks down under traffic into small interlocking pieces, the size of hard core, separated by fine cracks, and thus behaves in a similar manner to a flexible base. The present work shows that the weaker cemented materials break down to give a material having an elastic modulus comparable to that of the original unbound compacted material.

ACKNOWLEDGMENT

The work described was carried out as part of the program of the Road Research Board of the Department of Scientific and Industrial Research. The article is published by permission of the Director of Road Research.

REFERENCES

1. Whiffin, A. C., and Lister N. W. The Application of Elastic Theory of Flexible Pavements. Proc. Internat. Conf. on Asphalt Pavements, Univ. of Michigan, Aug. 20-24, 1962, Ann Arbor, pp. 499-521, 1963.
2. Jones, R. Non-Destructive Testing of Concrete. Cambridge Engineering Series, Cambridge, England, Cambridge Univ. Press, 1962.
3. Jones, R. Following Changes in the Properties of Road Bases and Subbases by the Surface Wave Propagation Method. Civ. Eng., London, Vol. 58, No. 682, 613, 615, 617; No. 683, 777-80, 1963.
4. Jones, R. Surface Wave Technique for Measuring the Elastic Properties and Thickness of Roads: Theoretical Development. Brit. Jour. Appl. Phys., Vol. 13, No. 1, pp. 21-29, 1962.
5. Jones, R. In-Situ Measurement of the Dynamic Properties of Soil by Vibration Methods. Géotechnique, London, Vol. 8, No. 1, pp. 1-21, 1958.
6. Maclean, D. J., and Robinson, P. J. M. Methods of Soil Stabilization and Their Application to the Construction of Airfield Pavements. Proc. Inst. Civ. Engineers, Pt. II, Vol. 2, No. 2, pp. 447-486, 1953.

Laboratory Investigation of Stabilization of Soils Using Cutback Asphalt

C. E. G. JUSTO, Reader in Civil Engineering, University of Roorkee, Roorkee (U. P.), India
P. HARIHARAN, Lecturer in Civil Engineering, College of Engineering, Trivandrum, India

ABRIDGMENT

•VARIOUS FACTORS affect the properties and behavior of soils stabilized with cutback asphalts. Empirical rules are often used to design soil-asphalt mixtures.

Laboratory investigations were carried out on three soil samples, and the properties and behavior of soils stabilized with cutback asphalts were determined in terms of Iowa bearing value (IBV), water absorption, water content and swelling after soaking. The samples were also subjected to wetting and drying cycles.

MC-2 was best suited to stabilize the soil samples under the prevaling climatic conditions in India. The behavior of soils varied considerably with varying curing and soaking periods, which depend on the soil type. Every soil-water-cutback mix has a particular aeration period which gives maximum stability and minimum water absorption.

The mixing water content has considerable effect on the properties of the stabilized soil. A particular mixing water content could be selected corresponding to the maximum stability or maximum dry density or minimum water absorption. There is an optimum percentage of cutback which would give maximum stability. If the mixing water content is changed even slightly, there is a great loss in the stability of the mix. Hence, for every soil the optimum percentage of cutback and mixing water should be chosen if maximum stability after soaking is desired. This optimum percentage of water content for maximum stability is seldom equal to the optimum water content corresponding to the maximum dry density or the optimum moisture content calculated by some of the empirical rules.

Some of the secondary additives improved the stability of the soils stabilized with cutback asphalt.

TABLE 1

SOIL STABILITY

Soil Type	IBV of Untreated Soil (lb)	IBV of Stabilized Soil (lb)	Opt. Percentage MC-2	Opt. Mixing Water Content (%)
A	114	460	4.0	9.5
B	167	810	5.0	7.0
C	40	650	4.5	10.0

Paper sponsored by Committee on Soil-Bituminous Stabilization.

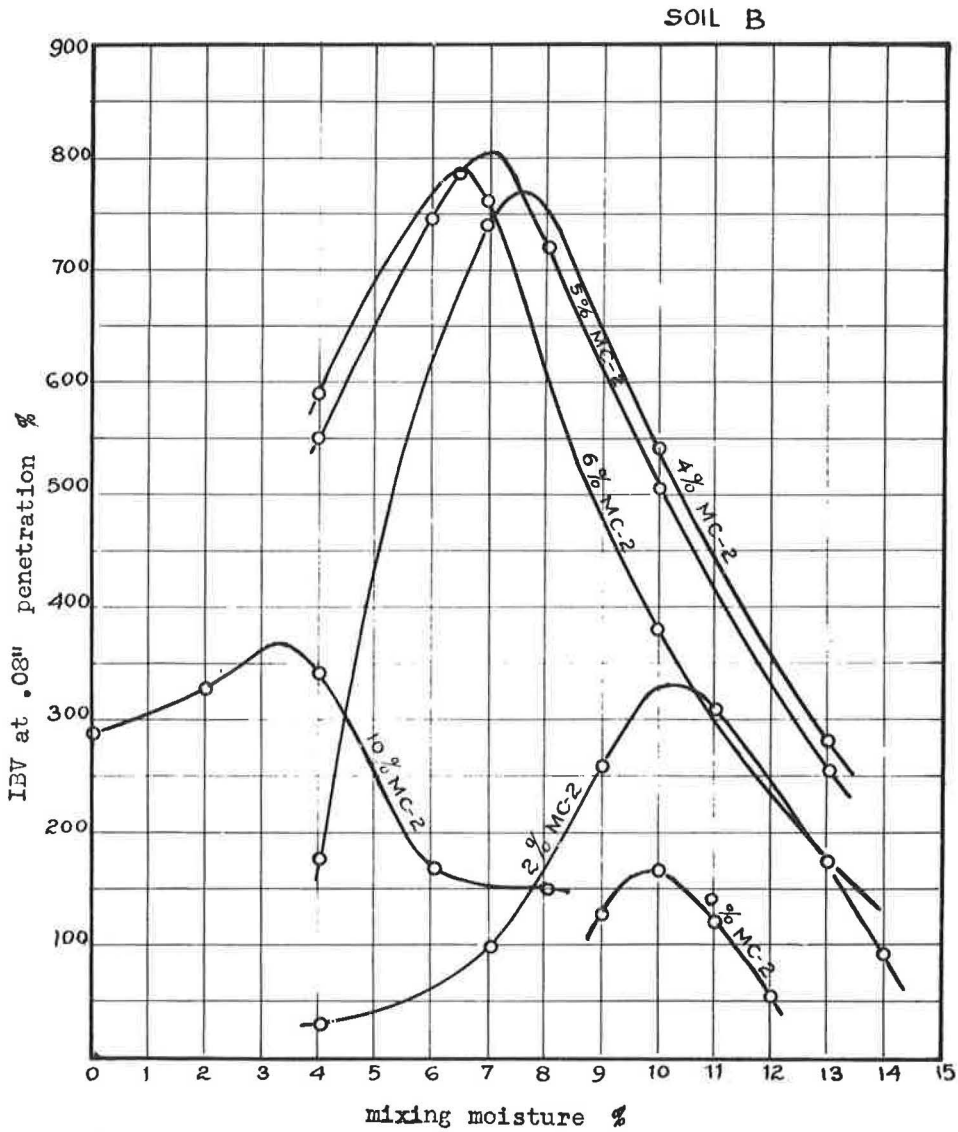

Figure 1. IBV vs mixing moisture content for soil B with different percentages of MC-2.

Figure 1 shows the variation in the IBV for varying percentages of bitumen and water contents for one of the soils. By selecting the optimum percentages of bitumen and mixing water, as suggested in the investigation, the stability of the soils increased considerably, as indicated in Table 1.